Complex formation and lactonization reactions in aqueous solutions containing Ca^{2+} or Nd^{3+} ions and sugar-type ligands

Ph.D. Dissertation

Bence Kutus

Supervisors: Prof. Pál Sipos

Prof. István Pálinkó

Doctoral School of Chemistry

Department of Inorganic and Analytical Chemistry,
Faculty of Science and Informatics, University of Szeged

Szeged

2018

Table of contents

1. Introduction

The interactions between metal ions and carbohydrate derivatives (*e.g.*, sugar alcohols and sugar acids) play a crucial role in numerous enzymatic reactions as well as industrial processes. For instance, sugar acids are considered to be very efficient chelating agents due to the presence of carboxylic and adjacent hydroxy groups. The most prominent member of this family, gluconic acid (HGluc), is produced in large amounts (60,000 tons annually) worldwide [1].

Owing to its moderate acidity, HGluc is used in food industry as an acidity regulator. Furthermore, the excellent metal-binding ability of gluconate ($Gluc^-$) is exploited in chelation therapy (*e.g.*, in the treatment of calcium deficiency). Of the numerous salts of gluconate, NaGluc is applied in paper and textile industry as well as in metallurgy as cleaning and derusting agent. Recently, NaGluc is used as an additive in the formulation of cementitious materials, since it helps to regulate the setting time and water resistance [1].

The underground repositories established to deposit low- and intermediate-level radioactive waste (like the Asse II salt mine in Germany [2]) are of general importance due to safety reasons. In these concrete-based repositories, hypersalic pore water is assumed to be formed by incidental water intrusion [2–5], while the pH may vary between 7 and 13 during the course of cement degradation [5].

Due to the reducing environment provided by the corroding steel containers [2], the preferred oxidation state of actinides is +3 or +4. Beside pH, the solubility of An(III/IV) ions is affected by complexing ligands as well. Gluconate, being an ingredient of Portland cement, is likely to be present in these systems and it is used as a model of organic contaminants [6]. Since the mobilization of radionuclides can be promoted through complexation, the quantitative description of these equilibria taking place both in neutral and alkaline media is of particular interest.

Furthermore, $Gluc^-$ is also a model compound of different organic substances that might be present in strongly caustic Bayer liquors [7], in which the solubility of $Ca(OH)_2(s)$ (used for NaOH recovery) can be affected by these complexing ligands [7,8]. Regarding waste repositories, Ca(II), which stems from Portland cement, may also have an impact on the solubility of actinides *via* the formation of ternary species consisting of Ca(II), An(III/IV) and $Gluc^-$ ions [2,6,9].

The affinity of $Gluc^-$ toward metal binding becomes more pronounced with increasing pH. Conversely, the quantitative description of the species formed between Ca(II)/Ln(III) ions and sugar-type ligands – especially at higher concentrations and pH – is still incomplete. Therefore we embarked on the study of the complexation reactions between $Gluc^-$ and Nd^{3+} ions, the latter being a frequently used model for trivalent actinides [2].

On the other hand, little is known about the effect of the configuration of sugar-type ligands. That is, the chemistry of coordination compounds prevailing under basic conditions can be further modulated by the difference in stereochemistry.

L-gulonic acid (HGul), being the diastereomer of HGluc, was chosen as a representative to study the impact of configuration. A profound comparison, however, requires the investigation of the whole pH range available. Hence, in this work we studied not only the complexation of Ca^{2+} ions by gulonate (Gul^-), but also the lactonization reactions of HGul occurring in acidic medium. Our experiments were augmented by both spectroscopic measurements and quantum chemical calculations to reveal the structure of the various species formed.

Additionally, the derivatives of D-glucose were investigated at neutral pH in order to draw general conclusions regarding the Ca^{2+} binding by polyhydroxy carboxylates having different oxidation state and structure.

2. Literature review

2.1. The properties of sugar acids in aqueous solutions

2.1.1. Synthesis from D-glucose

Aldohexoses, such as D-glucose (Glu), are readily oxidized in moderately acidic medium on reacting with bromine [10,11]. The thus formed aldonic acid, D-gluconic acid (HGluc), can be further oxidized with nitric acid resulting in the formation of D-glucaric (H_2Glucar) acid (also known as D-saccharic acid). Protecting the CHO group of Glu selectively, the terminal CH_2OH group can be transformed to COOH group yielding D-glucuronic acid (HGlucur). On the other hand, the formyl group can be reduced to D-sorbitol (Sor), a sugar alcohol, by using sodium borohydride. The reaction map with the corresponding glucose derivatives are seen in Figure 1.

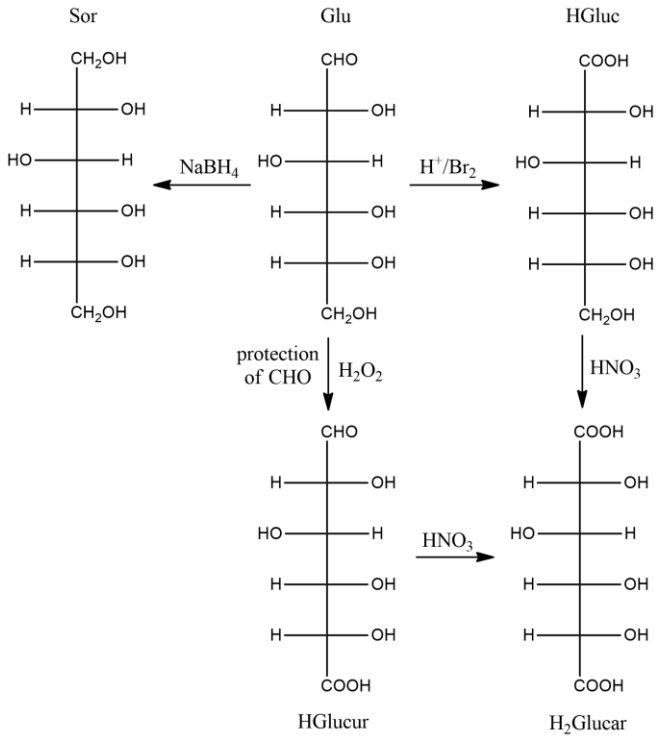

Figure 1 Oxidation and reduction processes of D-glucose (Glu). The structural formulae of Glu, D-sorbitol (Sor), D-gluconic acid (HGluc), D-glucuronic acid (HGlucur) and D-glucaric acid (H_2Glucar) correspond to the open-chain forms. Capital 'H' in the name represents the dissociable proton on the COOH functional group.

Oxidation processes other than the traditional chemical syntheses are based on the use of electric current [11–14], ultrasound [15] and catalysts such as Pt, Rh [16] or Au/C [17]. Alternatively, these compounds can be produced *via* the biochemical route. That is, HGluc is readily obtained from D-glucose by fermentation using filamentous fungi, yeast or bacteria [1]; the process was originally discovered by H. T. Herrick [18].

2.1.2. Protonation and subsequent lactonization processes of D-gluconate and L-gulonate

Having five electron-withdrawing hydroxy groups, HGluc and its diastereomer, HGul (Figure 2) have increased acidity compared to that of caproic (hexanoic) acid. The protonation reaction for the anion A^- and the corresponding equilibrium constant read as:

$$A^- + H_3O^+ = HA + H_2O \quad (1)$$

$$K_p = \frac{1}{K_a} = \frac{[HA]\cdot c}{[H_3O^+][A^-]} \quad (2)$$

where K_a is the acid dissociation constant of HA and c means the standard molar concentration, 1 mol·dm^{-3}.[1] Concerning gluconic acid, the thermodynamic protonation constant regarding to infinite dilution, log K_p^0,[2] was found to be 3.85 [19], 3.77 [20] as well as 3.92 [21] at 25 °C. Depending on the ionic strength and experimental technique used, the log K_p of $Gluc^-$ ranges from 3.23 to 3.86 determined *via* potentiometry [21,22–34], potentiometry combined with polarimetry [35] or with NMR spectroscopy [36,37]. These data (mostly correspond to T = 25 °C) are tabulated in Table 1 for the sake of perspicuity. For comparison, the log K_p of the caproate ion (same as the pK_a of caproic acid) was reported to be 4.85 [38].

L-gulonic acid (Figure 2) is known as an important intermediate forming in the enzymatic synthesis of L-ascorbic acid in mammals [39]. Contrary to HGluc, the protonation equilibria of Gul^- were studied sporadically. At infinite dilution, log K_p^0 was calculated to be 3.67 [40], whilst 3.48 [30] was deduced from potentiometric titrations at 0.1 M ionic strength (I) and 25 °C. This constant is considerably smaller than 3.70 reported for $Gluc^-$ in ref. [21]. Conversely, it agrees well with the range of 3.3–3.5 determined for $Gluc^-$ at I = 0.1 M (Table 1). In conclusion, the protonation constants for the two anions are very similar (within experimental uncertainty), thus, the role of configuration seems to be marginal.

[1] All stability products are defined as dimensionless quantities throughout this work.
[2] Hereafter, the equilibrium constants include the activity of water.

It is worth mentioning that the only available constant (3.38) for the structurally-related heptagluconate ($Hpgl^-$, Figure 2) with regard to I = 0.1 M [28] also falls into the above-mentioned range. By the same token, the actual value of the protonation constant is not affected either by the number of hydroxy groups. (The log K_p of 2.49 corresponding to I = 1 M [41] is probably an underestimation.)

Table 1 Protonation constants (log K_p) for D-gluconate ($Gluc^-$), L-gulonate (Gul^-) and D-heptagluconate ($Hpgl^-$). Data correspond to T = 25 °C unless indicated differently; ± 3 *SE* is given in parentheses.

Reaction	Ionic strength and backgr. electrolyte	log K_p	Reference	Method[a]
$Gluc^- + H_3O^+ = HGluc + H_2O$	$I \rightarrow 0$	3.85	19	POL/POT
	$I \rightarrow 0$	3.77(6)	20	POL/POT
	$I \rightarrow 0$	3.92(10)	21	POT
	≈ 0.004 M[b]	3.70	35	POL/POT
	0.015 M KCl	3.86	23[c]	POT
	0.1 M NaCl	3.46(6)	29	POT
	0.1 M $NaClO_4$	3.70(1)	21	POT
	0.1 M $NaClO_4$	3.50(9)	30	POT
	0.1 M $NaClO_4$	3.47(2)	31	POT
	0.1 M $NaClO_4$	3.30(6)	36[d]	^{13}C NMR/POT
	0.1 M $NaNO_3$	3.40(3)	28	POT
	0.1 M KNO_3	3.439(3)	26	POT
	0.15 M $NaClO_4$	3.572	24[d]	POT
	0.2 M KCl	3.556	22[c]	POT
	0.2 M KCl	3.36(2)	34	POT
	0.5 M $NaClO_4$	3.60(2)	21	POT
	0.5 M KNO_3	3.56(9)	27	POT
	1 M NaCl	3.23(3)	37	^{1}H NMR/POT
	1 M NaCl	3.24(3)	37	^{13}C NMR/POT
	1 M $NaClO_4$	3.63(1)	21	POT
	1 M $NaClO_4$	3.48(18)	25	POT
	1 M $NaClO_4$	3.30(10)	33	POT
$Gul^- + H_3O^+ = HGul + H_2O$	$I \rightarrow 0$	3.67	40	POL/POT
	0.1 M $NaClO_4$	3.48(6)	30	POT
$Hpgl^- + H_3O^+ = HHpgl + H_2O$	0.1 M $NaNO_3$	3.38(2)	28	POT
	1 M NaCl	2.49(15)	41	^{13}C NMR/POT

[a] POL = polarimetry, POT = potentiometry applying glass electrode, NMR = nuclear magnetic resonance spectroscopy.
[b] Corresponds to pH = 2.36 reported by the authors; no additional background electrolyte was used.
[c] The temperature was not indicated.
[d] The measurements were performed at 22 °C [36] and 37 °C [24], respectively.

In acidic medium, polyhydroxy carboxylic acids are transformed partially to various types of intramolecular cyclic esters. The so-called lactones occur in nature usually as five- (γ) and six-membered (δ) ring compounds [10,11]. They serve as building blocks as well as components of various aromas and odors, hence, they are utilized in the cosmetic and food industries.

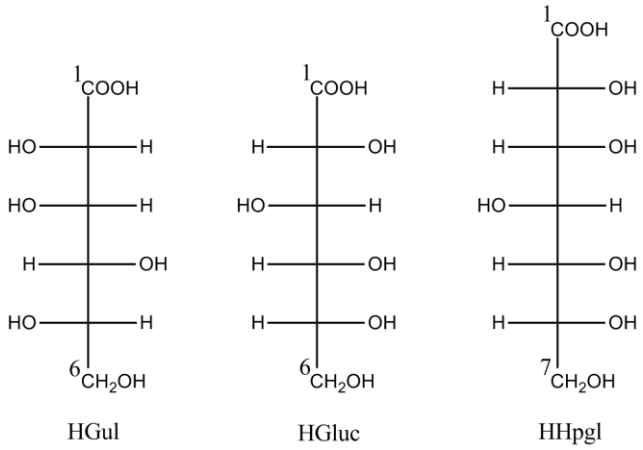

Figure 2 Fischer projection of L-gulonic acid (HGul), D-gluconic acid (HGluc) and D-heptagluconic acid (HHpgl). Capital 'H' in the name represents the dissociable proton on the COOH functional group.

D-gluconic acid δ-lactone (δ-HGluc, Figure 3) finds application as latent acid and leavening agent in baked goods and as acidifier in meat products. Moreover, it is a common additive in the dairy industry, too [1].

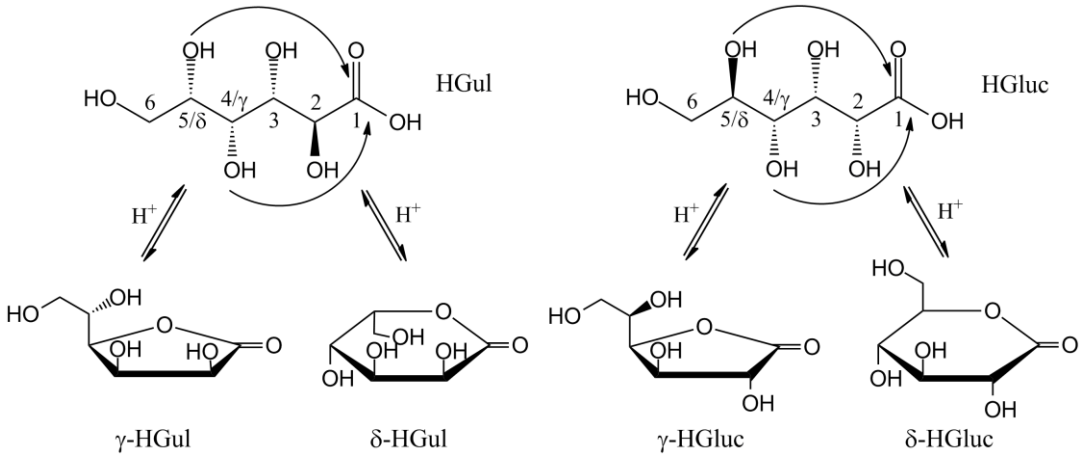

Figure 3 Structural formulae of L-gulonic (HGul) and D-gluconic acid (HGluc) as well as the Haworth projections of L-gulonic/D-gluconic acid γ- and δ-lactones (γ-HGul, γ-HGluc, δ-HGul, δ-HGluc). Arrows indicate the attack of the OH groups on the electrophilic carbon (C1) yielding the lactones.

Along with L-gulonic acid, its γ-lactone (γ-HGul, Figure 3) appears as key intermediate in the enzyme-catalyzed synthesis of vitamin C [39,42]. The reactions involving the formation of γ-HGul and ascorbic acid are discussed in detail in refs. [43–49]. Nowadays, the industrial production of ascorbic acid is mainly based on the Reichstein process applying the readily available

D-glucose instead of D-glucuronic acid [50]. Nevertheless, attempts were made to use directly γ-HGul or its 3,5-*O*-benzylidene derivative to obtain ascorbic acid [51].

In the course of non-enzymatic reactions, the formation of lactones below pH ≈ 5 is acid-catalyzed as follows from the mechanism of the Fischer-Speier esterification [52]. Accordingly, the carboxylic group undergoes protonation and the thus formed strongly electrophilic C1 atom is attacked by either the C4-OH or the C5-OH group (Figure 3). Structural rearrangement and subsequent loss of a water molecule leads to the formation of the cyclic esters.

A pioneering work related to the lactonization of HGul and HGluc (among other aldonic acids) was carried out by Levene and Simms [40,53]. The five- and six-membered lactones were found to be formed from D-gulonic, D-heptagluconic, D-galactonic, D-gluconic and D-mannonic acids. The authors observed that the δ-lactone was more dextrorotatory, whilst the γ-lactone was more levorotatory for the first three aldonic acids. On the other hand, gluconic and mannonic acids could only be converted into dextrototatory lactones.

These observations are formulated in Hudson's lactone rule [54], which stipulates that when the OH group involved in the ring closure lies on the right side on the Fischer projection of the acid, the lactone will be more dextrorotatory, otherwise it will be more levorotatory.

Concerning the lactonization kinetics, Levene and Simms [40,53] found that the initial rate of formation of δ-HGul was eight times faster than that of γ-HGul, while this ratio was twenty-one for HGluc. In conclusion, the δ-lactones are more readily formed. By the Baldwin's rules [55], the reactions yielding the γ- or the δ-lactone (*i.e.*, the 5-*exo-trig* and the 6-*exo-trig* types of ring closure) are both favoured.

The general acid-catalysed lactonization reaction reads as:

$$HA + H_3O^+ = HL + H_3O^+ + H_2O \quad (3)$$

where HA is the aldonic acid, HL denotes all of the lactones formed and H_3O^+ is the catalyst. The respective reaction rates can be expressed as:

$$r_1 = k_1[HA][H_3O^+] = k_1^*[HA] \quad (4)$$

$$r_{-1} = k_{-1}[HL][H_3O^+] = k_{-1}^*[HL] \quad (5)$$

It has to be mentioned that since kinetic measurements are usually conducted at only one and constant pH, only the pseudo-first order coefficients (k_1^* and k_{-1}^*) are given.

The rate of lactone formation and reverse hydrolysis for HGluc were previously studied *via* pH-metric, polarimetric, Electrospray Ionization Mass Spectrometric (ESI-MS) or High Performance Liquid Chromatographic (HPLC) measurements [19,20,35,36,56]. Generally, the results reported in the literature correspond almost exclusively to δ-HGluc. The rate coefficients obtained are around 10^{-5} s^{-1} for the lacton formation and around 10^{-4} s^{-1} for the hydrolysis inferring that these processes are considerably slow. In light of the above-mentioned literature sources, the work of Pocker and Green [20] is pivotal, since they determined the second-order rate constant, $k_{-1,\delta}$, as $2.9 \cdot 10^{-2}$ $M^{-1} \cdot s^{-1}$ (T = 25 °C, I = 0.5 M).

To the best of our knowledge, the study of Levene and Simms [40] is the only one with respect to HGul. From the initial reaction rates found at 25 °C, the $k_{1,\delta}^{*}$, $k_{-1,\delta}^{*}$, $k_{1,\gamma}^{*}$ and $k_{-1,\gamma}^{*}$ coefficients are as follows: $3.1 \cdot 10^{-5}$, $9.6 \cdot 10^{-5}$, $3.8 \cdot 10^{-6}$ and $9.6 \cdot 10^{-7}$ s^{-1}. It follows from these parameters that the slowest reaction is the hydrolysis of the presumably more stable γ-HGul.

Indeed, Levene and Simms [40] observed that the five-membered lactone was more stable than its isomer for all aldonic acids, except HGluc for which only the simultaneous formation of the two lactones was postulated [53]. The stability of the γ-lactone over its δ-isomer agrees with the qualitative finding that an *exo* double bond stabilizes the five-membered ring [57].

The overall lactonization constants K_L, is defined as

$$K_L = \frac{[\mathrm{HL}]}{[\mathrm{HA}]} \tag{6}$$

The term ‘overall’ refers to the sum of the two ‘individual’ constants, $K_{L,\delta}$ and $K_{L,\gamma}$:

$$K_L = \frac{[\gamma\text{-HL}]+[\delta\text{-HL}]}{[\mathrm{HA}]} = \frac{[\gamma\text{-HL}]}{[\mathrm{HA}]} + \frac{[\delta\text{-HL}]}{[\mathrm{HA}]} = K_{L,\gamma} + K_{L,\delta} \tag{7}$$

The lactone formation and hydrolytic processes concerning HGluc were studied in many instances with various experimental means like potentiometry, polarimetry and/or HPLC [19–21,35,36,56]. Due to the faster formation of δ-HGluc, $K_{L,\delta}$ was reported in the vast majority of studies. Accordingly, log $K_{L,\delta}^{0}$ (referring to infinite dilution), was reported to be –0.95 [20] (T = 20 °C) [20] and –0.81 (T = 25 °C) [21]. At higher ionic strengths (up to 1 M) and in the range of 22–25 °C, log $K_{L,\delta}$ ranges from –1.15 to –0.54 [19,21,35,36,56]. The large scatter in

these constants can be accounted for the different experimentation used rather than for the varying ionic strength. The available literature data with respect to log $K_{L,\gamma}$ are –0.59 [19] and –0.62 [58] at 25 °C.

The log $K_{L,\delta}$ and log $K_{L,\gamma}$ constants can be estimated as –0.49 and 0.60, respectively, based on the initial rate coefficients reported in ref. [40]. Based on the difference between these two constants, γ-HGul exhibits markedly higher stability.

2.1.3. Deprotonation of hydroxycarboxylates in strongly alkaline medium

Alcohols are known to be very weak acids. For the acid dissociation reaction, the log K_a is –15.5 and –16.0 for methanol and ethanol, respectively [59]. Polyhydroxy carboxylates are expected to be stronger acids, since additional OH groups decrease the pK_a for statistical reasons [60]. The acid dissociation constant, K_a, for these anions can be expressed as:

$$A^- + H_2O = AH_{-1}^{2-} + H_3O^+ \quad (8)$$

$$K_a = \frac{1}{K_p} = \frac{[AH_{-1}^{2-}][H_3O^+]}{[A^-]\cdot c} \quad (9)$$

where K_p is the protonation constant of AH_{-1}^{2-} and c means the standard molar concentration, 1 mol·dm^{-3}.

Concerning Gluc$^-$, a surprisingly high log K_a, –11.18 was determined (T = 37 °C, I = 0.15 M) employing glass electrode [24]. Using hydrogen electrode, values of –13.66 [61] and –13.68 [62] were deduced (T = 25 °C, I = 1 M), whilst –13 was proposed on the basis of ^{13}C NMR experiments (T = 22 °C, I = 0.1 M) [36]. Interestingly, it was found that gluconate ion could be deprotonated twofold; the log K_a of $GlucH_{-1}^{2-}$ was found to be –14.02 [61].

For Hpgl$^-$, log K_a was reported to be –13.41, determined by H_2/Pt potentiometric measurements (T = 25 °C, I = 1 M) [41]. The higher acidity of Hpgl$^-$ can be explained by the statistical effect of the higher number of OH functional groups [60]. With regard to the deprotonation of Gul$^-$, no literature data was reported to date.

2.2. Complexation of calcium(II) by sugar-type ligands

2.2.1. General aspects and experimental methods

Carbohydrates and their derivatives, like aldoses, ketoses and sugar alcohols, tend to interact weekly with alkaline earth metal ions owing to the relatively low electron density on the oxygen donor atoms. Hence, the hydroxy, formyl and oxo groups are not efficient competitors for the strongly bonded water molecules. As a result, the complexes formed in acidic and neutral solutions have almost exclusively low stability and 1:1 stoichiometry [63].

These features are accompanied with difficulties in the quantitative characterization *via* conventional methods (such as potentiometry, conductometry, calorimetry). Consequently, high metal and ligand concentrations are necessary to be used. Furthermore, the speciation is often modulated by the simultaneous formation of conformational isomers. Studying the association reactions between, for instance, Ca^{2+} ions and carbohydrate derivatives, only the average variations are detectable by the above-mentioned methods. Consequently, only the macro-equilibrium constants can be determined.

Other properties, such as electron density, optical activity or X-ray absorption can be utilized for studying conformational equilibrium. The respective spectroscopic methods, such as Nuclear Magnetic Resonance (NMR), Circular Dichroism (CD), polarimetry, Optical Rotatory Dispersion (ORD) or Extended X-ray Absorption Fine Structure (EXAFS) have proven to be useful to pinpoint the metal-binding sites of the ligands as well as to provide additional structural information (*e.g.*, bond lengths and angles). Other experimental means like infrared or Raman spectroscopies and X-ray diffraction are essential to characterize the coordination compounds in the solid phase. Additionally, in the past few decades, quantum chemistry emerged as an important method to elucidate the nature of metal-ligand interactions.

2.2.2. Ca^{2+} complexes forming with D-glucose and sugar alcohols

In general, favorable arrangement of the OH groups is desirable for the formation of Ca^{2+}-sugar or -cyclitol complexes as identified by Angyal and others [64–70]. Accordingly, the best coordinating ligands are a) pyranose rings having three non-adjacent OH groups in *triaxial* (*ax-ax-ax*) arrangement or b) three adjacent OH groups in *axial-equatorial-axial* (*ax-eq-ax*) sequence or c) furanose rings with OH functional groups with the same *ax-eq-ax* motif [63]. These structural moieties are depicted in Figures 4a-c. Polyols in open-chain form, whose OH groups

are situated on the same side of the plane (*threo-threo*), are better complexing agents than those having *erythro-threo* or *erythro-erythro* arrangement (Figures 4d-f) [63,71–73].

Accordingly, the expected order of complex stability is as follows: *ax-ax-ax* > *ax-eq-ax (pyranose)* > *ax-eq-ax (furanose)* as well as *threo-threo* > *erythro-threo* > *erythro-erythro*.

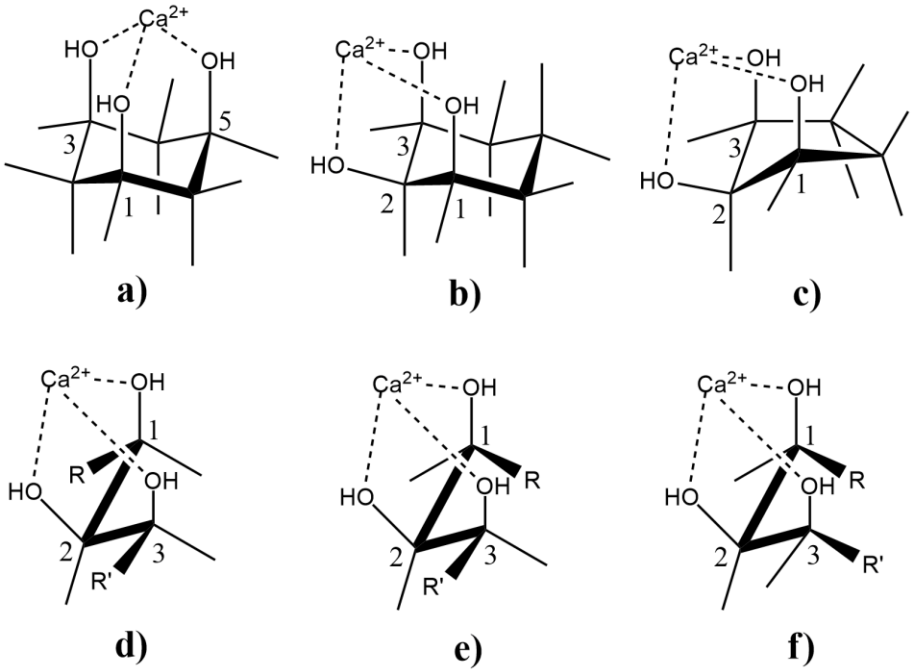

Figure 4 Steric arrangements of the OH groups for calcium(II) complexation in the order of decreasing stability of metal ion-ligand interactions. For cyclic triols: a) 1,3,5-*ax-ax-ax* triol and b) 1,2,3-*ax-eq-ax* triol on a six-membered ring; c) 1,2,3-*ax-eq-ax* triol on a five-membered ring. For acyclic triols: d) *threo*-1,2-*threo*-2,3, e) *erythro*-1,2-*threo*-2,3 and f) *erythro*-1,2-*erythro*-2,3 sequences. This figure is based on Figure 1 in ref. [63], p. 87.

On the basis of Angyal's rules, both α- and β-D-glucopyranose (Figure 5) lack any of the desired steric arrangements. Expectedly, D-Glu is not able to form stable complexes with Ca^{2+}, albeit the interactions with α-D-Glu might be more preferred to some extent due to the anomeric effect stabilizing the α-epimer.

The association reaction between the Ca^{2+} ion and glucose and the 1:1 stability constant are defined as

$$Ca^{2+} + Glu = CaGlu^{2+} \tag{10}$$

$$\beta_{11} = \frac{[CaGlu^{2+}] \cdot c}{[Ca^{2+}][Glu]} \tag{11}$$

This formation constant, however, could not be deduced from ^{1}H NMR spectroscopic [65], thin-layer chromatographic (TLC) [74] and potentiometric [75,76] (applying Ca^{2+} ion-selective electrode, Ca-ISE) measurements in the temperature range of 25–31 °C. It is noteworthy that contrary to Glu, α-D-allose, α-D-gulose and β-D-talose having the *ax-eq-ax* sequence all exhibited considerable extent of Ca(II) complexation [74].

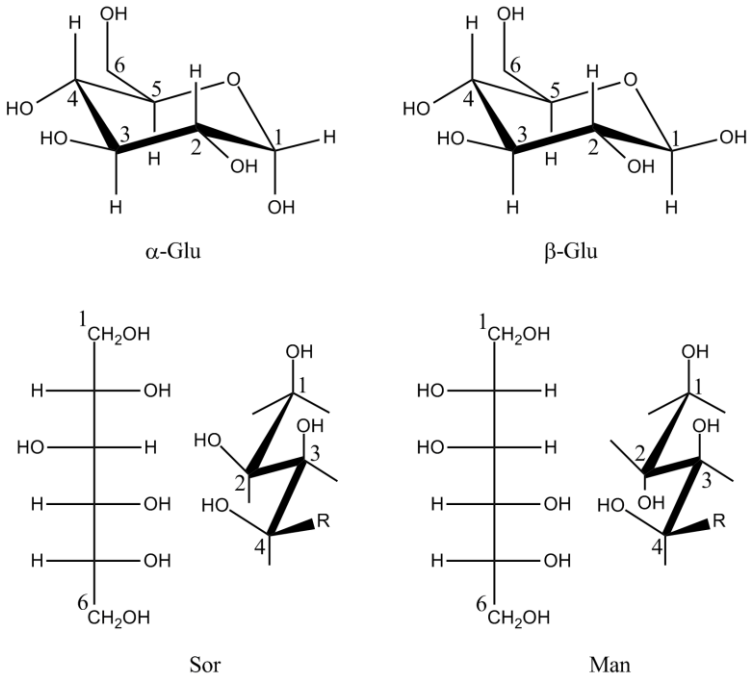

Figure 5 Structural formulae of α-D-glucose (α-Glu), β-D-glucose (β-Glu), D-sorbitol (Sor) and D-mannitol (Man). 'R' represents the C(5)HOH-C(6)H_2OH moiety.

The value of log β_{11} was suggested to be smaller than –1 by ref. [75]. This matches well with the value of –1.12 determined by conductometric experiments performed at 30 °C [77]. Additionally, the variations of the ^{13}C NMR shifts allowed the calculation of log β_{11} for the α (0.18) and β anomers (0.23) at T = 25 °C and I = 1 M [78]. The difference between these two constants does not bear any chemical information, since the standard error of log β_{11} is *ca.* 0.05. Furthermore, the change of each chemical shift upon addition of $CaCl_2$ was the same in direction and nearly the same in magnitude. Therefore, the observed variations might be caused by changing the background electrolyte from NaCl to $CaCl_2$.

Conversely, using the ^{1}H–^{43}Ca Heteronuclear Multiple Quantum Coherence (HMQC) two-dimensional NMR technique, the interaction between Ca^{2+} and the C1-OH group (adjacent to

the ethereal oxygen, Figure 5) was revealed for both epimers (Figure 6) [78]. On the other hand, molecular modeling performed at the HF/6–31G(d,p) level suggested the additional coordination of the ethereal oxygen as well as C6-OH [78]. The phenomenon of complex formation was also established qualitatively by Raman [79] and infrared spectrometric [80] methods indicating that α-D-glucose was the favored isomer in metal ion-binding. In conclusion, the interaction seems to occur in aqueous solutions; however, the formation constant is too low rendering the quantitative determination difficult.

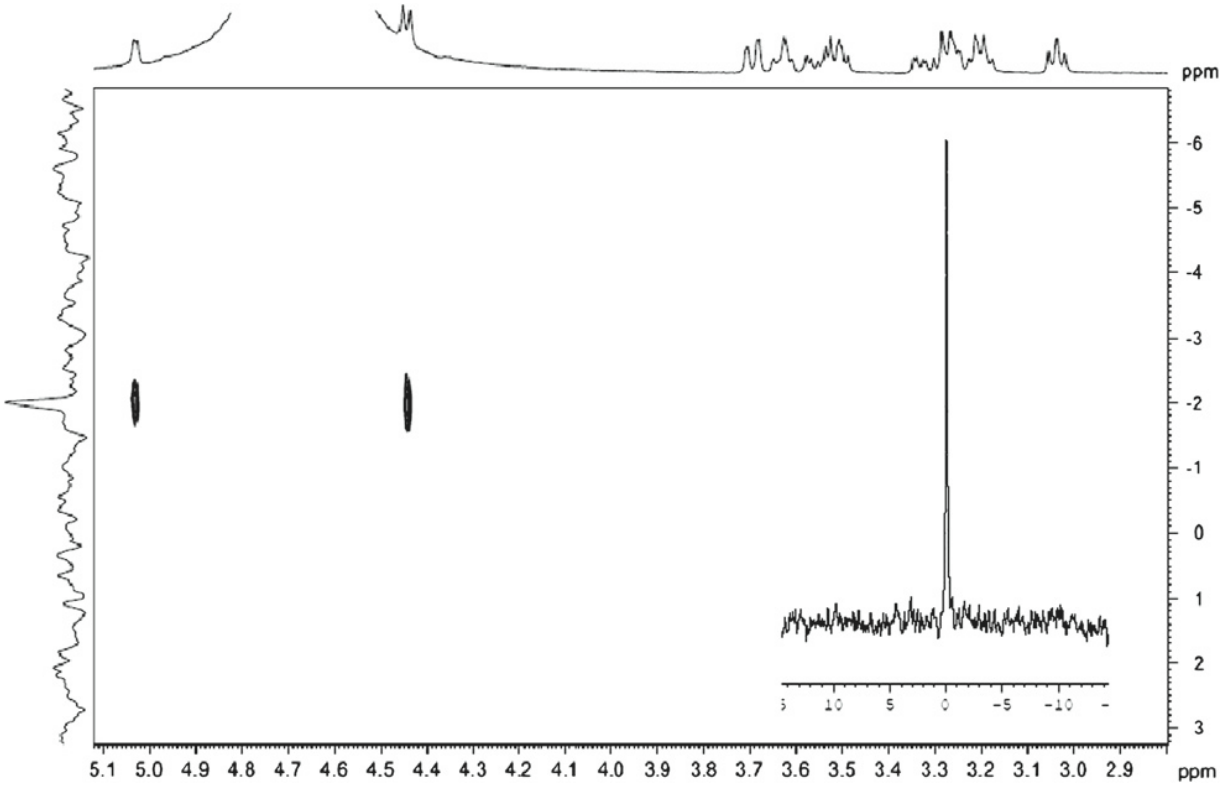

Figure 6 The 2D ^{1}H–^{43}Ca HMQC spectrum (^{1}H: x, ^{43}Ca: y axis) of the solution containing 0.2 M $CaCl_2$ and 0.2 M D-glucose (Glu, mixture of the two anomers). The peaks of α-H(C1) and β-H(C1) are seen around 5.0 and 4.4 ppm, respectively. Inset: the ^{43}Ca spectrum of 0.2 M $CaCl_2$. This figure was taken from ref. [78], p. 339.

Somewhat stronger complex formation is reported for D-sorbitol and D-mannitol (Figure 5). This finding can be elucidated with the flexibility of these ligands: the large number of coexisting conformations results in more favored reactions in view of entropy. TLC experiments [74] showed that the $CaSor^{2+}$ species was slightly more stable than the $CaMan^{2+}$ one. Concerning the $CaSor^{2+}$ species, conductometric measurements yielded log β_{11} as –0.79 (T = 30 °C) [77], while

–0.22 (T = 36 °C) [81] and 0.20 (T = 25 °C, I = 1 M) [78] were deduced from ^{13}C NMR spectroscopy. Using Ca-ISE potentiometry and/or the solubility method, the log β_{11} of the $CaSor^{2+}$ and $CaMan^{2+}$ complexes was reported to be –0.09 and –0.52 [73], 0.18 and –0.05 [82] as well as –0.52 and –0.62 (I = 0.7 M) [75] at 25 °C.

Summarizing these data, it can be stated that the extent of association is still small and is at the edge of measurability. On the other hand, literature data suggest that $\beta_{11}(CaMan^{2+}) < \beta_{11}(CaSor^{2+})$. This is in agreement with the predicted order based on structural differences [71], that is, Sor has *threo*-2,3-*threo*-3,4, while Man has *erythro*-2,3-*threo*-3,4 sequence (Figure 5).

The metal-binding sites of Sor were proposed as the C1-OH, C2-OH, C4-OH and C6-OH groups from the long-range couplings in the ^{1}H–^{43}Ca HMQC spectrum [78]. Conversely, C3-OH should be the coordinating group due to the *threo*-2,3-OH motif. Owing to the very broad ^{1}H peaks, however, the peak assignment was not obvious. Based on the assignment reported previously [83], the order of peaks is as follows: H2 > H3 > H6 > H5 > H1 > H4 > H6’ > H1’. Consequently, the most probable binding sites are, indeed, the C1-OH, C2-OH and the C3-OH groups, while the fourth one can be either the C4-OH or C6-OH.

2.2.3. Ca^{2+}-complexes of sugar carboxylates forming in neutral medium

Introducing a negatively charged anchoring group (*e.g.*, carboxylate) into the ligand results in significantly higher stability. For the most frequently studied $Gluc^{-}$ (Figure 7), the thermodynamic association constant, log β_{11}^{0}, was found to be 1.7–1.9 [37,84–86]. At varying ionic strength, log β_{11} varies in the range of 0.37–1.36 obtained from Ca-ISE potentiometric [22,62,75,87–90], solubility [82], ion-exchange [91] and ^{13}C NMR spectroscopic [37] measurements. The value of 0.37 [62] is probably underestimated, since it was obtained indirectly from pH-potentiometric titrations performed in alkaline solutions. At higher $[Gluc^{-}]_T/[Ca^{2+}]_T$ ratios, the formation of the 1:2 calcium complex, $CaGluc_2^{0}$, was also observed [87,92]. The log β_{12} was determined to be 1.88 (T = 25 °C, I = 0.5 M) from Ca-ISE potentiometric mseasurements [87], which is the only published data for this species.

For the structurally-related Gul^{-} and $Hpgl^{-}$ (Figure 7), log β_{11} was reported to be 1.6 (Gul^{-}, T = 25 °C, I = 0.1 M) [88] as well as 0.85 and 1.21 ($Hgpl^{-}$, T = 25 °C and I = 1 M) [41].

Regarding the structure of the $CaGluc^{+}$ solution species, the coordination sites of $Gluc^{-}$ were suggested to be the COO^{-}, C2-OH and the C4-OH groups (originally, the latter was interpreted

as C3-OH) by the variations of ^{13}C NMR chemical shifts [93]. The observed changes were, however, the result of simultaneous deprotonation and complexation reactions, thus, the proposed coordination motif is questionable. In a recent publication, a ^{1}H–^{43}Ca HMQC NMR measurement (Figure 8) attested the coordination of the C2-OH and C3-OH groups [37]. The authors suggested the simultaneous formation of linkage isomers in which either the C2-OH or both the C2-OH and C3-OH functional groups act as binding sites. Quantum chemical calculations shpwed that the latter was more stable. It has to be noted that Gluc^{-} has *threo*-2,3-*threo*-3,4-triol sequence (Figure 7), thus, the Ca(II) chelation by C2-OH, C3-OH and perhaps C4-OH is preferred.

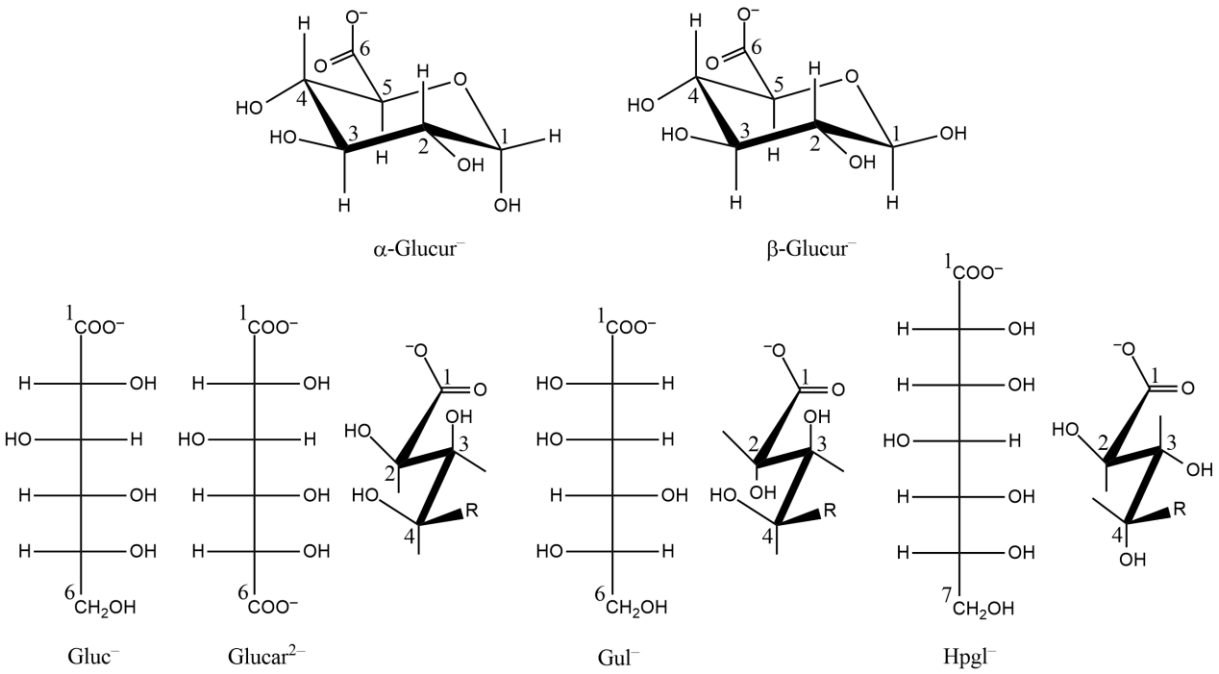

Figure 7 Structural formulae of α-D-glucuronate (α-Glucur^{-}), β-D-glucuronate (β-Glucur^{-}), D-gluconate (Gluc^{-}), D-glucarate (Glucar^{2-}), L-gulonate (Gul^{-}) and D-heptagluconate (Hgpl^{-}). 'R' represents the C(5)HOH-C(6)H_2OH (Gluc^{-}, Gul^{-}), C(5)HOH-C(6)OO^{-} (Glucar^{2-}) or the C(5)HOH-C(6)HOH-C(7)H_2OH (Hpgl^{-}) moiety.

In the case of Hpgl^{-}, the two-dimensional NMR measurement revealed the probable coordination of all the three OH functional groups [41] inferring the coexistence of coordination isomers. The Ca(II) ion, on the other hand, was bound to four heptagluconate anions acting as bidentate ligands and to a water molecule in the $CaHgpl_2.4H_2O$ single crystal [94]. Interestingly, the carboxylate group bound Ca^{2+} in a monodentate manner.

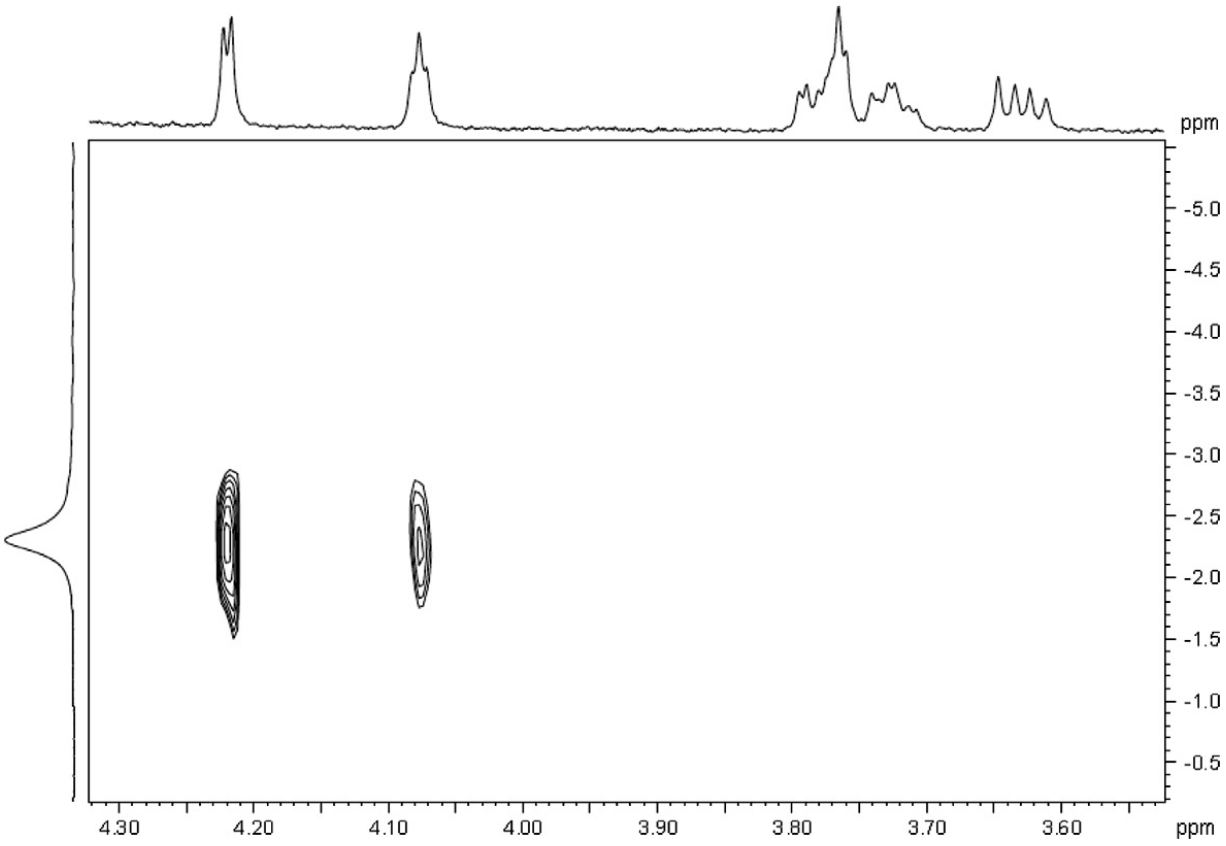

Figure 8 The 2D ^{1}H–^{43}Ca HMQC spectrum (^{1}H: x, ^{43}Ca: y axis) of the solution containing 0.2 M $CaCl_2$ and 0.2 M sodium D-gluconate (NaGluc). The peaks of H(C2) and H(C3) are seen around 4.24 and 4.08 ppm, respectively. This figure was taken from ref. [37], p. 1862.

Due to the presence of the CHO group, D-glucuronate is known to exist in α and β pyranose forms, from which β-Glucur^{-} is present to a larger extent in equilibrium [95], similarly to D-glucose. Another similarity is that the α-isomer of Glucur^{-} is probably the more preferred diastereomer in binding of Ca(II), since log β_{11}(α) and log β_{11}(β) were reported to be 1.57 and 1.45, respectively [95]. The preference for α-Glucur^{-} was further corroborated by IR measurements as well [96]. Utilizing different experimental means and various background electrolyte concentrations, the macro-equilibrium constant, log β_{11}, was found to be in the range of 0.72–1.50 [75,88,95,97,98].

The analysis of the CaBr-α-D-Glucur.3H_2O and CaNa-(D-Glucur)$_3$.6H_2O single crystals revealed that Ca^{2+} was coordinated by three glucoronate moieties in a bidentate manner [99–101]. Interestingly, the ring oxygen was found to be the main binding site beside the COO^{-} group, albeit other OH groups can also act as chelating groups.

Relative to the Ca(II) complexes of gluconate, further stability enhancement is expected to appear when an additional COO^- functionality is present like in D-glucarate (Figure 7). Applying Ca-ISE, the calcium complexation ability of $Glucar^{2-}$ was observed in ref. [102]. Additionally, the logarithmic association constant of the 1:1 complex was calculated to be 3.01 (T = 25 °C, $I \rightarrow 0$) [103] and 2.2 (T = 25 °C I = 0.1 M) [88], respectively.

Concerning the solid state, the metal centre is coordinated by eight oxygen atoms in the $CaGlucar.4H_2O$ single crystal [104]. That is, the two glucarates bind the metal ion in bidentate (COO^- and C2-OH) or tridentate manner (COO^-, C3-OH and C4-OH). The coordination sphere is completed with three water molecules.

2.2.4. Multinuclear Ca^{2+}-complexes of polyhydroxy carboxylates in alkaline solutions

Having the OH group deprotonated, the alcoholate formed is a much more effective binding site for bi- and trivalent metal ions (due to its increased basicity). The calcium(II) ion, in turn, facilitates the deprotonation of the OH groups and the parallel complex formation. In other words, Ca^{2+} decreases the pK_a of the ligand, since it is a strong competitor of H^+ for the alcoholate moiety. This process is the so-called metal ion promoted deprotonation.

Van Duin and co-workers proposed a general ionization scheme for metal polyhydroxy carboxylate complexes [105]. Accordingly, after the deprotonation of the COOH group, the adjacent α-OH group loses its proton. Finally, a further H^+ is displaced from another (not necessarily the β-) OH functional group, hence, the metal ion will be coordinated by a diolate moiety. The authors estimated that the ligand deprotonation for the alkaline earth metal ions occurred above pH = 10.

Being the metal ion-alcoholate interactions stronger than those with hydroxy groups, complexes forming *via* ligand deprotonation have higher stability. The calcium sequestering capacity was enhanced with increasing pH in the presence of $Gluc^-$, $Hpgl^-$ and $Glucar^{2-}$ [106,107], indeed.

The general complexation reactions and the corresponding β_{pq-r} stability products can be expressed as:

$$p\,Ca^{2+} + q\,A^- + r\,H_2O = Ca_pA_qH_{-r}^{(2p-q-r)+} + r\,H_3O^+ \qquad (12)$$

$$\beta_{pq-r} = \frac{[Ca_pA_qH_{-r}^{(2p-q-r)+}][H_3O^+]^r}{[Ca^{2+}]^p[A^-]^q c^{1+r-p-q}} \qquad (13)$$

where A^- stands for polyhydroxy carboxylate anions. For $Gluc^-$, the proton displacement from the $CaGluc^+$ complex was observed polarimetrically in the pH range of 10–11 [92]. Later, pH-potentiometric measurements revealed the formation of the $CaGlucH_{-1}^0$ [62], $CaHpglH_{-1}^0$ [41] as well as the $CaGlucurH_{-1}^0$ [98] species. The respective $\log \beta_{11-1}$ values were found to be –10.94 [62], –10.35 [41] as well as –10.40 [98]; each was determined at 25 °C and 1 M ionic strength.

A further proton removal from hydroxy carboxylates and the simultaneous formation of remarkably stable multinuclear complexes were observed with numerous transition metal ions (*e.g.*, with Cu(II) [28,30,108]). Surprisingly, Sipes [92] found a Ca(II) gluconate complex of 2:1 metal:ligand stoichiometry at higher pH indicating that such species is likely to form with Ca^{2+} as well. Later, the $Ca_2GlucH_{-3}^0$ ($\log \beta_{21-3} = -33.24$), the $Ca_3Gluc_2H_{-4}^0$ ($\log \beta_{32-4} = -42.60$) [41] and the $Ca_3Hpgl_2H_{-4}^0$ ($\log \beta_{32-4} = -41.28$) [62] complexes were identified through potentiometric titrations (T = 25 °C, I = 1 M). Additionally, the existence of the bi- and trinuclear gluconate-containing species was supported by ESI-MS and EXAFS [62].

The coordination sites of $Gluc^-$ and $Hpgl^-$ were revealed as the COO^-, C2-OH and C3-OH groups *via* $CaCl_2$- and temperature-dependent ^1H NMR spectra [41,62]. In both cases, the structure of the 3:2:–4 complex was optimized by quantum chemical calculations at the HF/6–31(d,p) level (the structure of the $Ca_3Gluc_2H_{-4}^0$ complex is displayed in Figure 9). Accordingly, each Ca^{2+} is bound to the carboxylate and either to the C2-O^- or to the C3-O^- groups establishing two five- and two six-membered chelate rings. Furthermore, carboxylate acts as a bridging ligand between these two metal ions.

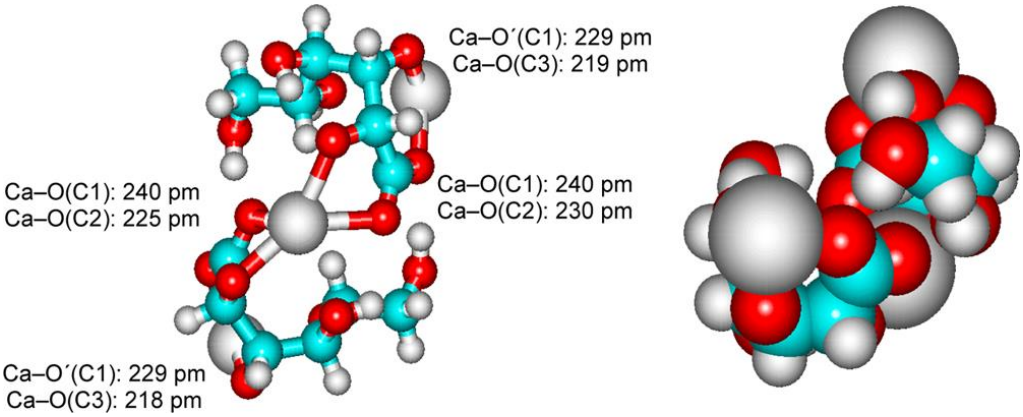

Figure 9 Optimized geometry of the $Ca_3Gluc_2H_{-4}^0$ complex (ball-and-stick and space-filling models). The corresponding metal-ligand bond length are indicated. This figure was taken from ref. [62], p. 6609.

These recent findings highlight that the chemistry of calcium(II) carbohydrate complexes in strongly alkaline medium is completely different from the one prevails at neutral pH. Based on structural similarity, similar bi- and/or trinuclear Ca(II) complexes are expected to form with gulonate and with other sugar carboxylates, respectively.

2.3. Complex formation between gluconate and Nd^{3+} or other lanthanide ions

2.3.1. Relevance to radioactive waste repositories and the role of neodymium(III)

In deep geological sites, which are considered to be possible low- and intermediate-level nuclear waste repositories, salt-rock formations consisting of NaCl and $MgCl_2$ are likely to be present. The incidental intrusion of water is assumed to yield strongly saline aqueous solutions, in which the pH can increase up to 12 ($MgCl_2$ systems) or 13 (NaCl systems) [2–5]. The interaction of these brines with the concrete-based containers can facilitate the mobilization of actinides from the pores into the surroundings. Hence, the long-term stability assessment of these repositories and the characterization of chemical equilibria taking place in these microenvironments are of particular importance.

Under reducing conditions (regulated by the eroding steel containers), Am and Cm appear mainly in their trivalent oxidation states, while Pu is in the forms of Pu(III) and Pu(IV) in aqueous medium [2,109,110]. In order to establish chemical models predicting actinide(III) solubility under the conditions of waste repositories, detailed knowledge is required concerning the effects of 1) pH, 2) ionic strength, 3) temperature and 4) complexing ligands [111].

Nd(III) is generally used as a model for studying the behavior of trivalent actinides. This replacement is justified by its stable +3 oxidation state, availability and safe usage. Moreover, the physicochemical properties and thus the thermodynamic data of tervalent metal ions correlate well with ionic radii [2,109,112]. These data for the eightfold aqua complexes of Nd(III), Pu(III), Am(III) and Cm(III) are as follows: 111, 112, 111 and 109 pm, respectively [112]. Accordingly, coordination interaction of similar strength and therefore similar stability constants are expected for the complexes of these metal ions.

2.3.2. The solubility and hydrolysis of neodymium(III)

In $MgCl_2$-containing brines the pH is buffered to 8–10 by $Mg(OH)_2$ or $Mg_2(OH)_3Cl.4H_2O$ for the first years in the time-scale of the cement degradation [5,113]. With regard to

$Nd(OH)_3(s)$,[3] The dissolution reaction with the corresponding solubility product, K_{sp}, is the following:

$$Nd(OH)_3(s) + 3H_3O^+ = Nd^{3+} + 6H_2O \quad (14)$$

$$K_{sp} = \frac{[Nd^{3+}] \cdot c^2}{[H_3O^+]^3} \quad (15)$$

At 25 °C, log K_{sp}^0 was reported to be 18.66 for amorphous, freshly precipitated hydroxide [114] as well as 16.02, 16.0 and 14.96 [114–116] for crystalline/aged hydroxide. Solubility measurements at 1 M $NaClO_4$ and 22 °C resulted in log K_p as 19.4 [117]. These findings shed light on the importance of the solid phase studied: the crystalline $Nd(OH)_3(s)$ is less soluble than the amorphous one. The increase in the ionic strength brings about marked increase in the solubility (defined as log ($[Nd^{3+}]_T/c$), where 'T' denotes the total concentration of the metal ion and c means 1 mol·dm^{-3}). That is, $-5.5 < \log([Nd^{3+}]_T/c) < -3.2$ for 0.1 M < I < 5.0 M (crystalline) [2], while a value of −4 for I = 1 M (amorphous) was reported (T = 22 °C, pH = 8).

The Nd^{3+} aqua ion is known to form various hydroxido complexes in the general reaction of:

$$pNd^{3+} + rH_2O = Nd_pH_{-r}^{(3p-r)+} + rH_3O^+ \quad (16)$$

In this equation, Nd^{3+} represents the $Nd(H_2O)_x^{3+}$ aqua ion and the $Nd_pH_{-r}^{(3p-r)+}$ species are equivalent to the $Nd_p(OH)_r^{(3p-r)+}$ ones. The dimensionless stability constants are defined by the equation of:

$$\beta_{p-r} = \frac{[Nd_pH_{-r}^{(3p-r)+}][H_3O^+]^r}{[Nd^{3+}]^p c^{1+r-p}} \quad (17)$$

At I = 1 M ionic strength, log β_{1-1}, log β_{1-2}, log β_{1-3} and log β_{2-2} were determined to be −8.1, −16.2, −24.3 and −11.6 *via* solubility measurements (T = 22 °C) [117], whilst log β_{1-1} and log β_{2-2} were calculated to be –8.51 and –14.03 from potentiometric titrations (T = 25 °C) [118].

2.3.3. Complex formation between Nd^{3+} and D-gluconate ions

The solubility of trivalent lanthanides and actinides is expected to increase in the presence of complexing agents, like D-gluconate, which is used as a cement additive [1]. Concerning the Nd^{3+} aqua ion, it is advantageous that its water exchange rate falls between those of Fe^{2+} and

[3] The term 's' in parentheses represents the solid state. If not indicated, the species or component is in the aqueous phase.

Cu^{2+} [119] resulting in relatively fast complexation equilibria easy to study with conventional methods. Furthermore, the visible spectrum of Nd^{3+} is sensitive to its coordination environment. These so-called hypersensitive transitions [120] (centered at 575 nm in water [89]) allow the application of spectrophotometry in addition to pH-metry. Concerning gluconate complexes forming in acidic medium, the increase of the ligand number results in remarkable redshift and larger absorption coefficient in the molar absorbance spectra [89] (Figure 10).

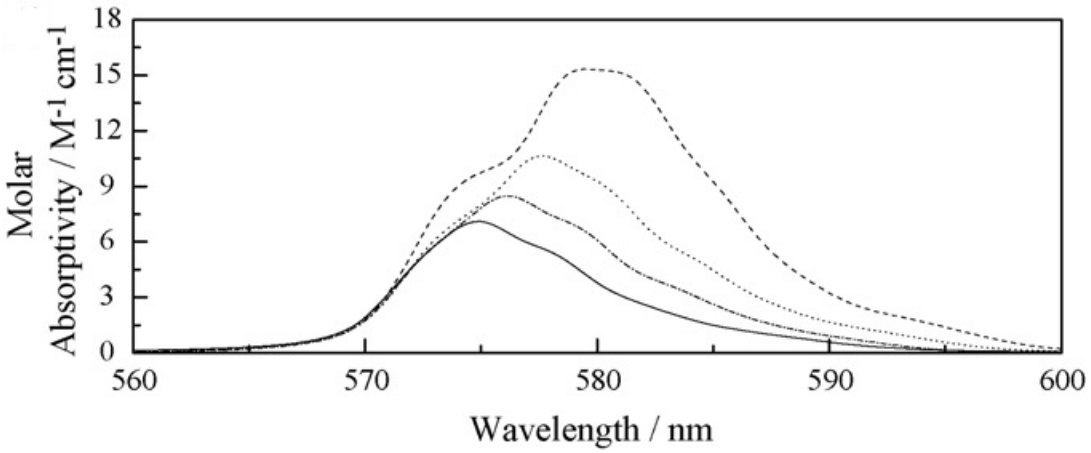

Figure 10 Molar absorbance spectra of Nd^{3+} (solid line) and the Nd^{3+}-gluconate ($Gluc^{-}$) complexes (T = 25 °C, I = 1 M): $NdGluc^{2+}$ (dotted-dash line), $NdGluc_2^{+}$ (dotted line) and $NdGluc_3^{0}$ (dashed line). This figure was taken from ref. [89], p. 473.

The complexation of Nd^{3+} with $Gluc^{-}$ can be expressed by eqs. (18) and (19):

$$p\mathrm{Nd}^{3+} + q\mathrm{Gluc}^{-} + r\mathrm{H_2O} = \mathrm{Nd}_p\mathrm{Gluc}_q\mathrm{H}_{-r}^{(3p-q-r)+} + r\mathrm{H_3O}^{+} \quad (18)$$

$$\beta_{pq-r} = \frac{[\mathrm{Nd}_p\mathrm{Gluc}_q\mathrm{H}_{-r}^{(3p-q-r)+}][\mathrm{H_3O}^{+}]^r}{[\mathrm{Nd}^{3+}]^p[\mathrm{Gluc}^{-}]^q c^{1+r-p-q}} \quad (19)$$

In the acidic pH range, the $NdGluc^{2+}$, $NdGluc_2^{+}$ and the $NdGluc_3^{0}$ species were detected *via* potentiometry and spectrophotometry [89,121–125] showing that the metal ion is able to accommodate even three ligands. The respective formation constants are as follows: $\log \beta_{110}$ = 2.55–2.72, $\log \beta_{120}$ = 4.45–4.70 and $\log \beta_{130}$ = 5.53–5.60 at T = 25 °C [89,122,123] and $\log \beta_{110}$ = 2.37 at T = 32 °C [125].

Contrary to Ca^{2+}, the metal-promoted deprotonation of bound $Gluc^{-}$ occurs at significantly lower pH in the presence of Nd^{3+} owing to its +3 charge. That is, the pK_a of $NdGluc^{2+}$ was reported to be 5.90 (T = 32 °C) [125], while a value of 11.24 can be calculated for $CaGluc^{+}$ from

the data given in ref. [62]. The further deprotonation of the $NdGlucH_{-1}^{+}$ complex was also observed (pK_a = 6.64, T = 32 °C) yielding $NdGlucH_{-2}^{0}$ [125]. Both values are well below the pK_a (= $-\log \beta_{1-1}$) of the aqua ion, 8.1 or 8.51 [117,118]. Consequently, these deprotonation processes take place probably on the ligand instead of H_2O as was postulated in ref. [105]. The proton displacement from the OH group of gluconate also holds for other lanthanides, such as La^{3+}, Pr^{3+} and Eu^{3+} [31,126]. Along with the 1:1:–1 and 1:1:–2 species, complexes with the stoichiometry of 1:2:–1, 1:2:–2 and 1:2:–3 were also reported [121–124].

It is noteworthy that the dependence of the complexation on the metal ion concentration was not investigated in spite of its importance in detecting multinuclear complexes. Such species were found to be formed with copper(II) [28,30,108], calcium(II) [62] and europium(III) [126].

Furthermore, reliable information with respect to the binding sites of the ligand as well as the structure of the complexes in solution is still scarce. Nevertheless, the participation of the C2–OH group in the binding of Nd^{3+} coordination has been proposed earlier [89]. Based on the physicochemical similarities within the lanthanide series, the results for other Ln(III)/$Gluc^{-}$ systems *via* ^{1}H, ^{13}C NMR and CD spectroscopies [31,126,127] may be used for the description of the Nd(III) gluconate complexes. Generally, the COO^{-} and the C2–OH groups were revealed as the binding sites for the $LnGluc^{2+}$ species [126]. Eu(III) was also found to be bound to C3–OH at acidic pH [127]. On the contrary, the C4–OH instead of C3–OH was proposed to coordinate Pr^{3+} in the $PrGluc_2H_{-1}^{0}$ and $PrGlucH_{-2}^{0}$ complexes [31].

3. Aims of the thesis

The protonation of D-Gluc$^-$ as well as the lactonization processes of HGluc were studied in detail. Conversely, literature data for such reactions for the diastereomeric L-Gul$^-$ are sporadic. In the presence of Ca^{2+} ions, the mononuclear 1:1 complex forming with Gluc$^-$ and other D-glucose derivatives were detected in many instances. On increasing pH, the deprotonation of Gluc$^-$ and the structurally related Hpgl$^-$ were observed together with the formation of highly stable, multinuclear complexes. The complex stability as well as the metal ion-binding sites of the ligand were deduced both at neutral and alkaline pH. Little is known, however, about the Ca(II) complexation of Gul$^-$, which would be useful for studying the effect of configuration on both stability and solution structure.

Concerning the underground radioactive waste repositories, Gluc$^-$ may have significant impact on the mobilization of trivalent actinides due to its exceptional metal chelating ability. The formation of mononuclear complexes between Gluc$^-$ and Nd^{3+} (the latter being used as analogue for actinides) were identified and discussed in detail. The existence of multinuclear complexes, however, was not reported, albeit such species are expected to affect significantly these complexation equilibria, especially at higher concentrations.

Hence, the main aims of the present work were as follows:

- to investigate the equilibria and kinetics of the protonation and lactonization reactions of Gul$^-$ and to compare the results to literature data available for Gluc$^-$;
- to perform a quantitative study on the calcium(II) complexes forming in the presence of Gul$^-$, Gluc$^-$ and other derivatives structurally related to D-glucose at neutral pH;
- to identify the multinuclear complexes may be formed with Gul$^-$ and to determine the corresponding stability constants;
- to reveal the Ca(II)-binding sites of Gul$^-$ both in neutral and alkaline media and to draw conclusions on the impact of stereochemistry relative to these complexation processes;
- to study the complexation of Nd^{3+} by Gluc$^-$ at pH = 2–8, to calculate the stability products and to find the groups responsible for metal ion coordination;
- to assess the impact of incidental multinuclear Nd(III) gluconate complexes at concentrations relevant to radioactive waste repositories.

4. Experimental part

4.1. Reagents and solutions

During this work, all materials (listed in Table 2) were used without further purification. All solutions were made using deionized Milli-Q water (by Merck Millipore) and the ionic strength was adjusted to 1 M with NaCl. The purpose of applying such high background electrolyte concentrations was (1) to minimize the effects arising from the variations of the activity and (2) to reach ionic strength values relevant to radioactive waste repositories.

Stock solutions of the hygroscopic $CaCl_2.2H_2O$ and $NdCl_3.6H_2O$ were standardized by EDTA titration.

The purity of γ-HGul was checked by its ^1H and ^{13}C NMR spectra (measured in 100% V/V D_2O). Accordingly, contaminants having peak area larger than 1% were not detected. *Prior to* measurements, the stock solutions of NaGul were prepared by neutralizing γ-HGul with NaOH. Rapid hydrolysis was observed, and the final pH was found to be 7–8. The completion of the ring-opening reaction was confirmed by the ^1H and ^{13}C NMR spectra.

The solution containing the acidic KHGlucar was titrated with NaOH until pH ≈ 7. The initial concentration of glucarate, $[Glucar^{2-}]_{T,0}$,[4] was set to about one order of magnitude lower (0.01–0.04 M) than that of the other compounds, because at higher concentrations, a white precipitate (CaGlucar(s)) appeared in samples stored for one day. Additionally, the high concentration of NaCl (≈ 1 M) resulted in that the contribution of K^+ ions to the total ionic strength was negligible.

HCl stock solutions of ≈ 1 M concentration were made by volumetric dilution of cc. HCl and it was standardized against $KHCO_3$. The carbonate-free, concentrated (50% w/w) NaOH solution was prepared following the procedure given in ref. [128]. A certain amount of the filtered solution (measured by weight) was brought to volume and the resulted ≈ 1 M NaOH was standardized by HCl.

[4] Hereafter for a component X, $[X]_{T,0}$ represents the initial total concentration (for titrations). Similarly, $[X]_T$ means the total concentration (for pointwise measurements), while [X] stands for the free or equilibrium concentration.

Table 2 List of compounds used throughout this work.

Name	Abbreviation	Purity	Supplier
L-gulonic acid γ-lactone	γ-HGul	95%	Sigma-Aldrich
D-gluconic acid δ-lactone	δ-HGluc	≥ 99%	Sigma-Aldrich
D-glucose	Glu	mixture of α and β anomers, ACS grade	Sigma-Aldrich
D-sorbitol	Sor	99%	Sigma-Aldrich
D-mannitol	Man	≥ 98%	Sigma-Aldrich
sodium D-gluconate	NaGluc	≥ 99%	Sigma-Aldrich
sodium D-heptagluconate	NaHpgl	≥ 99%	Sigma-Aldrich
sodium D-glucuronate monohydrate	NaGlucur.H_2O	mixture of α and β anomers, ≥ 97.5%	Sigma-Aldrich
potassium hydrogen glucarate	KHGlucar	≥ 98%	Sigma-Aldrich
sodium chloride	NaCl	a. r. grade	Molar Chemicals
calcium chloride dihydrate	$CaCl_2.2H_2O$	≥ 99%	Sigma-Aldrich
neodymium(III) chloride hexahydrate	$NdCl_3.6H_2O$	99.9%	Sigma-Aldrich
sodium hydroxide pellets	NaOH	≥ 98.5%	VWR Chemicals
hydrochloric acid solution, 37 %w/w	HCl	a. r. grade	Scharlab
deuterium oxide	D_2O	99.9%	Sigma-Aldrich

4.2. Potentiometry

Potentiometric titrations were carried out with a Metrohm 888 automatic titration instrument in a double-jacketed glass cell of in-house construction. For each system, the samples were stirred continuously and were thermostated to (25.0 ± 0.1) °C with a Julabo M12-MB thermostat. During the measurements, 70 cm^3 of the sample was titrated with $CaCl_2$, HCl or NaOH depending on the system in question.

The cell potentials were recorded in three ways:

1) The concentration of free Ca^{2+} ions (*i.e.*, $[Ca^{2+}]$) was measured with a combined Ca-ISE (type 6.0510.100 by Metrohm). The ionic strength of the reference electrolyte (NaCl) was the same as in the test solution. *Prior to* measurements, the electrode was calibrated by titrating a solution containing 10^{-4} M $CaCl_2$ with 0.2 M $CaCl_2$ at the same temperature and ionic strength. The calibration points can be fitted assuming a linear relationship between the cell potential and log ($[Ca^{2+}]/c$) by the Nernst equation. This procedure provides good linearity (*i.e.*, the correlation coefficient, R^2, is ≥ 0.9998) only above log ($[Ca^{2+}]/c$) = −3.3. The points corresponding to the range of log ($[Ca^{2+}]/c$) < −3.3 range, however, might bear essential information. That is, the

formation of the CaA_2^0 complexes is expected to occur in this range. Hence, a nonlinear calibration was applied by fitting splines to the calibration curves utilizing the Spline Calculus program [129]. By this procedure, the whole calibration range could be taken into account.

2) The pH[5] in the range of 2–8 was measured employing combined glass electrodes (type Sentix 62 by WTW or type 924005 by Jenway). To minimize the errors caused by lactonization [19–21,35,36,40,53,56], titrations were started in the alkaline region employing HCl as titrant. The electrodes were calibrated *via* titrating 0.02 M NaOH with 0.2 M malonic acid according to the non-linear evaluation method established in the pHCali program [130]. (The advantage of using malonic acid is that it can be weighed accurately, therefore a solution of known concentration can be prepared.) The program is not only able to calculate the intercept and slope of the electrode but the effect of dissolved CO_2 can also be taken into account. In order to minimize this dissolution, N_2 atmosphere was applied. The calibration and the measurements were performed under the same conditions, thus, the potentials could be converted into pH_c values.

In the case of pointwise measurements (coupled with either NMR or polarimetric experiments), the electrode system was calibrated with dilute buffers (by WTW). Since the ionic strength of the samples differs from that of the buffers, the observed pH_{exp} may be slightly different from pH_c. The difference is the so-called Irving or *A* factor [113,131], which comprises the difference in the activity coefficient of H^+ and the liquid junction potential.

$$pH_c = -\log([H^+]/c) = pH_{exp} + A \qquad (20)$$

Differences in the calibration procedure, therefore, can affect the actual value of the protonation constant; this will be discussed in Section 5.1.2.

In both cases, the electrode response was found to be Nernstian in the range studied.

3) The pH in the range of 11–13 was recorded by a platinized platinum electrode (H_2/Pt) constructed by us based on the procedure given in ref. [132]. The reason of using this electrode was that conventional glass electrodes show the so-called alkali error, usually above pH = 12. Furthermore, the CO_2 could be excluded by bubbling H_2.

As a reference, an outer Ag/AgCl electrode (also built in-house) was employed, and it was separated from the sample solution by a double junction salt bridge (1 M NaCl) to minimize the

[5] Hereafter for potentiometric titrations, pH is defined as $pH_c = -\log([H^+]/c)$. For pointwise measurements, pH is referred to as pH_{exp} which can be recorded directly with the pH meter.

variations of the liguid junction potential. The equilibrium cell potentials were recorded in the following cell construction:

Pt(s) | H_2(g) | H^+ (test sol.), NaCl (I = 1 M) ¦ 1 M NaCl ¦ 1 M NaCl, AgCl | AgCl(s) | Ag(s)

During the course of calibrations, a $[NaOH]_{T,0}$ = 0.005 M (I = 1 M) solution was titrated with 1 M NaOH. An exemplary calibration curve is depicted in Figure 11. It is clearly seen that the E *vs*. pH_c function shows good linearity and the slope (59.22 mV) agrees with the theoretical one (59.16 mV). The pH_c values were obtained from the log ($[OH^-]/c$) ones using pK_w = 13.76 (measured with the same experimental technique) [132]. The maximum difference between the measured and calculated points remains below 1 mV.

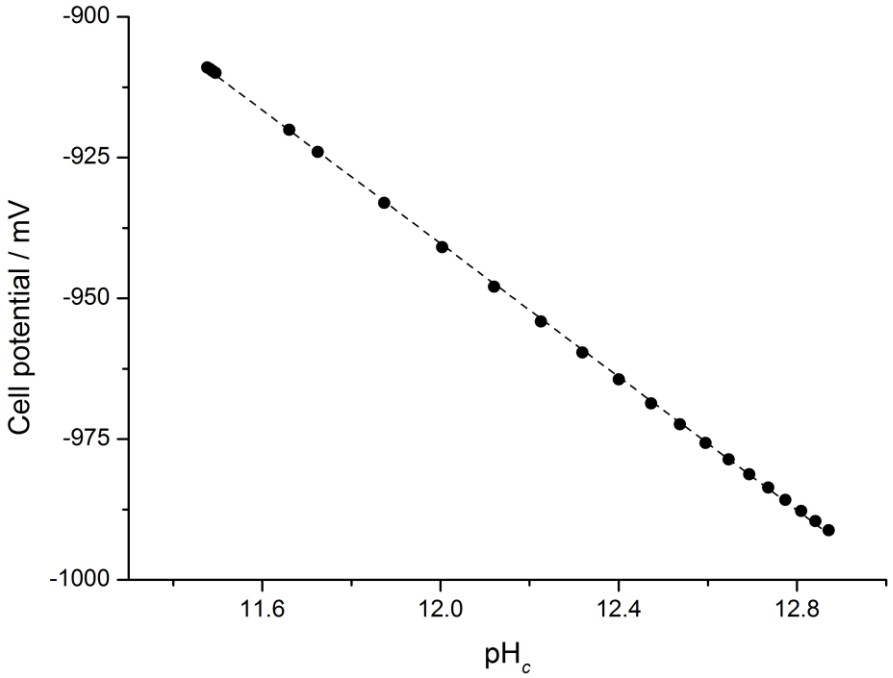

Figure 11 Calibration curve obtained with a H_2/Pt indicator and an Ag/AgCl reference electrode
The measured cell potentials are plotted as a function of pH_c. Experimental conditions: T = (25.0 ± 0.1) °C, I = 1 M, V_0 = 70 cm^3; $[NaOH]_{T,0}$ = 0.005 M (titrand); $[NaOH]_T$ = 1.042 M (titrant). The results of the fitting: intercept = –229.7 mV, slope = 59.22 mV, R^2 = 0.9998.

4.3. Spectrophotometry

The spectra in the $NdCl_3$-containing solutions were recorded in the wavelength range of 400–700 nm on a Shimadzu 1650-PC UV-Vis double beam spectrophotometer. The optical path length of the quartz cuvette was 1 cm. All solutions were measured at (25 ± 2) °C, and the ionic strength was adjusted to 1 M. These samples were prepared by varying $[NaGluc]_T$, $[NaOH]_T$,

$[HCl]_T$ or $[NdCl_3]_T$. For the samples with $[Gluc^-]_T/[Nd^{3+}]_T \leq 2.5$ and $[OH^-]_T > 0.1$ M, a mauve-colored precipitate appeared several hours after the measurements; these spectra were omitted from the calculations.

The rate of lactonization of HGluc [19–21,35,36,53,56] is expected to be slower in the Nd(III)-containing samples, since the ligand is bound to the metal ion. Nevertheless, to minimize the effect of this side reaction, the samples were measured right after their preparation.

During the calculations, the 550–610 nm wavelength region was used and the spectra of $NdCl_3$ (peak maximum at 575 nm) was obtained from calibration measurements. It was found that the absorbance values obey the Beer–Lambert law in the concentration range studied (0.025–0.075 M). The molar absorptivity was found to be 6.70 $dm^3 \cdot mol^{-1} \cdot cm^{-1}$ at 575 nm.

4.4. Polarimetry

The optical rotation of the samples was recorded with an Optech PL1 polarimeter equipped with a sodium lamp and having an accuracy of ± 0.05°. The length of the polarimeter tube was 2 dm. All experiments were performed at room temperature, ((25 ± 2) °C) and at I = 1 M.

The specific rotations of L-Gul^-, γ-L-HGul and D-$Gluc^-$ were determined by calibration at 1 M ionic strength. The thus obtained values are as follows: –13.5°, 57.8° and 13.0°. Previously, the specific rotation of –55.0° was calculated for γ-D-HGul [40]. For D-$Gluc^-$, values of 12.0–15.6° were reported [19,20,35].

To determine the specific rotations of L-HGul and D-HGluc, solution series with constant $[Gul^-]_T$ or $[Gluc^-]_T$ and varying $[HCl]_T$ were measured. Both optical rotation and pH readings were registered simultaneously and right after sample preparation. Additionally, a sample with $[Gul^-]_T$ = 0.42 M and $[HCl]_T$ = 0.46 M was used to follow the lactonization kinetics of HGul.

Experiments for the Ca^{2+}-containing systems were performed applying different ligand to metal ratios. For gulonate, additional measurements were carried out at $[Gul^-]_T/[Ca^{2+}]_T = 2$ and at varying $[OH^-]_T$.

4.5. NMR spectroscopy

The ^{1}H and ^{13}C NMR spectra were recorded on a Bruker Avance DRX 500 MHz NMR spectrometer equipped with a 5 mm inverse broadband probe head furnished with z oriented magnetic field gradient capability. The magnetic field was stabilized by locking it to the ^{2}D signal of the solvent before the measurements. For the individual samples, 128 or 256–8192 interferograms were collected to record the ^{1}H NMR or ^{13}C NMR spectra. Spectra acquisitions were carried out at (25 ± 1) °C in most cases. The temperature dependence of the spectra of gulonate was studied in the range of 5–55 °C.

For parallel pH and NMR measurements, the samples were placed into PTFE liners, and these sample holders were taken into external quartz tubes containing D_2O. D_2O is known to affect the activity coefficient of H^+ [133]. In this set-up, however, D_2O was outside the sample, therefore the correction of the obtained pH values was not necessary. The pH-dependent spectra of Gul^- were recorded 4 days after sample preparation.

For HGluc, the lactone formation was found to be reversible [19–21,35,36,53,56]. In order to check the reversibility of the overall process for HGul, 0.42 M NaGul was acidified with 0.63 M HCl, and the equilibrium solution was re-neutralized with 0.63 M NaOH (see the NMR spectra in Figures 12a-b). As a result, no irreversible side reactions were observed to take place in the system containing Gul^-.

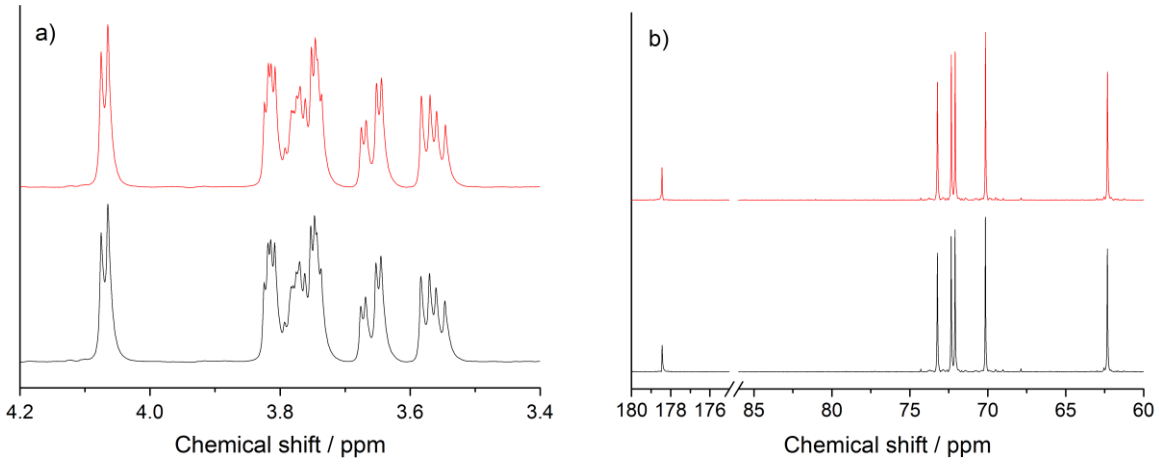

Figure 12 ^{1}H NMR (part a) and ^{13}C NMR (part b) spectra of L-gulonate (Gul^-). Experimental conditions: T = (25 ± 1) °C, 20% V/V D_2O; $[Gul^-]_T$ = 0.34 M. The spectra of freshly prepared (black) as well as acidified/re-neutralized (red) Gul^- are displayed.

Both kinetic and equilibrium studies concerning the lactonization of HGul and HGluc were performed in the presence of excess HCl. The completion of the reaction was checked periodically by polarimetry. Having reached the equilibrium, 20% V/V D_2O was added to all samples prior to spectra acquisition resulting in dilution of 0.8 ratio and I = 0.8 M; for the other systems I was set to 1 M.

4.6. Molecular modeling

Geometry optimizations were carried out *via* the Gaussian 09 (for γ-HGul, δ-HGul and $CaGul^+$) [134] and the ORCA (v. 3.0.3, for $NdGlucH_{-2}^0$) [135] software packages, respectively.

For γ-HGul and δ-HGul, the M11 range-separated hybrid meta-GGA DFT (Density Functional Theory) functional [136] was applied coupled with the def2–TZVP [137] basis set. To find the respective conformers, optimizations were augmented with conformational analysis, that is, the dihedral angle was systematically changed by 60° along the freely-rotating C-C bonds.

To reveal the optimum structure for the $CaGul^+$ species, the calculations were performed at B3LYP/6–311++g(d,p) [138,139] level, which was used several times in computations relating to carbohydrates, such as α-D- and β-D-glucopyranoses [140]. For the $NdGlucH_{-2}^0$ complex, the computations were carried out by using the PBE0 [141,142] hybrid functional coupled with the Stuttgart/Dresden (SD) Effective Core Pseudopotential (ECP) [SD(60,MWB)] for Nd [143] and the def2-SVP basis set [144] for the lighter atoms as implemented in ORCA.

In each case, the solvent effect was taken into account by embedding the gas-phase structures into the framework of implicit water molecules. These calculations were carried out by applying the Integral Equation Formalism or the Conductor-like variants of the Polarizable Continuum Model (IEFPCM, for $CaGul^+$ and CPCM, for the lactones) as well as the Conductor-like Screening Model (COSMO, for $NdGlucH_{-2}^0$) [145] using the default set of radii from the Universal Force Field (UFF) [146]. Furthermore, explicit water molecules were introduced into the complex structures to model the first coordination sphere of the metal ions.

The stability of each structure was checked with frequency calculations.

4.7. Data evaluation

The time-dependence of the optical rotations in the gulonate-containing system was processed with the aid of the ChemMech program [147]. The protonation constants of gulonate and gluconate were calculated by the PSEQUAD [148] (potentiometric titrations) or the Origin [149] software (polarimetric and NMR measurements). The lactonization constants were obtained from NMR peak areas determined by the MestreC program [150]. For the metal ion-containing systems, the stability products, molar absorbance spectra, chemical shifts or specific rotations were computed using the PSEQUAD software.

The general expression for the complexation reactions between the M^{z+} and A^{w-} ions:

$$pM^{z+} + qA^{w-} + rH_2O = M_pA_qH_{-r}^{(zp-wq-r)+} + rH_3O^+ \tag{21}$$

$$\beta_{pq-r} = \frac{[M_pA_qH_{-r}^{(zp-wq-r)+}][H_3O^+]^r}{[M^{z+}]^p[A^{w-}]^q c^{1+r-p-q}} \tag{22}$$

For the sake of internal consistency, the A^{w-} ligand will be written on the left side in the equations in this work. In the case of the Ca^{2+}/$Gluc^-$ system, for instance, β_{011}, β_{01-1}, β_{110} and β_{11-1} represent the stability products of the HGluc, $GlucH_{-1}$, $CaGluc^+$ and the $CaGlucH_{-1}^0$ species, respectively. The above-mentioned programs determine the standard error (*SE*) of the equilibrium constant or other quantities. To broaden the confidence interval of these data, the ± 3 *SE* will be given in the appropriate sections.[6]

The average difference between the experimental and calculated data is described with the fitting parameter (*FP*):

$$FP = \sqrt{\frac{\sum_{i=1}^{n}\left(Y_{i,calc} - Y_{i,meas}\right)^2}{n-k}} \tag{23}$$

where $Y_{i,calc}$ and $Y_{i,meas}$ are the i^{th} calculated and measured data, n is the number of the measurements, while k means the number of the fitted parameters. (The $n–k$ expression is equal to the degree of freedom.) The computation of *FP* is the same for all programs used in this study, and it will be provided in the respective sections.

[6] For instance, the exact meaning of $\log \beta_{11} = 1.00(3)$ is 1.00 ± 0.03, where 0.01 is the *SE*. Analogously, $[\alpha] = 1.0(3)°$ represents $(1.0 \pm 0.3)°$ and the *SE* is 0.1°.

5. Results and discussion

5.1. The lactonization reactions of L-gulonic and D-gluconic acids

5.1.1. Assignment of the ^{1}H and ^{13}C NMR peaks

The NMR peaks of gluconate were identified previously [36,37]. The ^{1}H peaks of gulonate were assigned by calculating the vicinal or geminal coupling constants ($|^{3}J_{H,H}|$ or $|^{2}J_{H,H}|$, presented in Table 3), both in neutral and alkaline media. Performing measurements at high pH was chosen because more resolved spectra with smaller line widths were obtained for gluconate [37] and heptagluconate [41], respectively. The present $|J_{H,H}|$ values (corresponding to pH ≈ 7) were compared to those measured in D_2O earlier [151]. The largest difference was found to be ≤ 0.2 Hz except for $^{3}J_{H4,H5}$ (3.6 Hz). Hence, a replicate experiment was done to decide whether our data were reproducible or not. The second spectrum yielded the same coupling constants (with the maximum deviation being 0.1 Hz), thus, we accepted our $^{3}J_{H4,H5}$ value. It is worth mentioning that the coupling constants were slightly sensitive to the presence of NaOH, which is probably associated with the partial deprotonation of the anion.

Table 3 Absolute values of $J_{H,H}$ coupling constants (in Hz, at T = 25 °C) of Na-L-gulonate in different media.

Medium/pH$_{exp}$	$J_{H2,H3}$	$J_{H3,H4}$	$J_{H4,H5}$	$J_{H5,H6}$	$J_{H5,H6'}$	$J_{H6,H6'}$	Reference
0.5 M NaOH	5.1	2.8	4.7	4.1	6.3	11.7	p. w.[a]
H_2O/6.34	5.3	3.0	4.9	3.7	6.7	11.7	p. w.
0.2 M HCl/2.02	6.1	3.8	4.5	4.0	6.7	11.7	p. w.
D_2O/7.5	5.1	3.1	1.3	3.9	6.5	11.8	151[b]
D_2O/3.0	5.9	3.5	1.3	3.9	6.5	11.8	151

[a] Present work; the measurements correspond to 0.2 M NaGul (H_2O and HCl) or 0.15 M NaGul (NaOH).
[b] In ref. [151], the measurements correspond to 0.10 M NaGul.

Concerning the ^{13}C spectrum, peaks were identified on the basis of the ^{1}H–^{13}C Heteronuclear Single Quantum Coherence (HSQC) measurement (Figure 13). The order of the carbon peaks as a function of decreasing chemical shift (C1, C2, C5, C3, C4, C6) matches with that was reported previously [151].

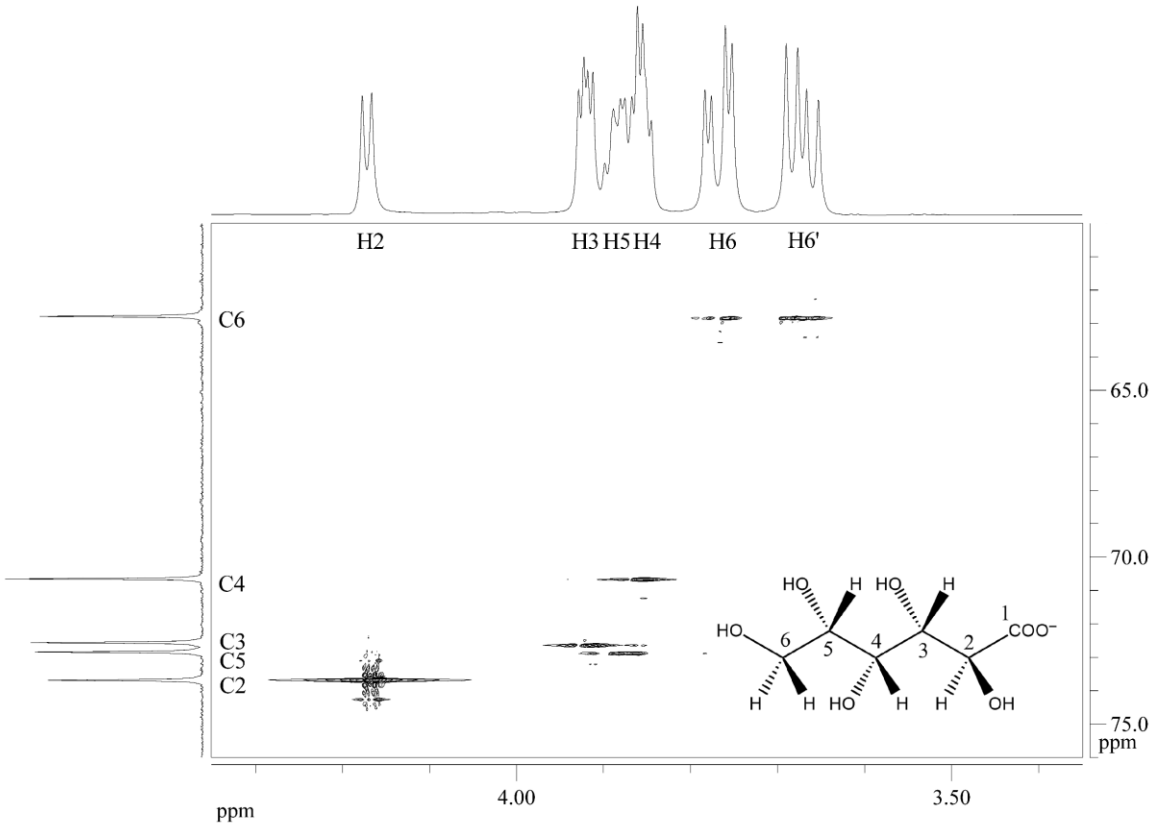

Figure 13 ^{1}H–^{13}C HSQC spectrum of L-gulonate (Gul^{-}). Experimental conditions: T = (25 ± 1) °C, 20% V/V D_2O; $[NaGul^{-}]_T$ = 0.50 M. The structural formula of Gul^{-} and the peak assignments are indicated (C1 centered at about 178.9 ppm is not shown).

Upon decreasing pH, marked spectral changes were detected in the solutions of Gul^{-} and $Gluc^{-}$, respectively. The appearance of new peaks is the consequence of lactone formation. Even though the ^{1}H spectra of the acid-lactone systems are not well-resolved, their position is known not to vary with pH, thus, the lactone signals can readily be distinguished from those of the aldonic acid/aldonate. This spectral property of the lactones must hold for the ^{13}C NMR peaks as well. Indeed, at least ten new peaks were found for both Gul^{-}- and $Gluc^{-}$-containing samples attesting the formation of the two different lactones. (The signals belonging to the ester carbon could not be observed in some cases due to their very low intensities.) Two exemplary spectra of Gul^{-} (pH_{exp} = 6.34 and 2.02) are shown in Figures 14a-b. Concerning $Gluc^{-}$, the shape of the ^{13}C NMR spectra obtained in acidic medium is identical to that presented in ref. [36].

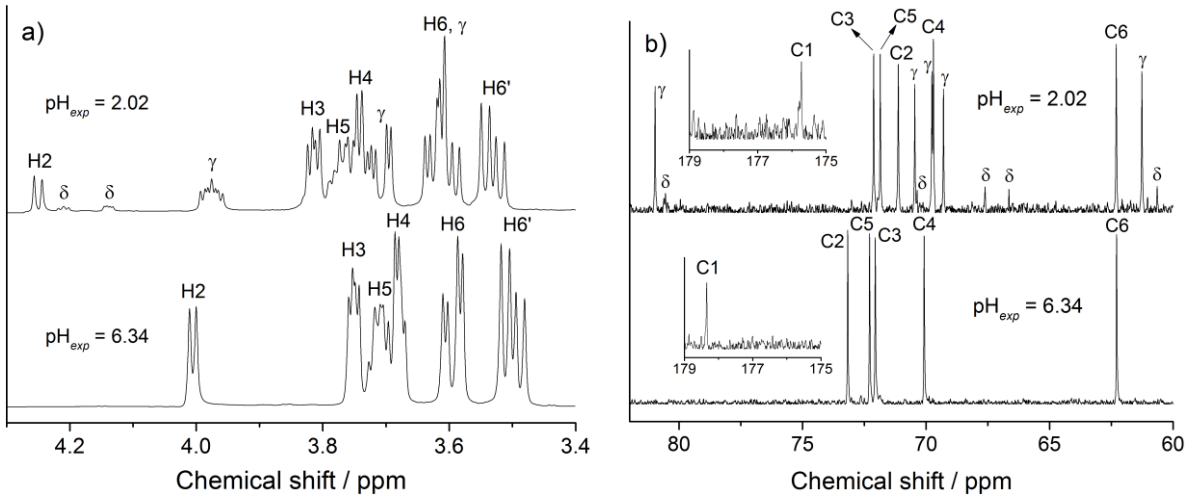

Figure 14 ^{1}H NMR (part a) and ^{13}C NMR (part b) traces of a close-to-neutral/acidic (lower/upper spectrum) of L-gulonate (Gul^{-}). Inset of part b: region of carboxylate and carbonyl resonances. Experimental conditions: T = (25 ± 1) °C; $[Gul^{-}]_T$ = 0.20 M and $[HCl]_T$ = 0.20 M. Spectra were recorded and pH$_{exp}$ was measured after 4 days of preparation. The peak assignments (H2–H6' or C1–C6) refer to Gul^{-} and HGul, respectively.

Furthermore, the ^{1}H as well as the ^{13}C spectra were recorded for γ-HGul and δ-HGluc (in 100 and in 20% V/V D_2O, too). Hence, it was possible to decide which peaks belong to which isomer. It is worth mentioning that contrary to γ-HGul, large portion of δ-HGluc underwent hydrolysis several hours after its dissolution.

5.1.2. Protonation constants of gulonate and gluconate *via* various experimental methods

The pH potentiometric titrations for the Gul^{-}- and Gluc^{-}-containing solutions using glass electrode were performed at 1 M ionic strength and in the concentration range of 0.1–0.3 M (Figures 15a-b). The four sets of experimental data were fitted simultaneously, and the ionic product of water, pK_w, was taken as 13.76 [132]. The fitting parameter (*FP*) was found to be 0.7 mV (Gul^{-}) and 1.1 mV (Gluc^{-}), and it is in the range of the usual error of the pH electrodes. The calculated values of log K_p for the two ligands are very similar (Table 4), which is justified by the structural similarity.

According to the empirical reaction rate equation, one would expect higher reaction rate for lactonization with increasing aldonate concentration. To decide whether this reaction proceeded in these systems or not, the curves were fitted individually as well. If the lactonization goes to completion, the apparent protonation constant ($K_{p,ap}$) of the anion can be expressed as:

$$K_{p,ap} = \frac{([\mathrm{HA}]+[\gamma\text{-}\mathrm{HA}]+[\delta\text{-}\mathrm{HA}])\cdot c}{[\mathrm{H_3O^+}][\mathrm{A^-}]} = K_p\left(1+K_{L,\gamma}+K_{L,\delta}\right) \qquad (24)$$

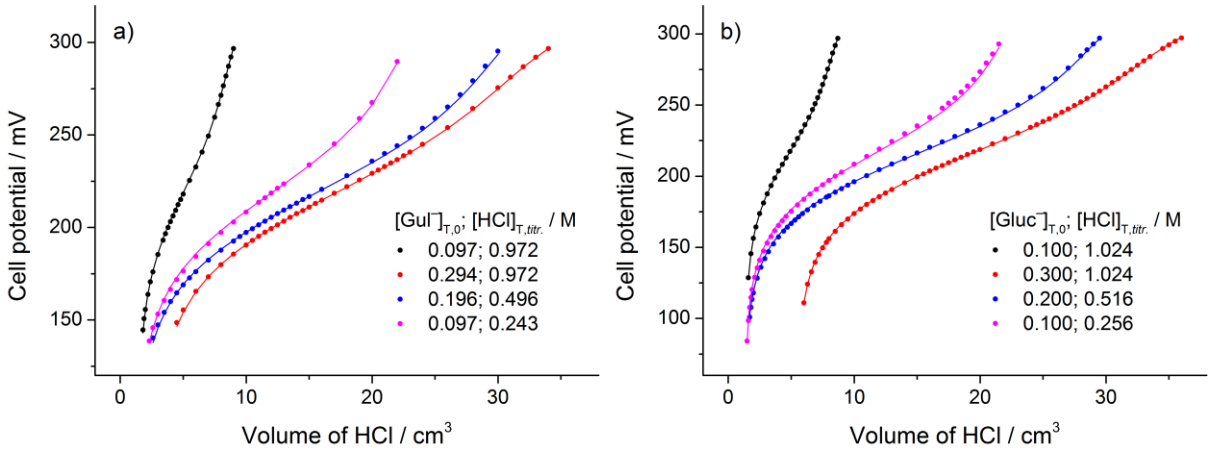

Figure 15 The pH-potentiometric titration curves of L-gulonate (Gul^-, part a) and D-gluconate ($Gluc^-$, part b). Experimental conditions: T = (25.0 ± 0.1) °C, I = 1 M (NaCl), V_0 = 70 cm^3. The initial concentrations of the anion as well as the titrant HCl are indicated in the legend. The titrations started in the alkaline region with $[OH^-]_{T,0}$ = 0.01–0.02 M. Symbols and solid lines refer to the measured and calculated data, respectively.

Table 4 Protonation constants (log K_p) for L-gulonate (Gul^-) and D-gluconate ($Gluc^-$).[a] Data correspond to T = 25 °C; ± 3 *SE* is given in parentheses.

Reaction	Ionic strength and backgr. electrolyte	log K_p	Reference	Method[b]
$Gul^- + H_3O^+ = HGul + H_2O$	$I \rightarrow 0$	3.67	40	POL/POT
	0.1 M $NaClO_4$	3.48(6)	30	POT
	1 M NaCl	3.325(4)[c]	p. w.[d]	POT
	1 M NaCl	3.33(3)[e]	p. w.	POT
	1 M NaCl	3.14(9)	p. w.	POL/POT
	1 M NaCl	3.21(3)	p. w.	^{1}H NMR/POT
	1 M NaCl	3.19(1)	p. w.	^{13}C NMR/POT
$Gluc^- + H_3O^+ = HGluc + H_2O$	1 M NaCl	3.371(5)	p. w.	POT
	1 M NaCl	3.37(3)	p. w.	POT
	1 M NaCl	3.26(6)	p. w.	POL/POT
	1 M NaCl	3.23(3)	37	^{1}H NMR/POT
	1 M NaCl	3.24(3)	37	^{13}C NMR/POT
	1 M $NaClO_4$	3.63(1)	21	POT
	1 M $NaClO_4$	3.48(18)	25	POT
	1 M $NaClO_4$	3.30(10)	33	POT

[a] Data for $Gluc^-$ are restricted to I = 1 M; further data are presented in Table 1 on p. 7.
[b] POL = polarimetry, POT = potentiometry applying glass electrode, NMR = nuclear magnetic resonance spectroscopy.
[c] Protonation constant calculated *via* simultaneous curve fitting.
[d] Present work.
[e] Suggested value for the protonation constant obtained from individual curve fitting.

It follows from eq. 24 that $K_{p,ap} \geq K_p$ and only $K_{p,ap}$ can be determined by potentiometry, since this method is not able to distinguish whether the pH change is caused by protonation or lactonization. The apparent constant would also be higher if the lactonization processes took

place only partially; in this case K_L is to be replaced by the reaction quotient, Q_L. Each curve, however, provided the same log K_p values within 0.01 unit of uncertainty. This concentration-independence corroborates that $K_{p,ap} = K_p$, thus, our constants truly represent the protonation processes.

Polarimetric measurements were also carried out with samples containing $[Gul^-]_T = 0.3$ M and $[Gluc^-]_T = 0.4$ M; the results are presented in Figures 16a-b. Upon increasing $[HCl]_T$, the optical rotation of Gul^- markedly increases, whilst remarkable decrease can be observed for $Gluc^-$. This opposite direction can be explained on the basis of different relative configurations. It is worth mentioning that the reverse change was detected from $[HCl]_T/[Gul^-]_T = 1.13$ and $[HCl]_T/[Gluc^-]_T = 1.02$ implying that the lactonization proceeded to a considerable extent.

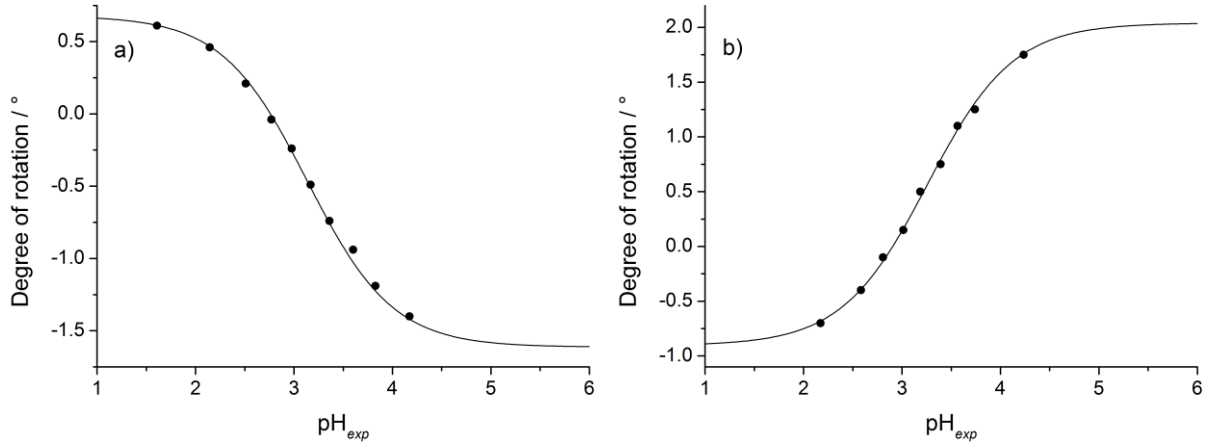

Figure 16 Optical rotation of L-gulonate (Gul^-, part a) and D-gluconate ($Gluc^-$, part b) as a function of pH_{exp}. Experimental conditions: $T = (25 \pm 2)$ °C, $I = 1$ M (NaCl); a) $[Gul^-]_T = 0.306$ M, $[HCl]_T = 0.031$–0.311 M, b) $[Gluc^-]_T = 0.403$ M, $[HCl]_T = 0.041$–0.369 M. Symbols and solid lines refer to the measured and calculated data, respectively.

Nevertheless, the observed optical rotation was found to be sensitive to pH_{exp} allowing to calculate the protonation constants. The observed rotation (α) depends on the concentrations of A^- and HA through eq. 25:

$$\alpha = \alpha_{A^-}[A^-] + \alpha_{HA}[HA] \tag{25}$$

where $[A^-]$ and [HA] are the corresponding free concentrations (in mol·dm^{-3}), while α_{HA} and α_{A^-} denote the products of the molar rotation and the optical path length (in °·dm^3·mol^{-1}).

Using the definition of K_p (eq. 2) and the mass balance equation for A^-:

$$[A^-]_T = [A^-] + [HA] \tag{26}$$

the rotation can be expressed as:

$$\alpha = [\mathrm{A}^-]_\mathrm{T} \frac{K_p 10^{-\mathrm{pH}_{exp}} \alpha_\mathrm{HA} + \alpha_{\mathrm{A}^-}}{1 + K_p 10^{-\mathrm{pH}_{exp}}} \tag{27}$$

where $[A^-]_T$ is the total concentration of the anion. During calculations, α_{HA} was held constant at the value determined from calibrations. As a result, *FP* was found to be 0.03° (for Gul^-) and 0.04° (for $Gluc^-$).

The protonation constants obtained are shown in Table 4. The difference between the constants of the two anions (0.12) might be explained by the broader pH range available for Gul^-. Both protonation constants; however, deviate from the values obtained by titrations (Table 4). Therefore, it seems plausible that the Irving factor (eq. 20) is not zero, which follows from the different calibration procedures.

The main aim of these measurements, however, was to deduce the specific rotations of HGul and HGluc, which are affected by the available experimental range rather than the actual value of K_p. The calculated rotations were converted to traditional units yielding $[\alpha_{HGul}] = 5.7(8)°$ and $[\alpha_{HGluc}] = –5.7(8)°$. Similarly to the conjugate bases, the absolute specific rotations for the two acids are identical. On the other hand, $[\alpha_{HGul}]$ and $[\alpha_{HGluc}]$ as well as $[\alpha_{Gul^-}]$ and $[\alpha_{Gluc^-}]$ have opposite signs, as a consequence of the different configuration of the two anions.

The specific rotation of HGluc at T = 20–25 °C was reported to be between –6.9° and 5.80° [19,20,35,56,152,153] pointing to the uncertainty of the experimental data. Nevertheless, –6.7° [152] and –6.9° [153] were determined from freshly prepared HGluc, which is close to our value and to those reported previously [19,56]. Based on this agreement, the specific rotation found for HGul seems to be reliable.

The protonation constant of gulonate was determined *via* ^1H and ^{13}C NMR spectroscopies, too. Similarly to the observations made for $Gluc^-$ [36,37], all the ^1H peaks of Gul^- shift downfield with decreasing pH and the extent of the displacement decreases with the distance from the protonation site. The vicinal coupling constants at pH = 2.02 are listed in Table 3. The most pronounced changes relative to those obtained in neutral medium are seen for $|^3J_{2,3}|$ and $|^3J_{3,4}|$ (0.8 Hz increase). This reflects the changes of the H2C2C3H3 and H3C3C4H4 dihedral angles by the Karplus equation [154]. The alteration of hydrogen bonds (may be formed between the COO^- and the C2-OH/C3-OH groups) upon protonation can account for these variations.

As the pH decreases, the ^{13}C peaks of C1, C2, C4 and C5 move upfield in contrast with the ^{1}H signals (the position of C3 and C6 remains practically unchanged). Of these displacements, the variations of C1 and C2 are the largest reflecting the vicinity of the protonation site. It is worth mentioning that the extent of change (C1 > C2 >> C4 ≈ C5) does not show complete correlation with the proximity to the carboxylic group. This implies that the shielding factor is sensitive not only to the protonation but to the simultaneous conformational changes as well.

Since the exchange of H^+ between Gul^- and HGul is fast on the NMR timescale, the chemical shift is proportional to the molar fraction of these forms:

$$\delta = \delta_{\mathrm{Gul}^-} \frac{[\mathrm{Gul}^-]}{[\mathrm{Gul}^-]+[\mathrm{HA}]} + \delta_{\mathrm{HGul}} \frac{[\mathrm{HGul}]}{[\mathrm{Gul}^-]+[\mathrm{HGul}]} \tag{28}$$

where δ_{Gul^-} and δ_{HA} (in ppm) denote the limiting chemical shifts of Gul^- and HGul, respectively. Contrary to polarimetric measurements, eq. 26 is not valid here since the concentrations of the lactones must be included in the mass balance equation. (Prompt and simultaneous NMR and pH measurements could not be undertaken in this case.) However, expressing [HGul] by eq. 2 results in the following relationship:

$$\delta = \frac{\delta_{\mathrm{HA}} K_p 10^{-\mathrm{pH}_{exp}} + \delta_{\mathrm{A}^-}}{1 + K_p 10^{-\mathrm{pH}_{exp}}} \tag{29}$$

The protonation constant was obtained from the fitted curves, while the ^{1}H and ^{13}C chemical shifts of Gul^- were fixed during calculations. The *FP* was found to be $2.2 \cdot 10^{-3}$ ppm (^{1}H) and $9.4 \cdot 10^{-3}$ ppm (^{13}C); the fitted curves are plotted in Figures 17a-b while the calculated chemical shifts of HGul are presented in Table 5. It is seen that the log K_p agrees reasonably well with the polarimetrically obtained constant (Table 4), and also deviates to some extent from that determined v*ia* titrations. Additionally, there is a close agreement between the protonation constants for Gul^- (present work) and $Gluc^-$ (ref. [37]).

For the pH-potentiometric measurements, the electrode was calibrated at the same ionic strength as that of the titrations. Hence, the measured pH_c is equal to $-\log([H^+]/c)$. When the electrode is calibrated against dilute buffers, the pH_{exp} obtained differs from pH_c by the Irving factor (eq. 20). Applying the mass balance equations for $[A^-]_T$ and $[H^+]_T$ as well as eqs. 1 and 20, it can be deduced that above pH ≈ 2:

$$A \approx \log K_{p,c} - \log K_{p,exp} \tag{30}$$

where log $K_{p,c}$ or log $K_{p,exp}$ were calculated from the appropriate values of pH_c or pH_{exp}. That is, the estimated values of A are 0.19 (POL) and 0.13 (NMR) for Gul^- as well as 0.11 (POL) and 0.13 (NMR) for $Gluc^-$. Although, these deviations are not so large considering the various experimental method used, the log K_p determined *via* potentiometry can be proposed as the most realistic conditional constant.

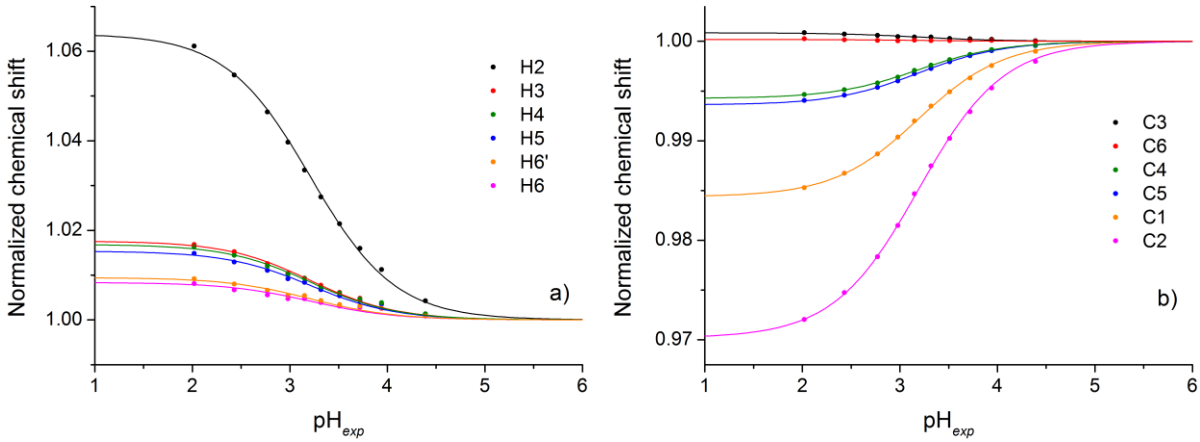

Figure 17 ^1H (part a) and ^{13}C (part b) chemical shifts of L-gulonate (Gul^-) as a function of pH_{exp}. Experimental conditions: T = (25 ± 1) °C, I = 1 M (NaCl); $[Gul^-]_T$ = 0.200 M, $[HCl]_T$ = 0–0.200 M. Symbols and solid lines refer to the measured and calculated data, respectively. The data were normalized to those of Gul^- at $pH_{exp} \approx 7$.

Table 5 ^1H and ^{13}C chemical shifts of HGul and their relative difference to those of L-gulonate (Gul^-). Experimental conditions: T = (25 ± 1) °C and I = 1 M (NaCl). The shifts of Gul^- were observed experimentally while those of HGul were calculated. Additionally, ± 3 *SE* is given in parentheses.

Nucleus	δ_{HGul} / ppm	$\delta_{HGul} - \delta_{Gul^-}$ / ppm	Nucleus	δ_{HGul} / ppm	$\delta_{HGul} - \delta_{Gul^-}$ / ppm
H2	4.262(6)	0.256	C1	175.56(2)	–2.79
H3	3.817(3)	0.066	C2	70.99(2)	–2.18
H4	3.740(3)	0.062	C3	72.12(2)	0.06
H5	3.769(3)	0.057	C4	69.68(2)	–0.40
H6	3.624(3)	0.030	C5	71.83(2)	–0.46
H6’	3.532(3)	0.033	C6	62.30(2)	0.01

5.1.3. Lactonization equilibria of L-gulonic and D-gluconic acids

Applying excess HCl, remarkable conversion of HGul and HGluc to their lactones was observed both in the ^{13}C and the ^1H NMR spectra (Figures 18a-b). The ^1H spectra, however, were not well-resolved preventing their use from further quantitative analysis.

It is clearly shown in Figure 18 that of the four lactones, γ-HGul is formed in the largest amount while the concentrations of the gluconolactones can be regarded as nearly equal. The extreme stability of γ-HGul over δ-HGul reflects the qualitative rule that an *exo* double bond

stabilizes the five-membered and destabilizes the six-membered rings [57]. Conversely, this relation is not applicable for the lactones of HGluc for which other factors may have important role as well.

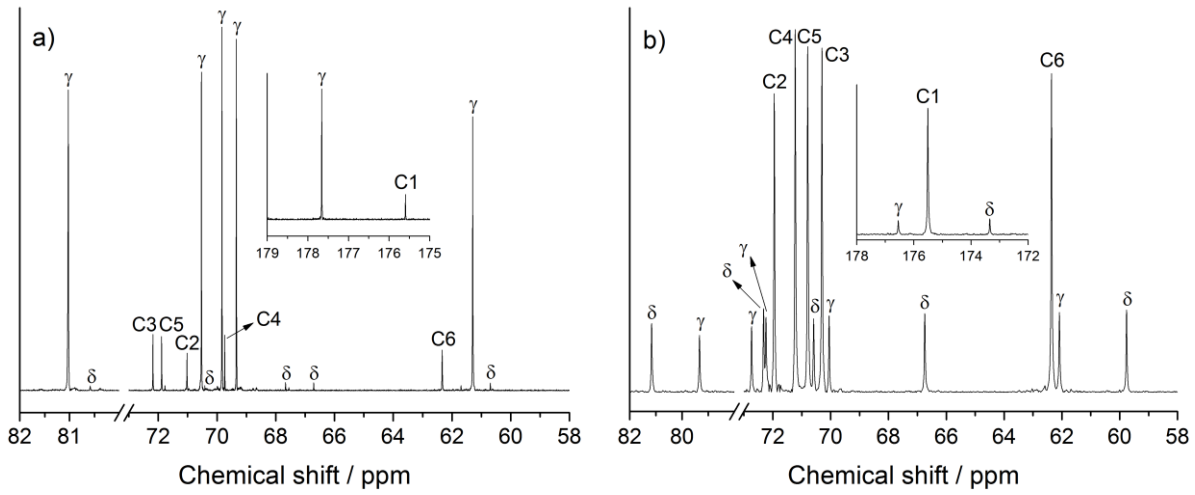

Figure 18 ^{13}C NMR spectrum of L-gulonic (HGul, part a) and D-gluconic (HGluc, part b) acids and their γ- and δ-lactones (γ-HGul, δ-HGul, γ-HGluc, δ-HGluc). Inset: region of carboxylate and carbonyl resonances. Experimental conditions: T = (25 ± 1) °C, I = 0.8 M (NaCl), 20% V/V D_2O; a) $[Gul^-]_T$ = 0.336 M, $[HCl]_T$ = 0.368 M, b) $[Gul^-]_T$ = 0.320 M, $[HCl]_T$ = 0.369 M. The peaks of aldonic acids are labeled as C1–C6.

Though the actual structure of the acids and their lactones are rather different, the number of the O and H nuclei attached to the same carbon atom remains unaltered leading to similar relaxation times and hence, similar peak areas. Consequently, the sum of the integrals of C1–C6 may be applied for estimating the ratio of the actual concentrations within a certain spectrum. In addition to the well-separated peaks of the ^{13}C nuclei, 1) the position of the lactone signals is independent of the pH, 2) the concentration of the free anion is negligible in excess of HCl, and 3) this method does not require the exact value of pH (contrary to the determination of K_p). Moreover, this procedure was successfully employed to determine the K_L of xylonic acid [155].

Based on these assumptions, $K_{L\gamma}$ and $K_{L,\delta}$ can be estimated by eqs. (31) and (32):

$$\frac{A_{\gamma\text{-HA}}}{A_{\text{HA}}} \approx \frac{[\gamma\text{-HA}]}{[\text{HA}]} = K_{L,\gamma} \tag{31}$$

$$\frac{A_{\delta\text{-HA}}}{A_{\text{HA}}} \approx \frac{[\delta\text{-HA}]}{[\text{HA}]} = K_{L,\delta} \tag{32}$$

where *A* belongs to the respective total integrated areas of nuclei C1–C6 for the anion and the lactones. It is seen in Figure 18a that δ-HGul is formed to a very low extent. Thus, a reliable estimate for its concentration required long spectral acquisition (8192 scans), which was then applied for $Gluc^-$ as well. It is noteworthy that the C1 (carbonyl) peak of δ-HGul did not appear even after such long accumulation time due to its long relaxation time.

The lactonization constants calculated this way are presented in Table 6 and the corresponding speciation diagrams are depicted in Figures 19a-b. (The protonation constants obtained from potentiometry were used for these speciation calculations.) The log $K_{L,\gamma}$ of HGul is in fair agreement with the one calculated from the rate coefficients given in ref. [40]. On the other hand, the present value of log $K_{L,\delta}$ is lower by ≈ 0.4 units. Both literature data, however, are based on estimated initial reaction rates.

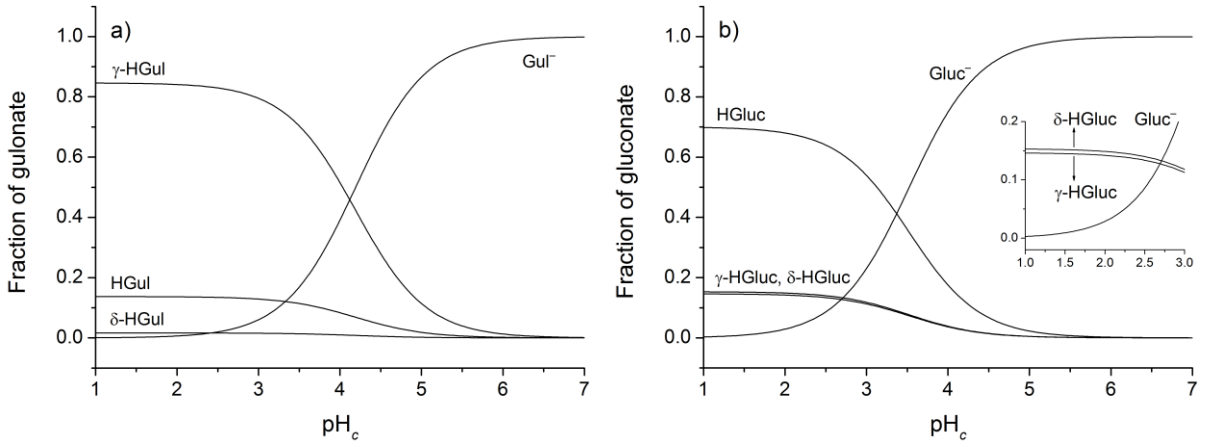

Figure 19 Speciation diagram of the gulonate- (Gul^-, part a) and gluconate-related ($Gluc^-$, part b) species as a function of pH_c. Inset of part b: pH_c region of 1–3. The calculations correspond to T = 25 °C, I = 0.8–1.0 M and $[Gul^-]_T$ or $[Gluc^-]_T$ = 0.300 M.

For $K_{L,\delta}$ of HGluc (at $I > 0$), the deviation of our values from literature data is not higher than 0.2 logarithmic unit (except for those reported in ref. [21]). Although our constants might be affected by the presence of 20% V/V D_2O, and the different ionic strength (0.8 M), the difference is lower than the scattering range of the reported values. Thus, the lactonization constants of HGluc given here are reliable at least at the semi-quantitative level which validates the constants of HGul, too.

Two important conclusions can be drawn from these calculations. First, HGul tends to form lactones more readily than HGluc. Second, the surprisingly high γ-lactonization constant of

HGul implies that this species should be considered when complexation equilibria between metal ions and Gul^- are studied in the acidic pH range. This is even more important when the metal ion is inert preventing the use of fast potentiometric titrations.

Table 6 Lactonization constants (log K_L) for L-gulonic (HGul) and D-gluconic (HGluc) acids. Data correspond to T = 25 °C unless indicated differently; ± 3 *SE* is given in parentheses.

Reaction	Ionic strength and backgr. electrolyte	log K_L	Reference	Method[a]
HGul = γ-HGul + H_2O	0.8 M NaCl	0.79(3)	p. w.[b]	^{13}C NMR
	1 M NaCl	0.73(3)	p. w.	POL
	not indicated	0.60[c]	40	POL
HGul = δ-HGul + H_2O	0.8 M NaCl	–0.91(6)	p. w.	NMR
	not indicated	–0.49[c]	40	POL
HGluc = γ-HGluc + H_2O	0.8 M NaCl	–0.68(3)	p. w.	^{13}C NMR
	not indicated	–0.59(6)	19	POL/POT
	not indicated	–0.62	58	GC
HGluc = δ-HGluc + H_2O	$I \rightarrow 0$	–0.95	20	POL/POT
	$I \rightarrow 0$	–0.81(9)	21	POT
	≈ 0.004 M[d]	–0.89	35	POL/POT
	0.1 M $NaClO_4$	–0.91(6)	21	POT
	0.1 M $NaClO_4$	–0.54(12)	36[e]	^{13}C NMR/POT
	0.5 M $NaClO_4$	–0.93(10)	21	POT
	0.8 M NaCl	–0.65(1)	p. w.	^{13}C NMR
	1 M $NaClO_4$	–1.15(6)	21	POT
	not indicated	–0.73(3)	19	POL/POT
	not indicated	–0.66	56[e]	HPLC/POL
	not indicated	–0.67	58	GC

[a] NMR = nuclear magnetic resonance spectroscopy, POT = potentiometry applying glass electrode, POL = polarimetry, HPLC = high-performance liquid chromatography using refractive index detector, GC = gas chromatography using flame ionization detector.
[b] Present work.
[c] Calculated from the rate coefficients determined at pH ≈ 2 in ref. 40.
[d] Corresponds to pH = 2.36 reported by the authors; no additional background electrolyte was used.
[e] The measurements were performed at 22 °C (ref. [36]) and 20 °C (ref. [56]), respectively.

5.1.4. Lactonization kinetics of L-gulonic acid

The applicability of ^{13}C NMR spectroscopy to characterize the lactonization reaction was utilized to find which lactone was formed faster. In a solution containing 0.34 M NaGul and 0.37 M HCl, the integrals of the different species were calculated, while the reaction was followed for a sufficiently long time (11 hours). The six peaks of the acid and additional signals appeared 20 minutes after solution preparation. These peaks were at the same position as those of δ-HGul identified in the equilibrium measurements (Figure 18a).

New signals appeared in the spectra after 27 minutes; these peaks were assigned as those of γ-HGul. The peak intensity of the six-membered lactone, however, started to increase much

faster compared to its isomer. Consequently, the formation of δ-HGul is faster in agreement with the observations of Levene and Simms [40].

Similarly to the lactonization constants, the reaction quotient at a given time (Q_L), can be estimated by the relative peak areas:

$$\frac{A_{\gamma\text{-HGul},t}}{A_{\text{HGul},t}} \approx \frac{[\gamma\text{-HGul}]_t}{[\text{HGul}]_t} = Q_{L,\gamma} \tag{33}$$

$$\frac{A_{\delta\text{-HGul},t}}{A_{\text{HGul},t}} \approx \frac{[\delta\text{-HGul}]_t}{[\text{HGul}]_t} = Q_{L,\delta} \tag{34}$$

These reaction quotients are plotted in Figure 20. It is seen that after 4 hours, $Q_{L,\delta}$ reaches a constant value (indicated with dashed line); this limiting value can be regarded as $K_{L,\delta}$. In conclusion, δ-HGul reaches the equilibrium rapidly, even when the reaction is far from the overall equilibrium state. Additionally, the assumption that δ-HGul would be an unstable intermediate can be ruled out.

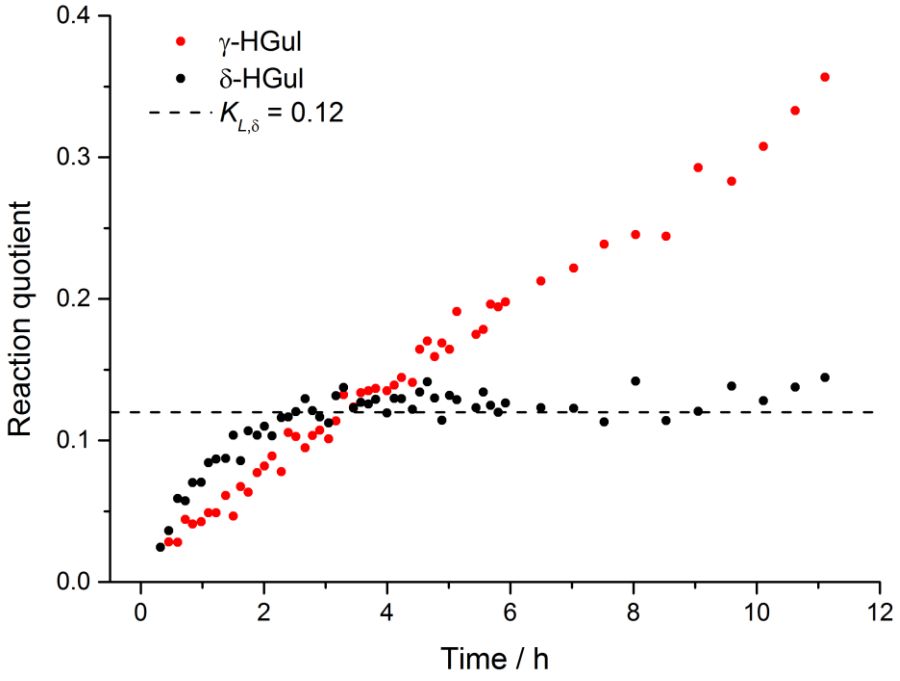

Figure 20 Reaction quotients (Q_L) for L-gulonic acid (HGul) γ- and δ-lactone (γ-HGul and (δ-HGul) as a function of time. Experimental conditions: T = (25 ± 1) °C, I = 0.8 M (NaCl), 20% V/V D_2O; $[Gul^-]_T$ = 0.34 M, $[HCl]_T$ = 0.37 M. $Q_{\gamma,L}$ and $Q_{\gamma,L}$ were defined as the ratio of the total ^{13}C peak area of the lactone and that of HGul. The dashed line represents the δ-lactonization constant, $K_{L,\delta}$, determined from equilibrium measurements.

For HGluc, the calculation of rate constants is based on the observation that the equilibrium between HGluc and δ-HGluc is established long before the formation of γ-HGul [19]. Conversely, the present measurements (Figure 20) provide spectroscopic evidence that this assumption is not applicable for the lactonization of HGul.

Despite the advantage of ^{13}C NMR in identifying the different lactones, accurate rate constants cannot be deduced due to the large uncertainty of the calculated integral ratios. Thus, polarimetry was chosen to study the kinetics of lactonization in detail, similarly to those published in the literature [19,20,35,40,53,56].

The optical rotation was recorded in a solution containing $[Gul^-]_T$ = 0.420 M and $[HCl]_T$ = 0.461 M; the measured points are depicted in Figure 21. The direction of the overall change is the opposite but, expectedly, its shape is the same as that observed by Levene and Simms [40] for the enantiomer D-gulonic acid.

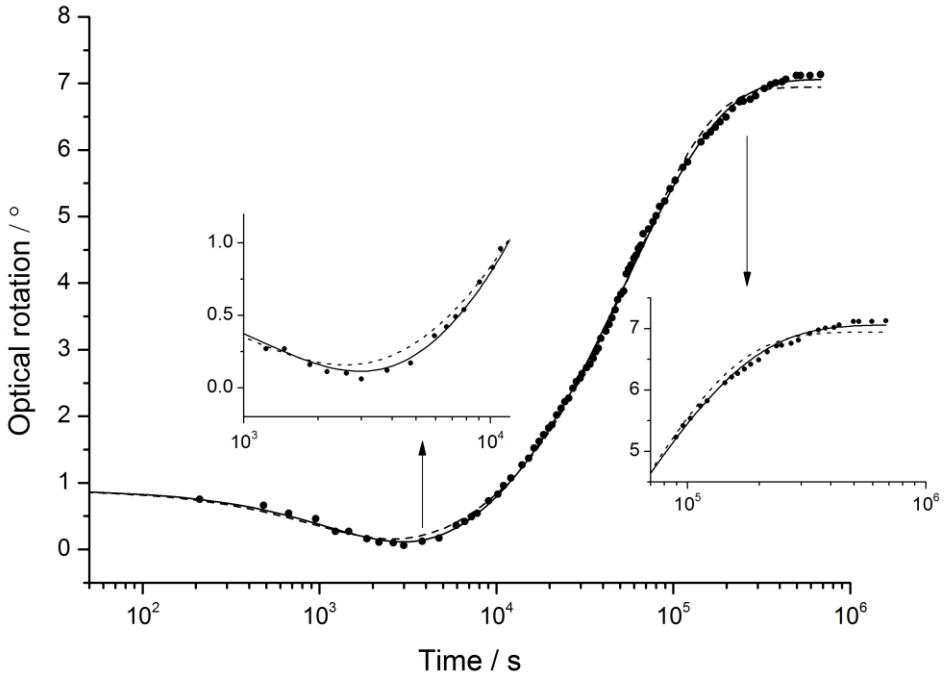

Figure 21 Optical rotations for L-gulonic acid (HGul) as a function of time. Experimental conditions: T = (25 ± 2) °C, I = 1 M (NaCl); $[Gul^-]_T$ = 0.420 M, $[HCl]_T$ = 0.461 M. Full circles represent the measured points. Dashed line: calculated points by assuming reactions 35 and 39 (model 1); solid line: calculated points by assuming reactions 35, 39 and 43 (model 2). Insets: zoomed regions where model 1 shows the largest deviation from the experimental curve.

The initial rotation is positive according to the specific rotation of HGul. The measured values then decrease slightly due to the formation of the δ-lactone. After 20 minutes, the formation

of γ-lactone exhibits a remarkable increase reaching a constant value of 7.1° implying the completion of the reaction.

If the specific rotation of δ-HGul was positive, it would be even smaller than that of the acid, which is very unlikely for a cyclic compound. Hence, $[\alpha_{\delta\text{-HGul}}]$ is a large negative value, contrary to $[\alpha_{\gamma\text{-HGul}}]$. Since the nucleophilic OH group lies on the right (δ) or left (γ) side on the Fischer projection of HGul, δ-HGul is more levorotatory while γ-HGul is more dextrorotatory than the acid. Accordingly, L-gulonic acid obeys Hudson's lactone rule [54], hence, $[\alpha_{\delta\text{-HGul}}] < [\alpha_{\text{HGul}}] < [\alpha_{\gamma\text{-HGul}}]$.

To model the experimental points, the acid-catalyzed lactonization and lactone hydrolysis for the two lactones were taken into account first.

$$\text{HGul} + \text{H}_3\text{O}^+ = \delta\text{-HGul} + \text{H}_3\text{O}^+ + \text{H}_2\text{O} \tag{35}$$

$$r_1 = k_1[\text{H}_3\text{O}^+][\text{HGul}] \tag{36}$$

$$r_{-1} = k_{-1}[\text{H}_3\text{O}^+][\delta\text{-HGul}] \tag{37}$$

$$K_{L,\delta} = \frac{k_1}{k_{-1}} \tag{38}$$

$$\text{HGul} + \text{H}_3\text{O}^+ = \gamma\text{-HGul} + \text{H}_3\text{O}^+ + \text{H}_2\text{O} \tag{39}$$

$$r_2 = k_2[\text{H}_3\text{O}^+][\text{HGul}] \tag{40}$$

$$r_{-2} = k_{-2}[\text{H}_3\text{O}^+][\gamma\text{-HGul}] \tag{41}$$

$$K_{L,\gamma} = \frac{k_2}{k_{-2}} \tag{43}$$

H_3O^+ acts as a catalyst in these reactions (model 1) and its concentration was nearly constant (≈ 0.044 M, *i.e.*, $pH_c \approx 1.35$) throughout the reaction, because of employing excess HCl. During the fitting procedure, the protonation constant (from potentiometry) and the specific rotations (from polarimetry) were kept constant. Regarding the lactonization, the low conversion of δ-lactonization results in strong correlation between $K_{L,\delta}$ and the unknown $[\alpha_{\delta\text{-HGul}}]$, thus, $K_{L,\delta}$ was fixed as well. On the other hand, $K_{L,\gamma}$ was treated as a parameter to be fitted.

The calculated rotations are depicted as dashed line in Figure 21. The optical rotation can be appropriately fitted for the majority of the points, however, significant deviations remain around the minimum (≈ 3000 s) and from 10^5 s. By this model, the *FP* was found to be 0.09°.

Beside H_3O^+, HGul may also serve as a proton source; its decrease would lead to the decrease of the reaction rate when significant amount of γ-HGul was formed at the expense of HGul. The model, therefore, was extended with the following reaction:

$$\mathrm{HGul} + \mathrm{HGul} = \gamma\text{-}\mathrm{HGul} + \mathrm{HGul} + \mathrm{H_2O} \tag{43}$$

$$r_3 = k_3[\mathrm{HGul}]^2 \tag{44}$$

$$r_{-3} = k_{-3}[\mathrm{HGul}][\gamma\text{-}\mathrm{HGul}] \tag{45}$$

$$K_{L,\gamma} = \frac{k_3}{k_{-3}} \tag{46}$$

The model augmented with eqs. 44–46 (model 2) provides satisfactory fitting for the whole duration of the reaction (solid line in Figure 21), since the two ranges of systematic deviations disappear. Accordingly, the *FP* decreased to 0.07°. The log $K_{L,\gamma}$ was found to be 0.73, 0.06 unit lower than the one obtained *via* ^{13}C NMR (log $K_{L,\gamma}$ = 0.79, Table 6). Nevertheless, this difference is acceptable considering the different experimental methods and the overlapping uncertainty intervals of the two constants. Additionally, the specific rotation of δ-HGul was calculazed to be –85(9)°.

The catalytic role of HGul may be unusual, but can be explained by its high concentration (≈ 0.42 M). Similar concentration of HGul, 0.25 M, was applied by Levene and Simms [40], which is in the same order of magnitude, however, they only analyzed the initial reaction rates (preventing direct comparison of the rate coefficients). It is worth mentioning that the effect of self-catalysis can only be observed near the minimum and at the end of the reaction. Hence, full curve fitting is necessary to pinpoint this process, as opposed to the method of initial rates.

Moreover, the self-catalysis of HGul for the lactonization and hydrolysis of δ-HGul was taken into account but the *FP* could not be lowered. Concerning HGluc, the direct interconversion of δ-HGul to γ-HGul (above pH ≈ 4) was proposed earlier [156–158]. (It should be noted here that our ^{1}H and ^{13}C NMR spectra of the partially hydrolyzed δ-HGluc (in D_2O) showed the presence of HGluc but γ-HGluc was absent.) Considering such reaction for the gulonate-containing system did not yield lower *FP*.

The rate coefficients obtained by assuming reactions (35), (39) and (43) are presented in Table 7. It is seen that both the rates of formation and hydrolysis are higher for δ-HGul. The ratio of k_1 and k_2 is = 6.8, while the ratio of k_{-1} and k_{-2} is = 325. Hence, the remarkable difference between $K_{L,\gamma}$ and $K_{L,\delta}$ does not arise from the rate of formation but from the rate of hydrolysis.

Since the k_{-1}/k_{-2} parameter is closely related to the relative stability of the lactone rings, our finding supports quantitatively that an *exo* double bond stabilizes the γ-lactone ring [57].

Table 7 Reaction rate coefficients for the δ- and γ -lactonization (k_1, k_2, k_3) and the reverse hydrolysis reactions (k_{-1}, k_{-2}, k_{-3}) of L-gulonic acid (HGul) at T = (25 ± 2) °C and I = 1 M (NaCl). The coefficients were determined *via* polarimetry; ± 3 *SE* is given in parentheses.

Reaction[a]	Rate coefficient	Reference
HGul + H_3O^+ = δ-HGul + H_3O^+ + H_2O	$k_1 = 1.5(5)\cdot10^{-3}$ $M^{-1}\cdot s^{-1}$	p. w.
	$k_{-1} = 1.3(3)\cdot10^{-2}$ $M^{-1}\cdot s^{-1}$	p. w.
	k_1^* [H_3O^+] = $3.1\cdot10^{-5}$ s^{-1}[c]	40
	k_{-1}^*[H_3O^+] = $9.6\cdot10^{-5}$ s^{-1}[c]	40
HGul + H_3O^+ = γ-HGul + H_3O^+ + H_2O	$k_2 = 2.2(6)\cdot10^{-4}$ $M^{-1}\cdot s^{-1}$	p. w.[b]
	$k_{-2} = 4.0(1.1)\cdot10^{-5}$ $M^{-1}\cdot s^{-1}$	p. w.
	k_2^*[H_3O^+] = $3.8\cdot10^{-6}$ s^{-1}[c]	40
	k_{-2}^*[H_3O^+] = $9.6\cdot10^{-7}$ s^{-1}[c]	40
HGul + HGul = γ-HGul + HGul + H_2O	$k_3 = 2.5(8)\cdot10^{-5}$ $M^{-1}\cdot s^{-1}$	p. w.
	$k_{-3} = 4.7(1.5)\cdot10^{-6}$ $M^{-1}\cdot s^{-1}$	p. w.

[a] Excess H_3O^+ or HGul given in the reaction equation act as a catalyst.
[b] Present work.
[c] Data correspond to T = 25 °C. The pseudo-first order rate coefficients were determined at pH ≈ 2.

Interestingly, the k_2 rate coefficient was found to be 8.6 times larger than k_3 inferring that the initial step of lactonization, which is the protonation of the carbonyl oxygen, proceeds much faster with H_3O^+ (H^+) than with HGul. In general acid catalysis the rate-determining step is the protonation of the COOH group. It follows from the mechanism that the stronger the acid the higher the reaction rate since H^+ can be released easier. HGul is weaker acid than H_3O^+, hence $k_3 < k_2$. (The same relation, $k_{-3} < k_{-2}$ holds for the reverse hydrolysis, too.) In conclusion, HGul is a general acid catalyst. Numerous general acid catalysts (*e.g.*, acetic acid, malonic acid) were studied for the hydrolysis of δ-HGluc in the work of Pocker and Green [20]. Our observations imply that if the aldonic acid in question is used in sufficiently high concentrations it can catalyze its own lactonization and lactone hydrolysis processes, like other acids.

5.1.5. The relative stability of L-gulonic acid γ- and δ-lactones

Previously, the equilibrium conformation of D-gulonic acid γ-lactone was studied by ^1H NMR spectroscopy [159]. Accordingly, γ-D-HGul favors the envelope conformation in equilibrium having the C2-OH group quasi-equatorially oriented. Additionally, the $HOCH_2$-CHOH side chain prefers the arrangement in which the interaction between the C5-OH and C3-OH

groups is absent. Concerning the results of other aldopentono-lactones, the authors proposed that intramolecular hydrogen bonds play role in the stabilization of the preferred structures.

These observations are supported by the optimized structure of the enantiomer γ-L-HGul (Figure 22a). It is worth mentioning that the C=O double bond is partially delocalized through the O-C=O ester group. As a result, the C1-O1A bond length becomes shorter (1.333 Å) than the C4-O1A one (1.461 Å). The envelope conformation is slightly distorted as the dihedral angle for the C2-C1-O1A-C4 moiety is 5.81° instead of 0°.

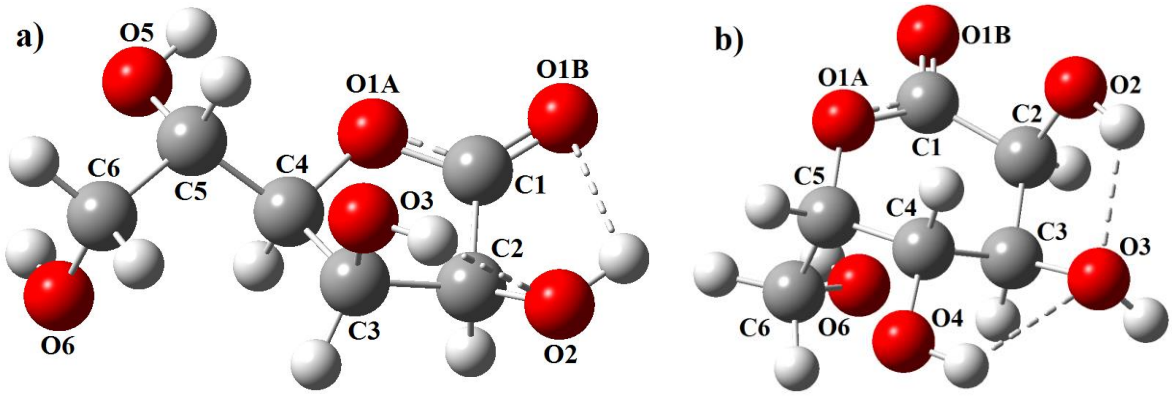

Figure 22 Optimized structure of L-gulonic acid γ- (γ-HGul, part a) and δ-lactone (δ-HGul, part b). The calculations were performed at the M11/def2-TZVP level while solvent effects were taken into account by the CPCM model. The hydrogen bonds are visualized with dashed lines.

Furthermore, two hydrogen bonds are formed between the O1B atom and the C2-OH group (2.373 Å) as well as between the C2-OH and C3-OH groups (2.178 Å).

Concerning δ-HGluc, the half-chair conformation was reported to prevail in aqueous medium [160] and it was also deduced that the relative arrangement of C2-OH and C5-OH functional groups had a key role. That is, if these two groups are *trans*-disposed (*e.g.*, for δ-D-HGluc and δ-D-HGul), the half-chair, otherwise the boat conformation is favored. This statement is confirmed by the present calculation for δ-L-HGul (Figure 22b) albeit its structure is somewhat distorted. That is, the dihedral angle for the C5-O1A-C2-C3 and the O1A-C1-C2-C3 moieties are –29.72° and 24.53° instead of 0°.

The lower thermodynamic stability of δ-HGul found by ^{13}C NMR spectroscopy was attested by these calculations since δ-HGul has lower free energy by 26.1 kJ·mol^{-1} at 298.15 K. (This is considerably higher than the energy of thermal motion, 2.5 kJ·mol^{-1}.) The delocalization of the π electrons again results that the C1-O1A bond length is shorter than the C4-O1A one (1.341

vs. 1.435 Å). The distances between C2-OH and C3-OH (2.043 Å) as well as between C4-OH and C3-OH (2.411 Å) indicate hydrogen bonding.

Conversely, there is no interaction between the C2-OH group and the carbonyl oxygen (O1B). This finding may in part explain the differences in the stability constants, but there can be other factors (*e. g.*, repulsion and overlapping orbitals), which affect the structure of the lactones. To disentangle all the interactions affecting the stability of these molecules would require more detailed computational analysis, which was beyond the scope of the present study.

5.2. Complexation of Ca^{2+} by D-glucose derivatives in neutral medium

5.2.1. D-glucose, D-sorbitol and D-mannitol

The titration curves obtained for systems containing $[Glu]_{T,0}$ = 0.200 and 0.800 M show that upon adding Glu to the solution, the cell potential does not decrease. That is, the drop in the concentration of the unbound calcium ions, $[Ca^{2+}]$, cannot be observed. Surprisingly, compared to the calibration curve, there is a small, but detectable increase (0.6 and 2.6 mV on average). A possible explanation for this feature may be the increase of the activity of Ca^{2+} ions. It was found from Ca-ISE measurements that this change in a solution containing 0.001 mol·kg^{-1} $CaCl_2$ and 0.1–1.0 mol·kg^{-1} Glu is 0.3–6.0% [161]. Two possible scenarios can be envisaged. One is that if we assume that this minor medium effect is the only one we observe and the complexation does not take place at all. The other is that this effect is somewhat larger than and opposite in direction caused by Ca(II) complexation. These two effects, however, are inseparable.

Although, the interaction between Ca^{2+} and Glu was not detectable by ^{1}H NMR spectroscopy [65], thin-layer chromatography [74] and potentiometry [75,76], conductometric [77], ^{13}C NMR spectroscopic [78], Raman [79] and infrared [80] measurements indicated complex formation. Moreover, the ^{1}H–^{43}Ca HMQC spectrum revealed the metal ion-binding of glucose. In conclusion, the association between Ca^{2+} and Glu can be established. Conversely, Ca-ISE potentiometry is not a suitable method as putative changes caused by metal coordination are minor compared to the changes in activity.

For the two sugar alcohols, $[Ca^{2+}]$ decreases upon the addition of Sor or Man (Figures 23a and b) implin the binding of Ca^{2+} ions. With respect to the last measured point (V = 120 cm^3), this change is *ca.* 1.8 mV between the calibration and the solution containing $[Sor]_{T,0}$ =

0.387 M. This effect is somewhat smaller even at higher concentration of Man (*ca.* 1.4 mV; $[Man]_{T,0}$ = 0.429 M). Consequently, Man appears to form weaker complexes with Ca^{2+} ions.

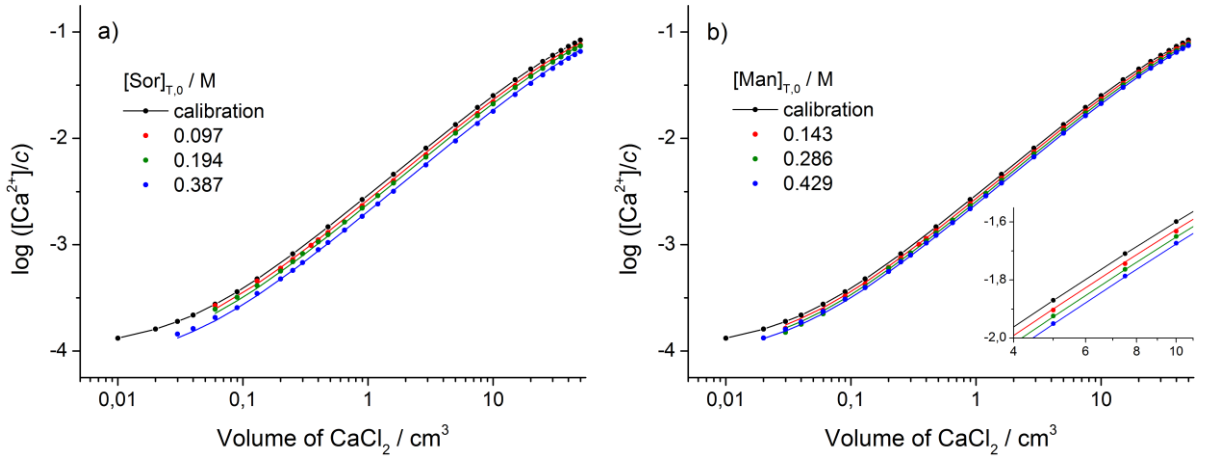

Figure 23 Ca-ISE titration curves of D-sorbitol (Sor, part a) and D-mannitol (Man, part b). Inset of part b: enlargement of the volume range of 4–11 cm^3. Experimental conditions: T = (25.0 ± 0.1) °C, I = 1 M (NaCl), V_0 = 70 cm^3; $[Ca^{2+}]_{T,0} = 10^{-4}$ M. The initial concentrations of the ligands are indicated in the legend. The concentration of the titrant $CaCl_2$ was 0.201 M. Symbols refer to the measured data, while solid lines were calculated by assuming the formation of the 1:1 complexes.

It has to be noted here that the medium effect might be large due to the high ligand concentrations applied. In this respect, it was pointed out that such weak interactions cannot be studied appropriately by Ca-ISE potentiometry if the ligand concentration is only several hundredths in $mol \cdot dm^{-3}$ [162]. On the other hand, the observed changes presented here are commensurable with the average error of the electrode (1 mV). Thus, the obtained stability constants should be considered as estimations.

Nevertheless, the systematic decrease allows the determination of the apparent association constants for both ligands. During calculations, the measured cell potentials were converted to log ($[Ca^{2+}]/c$) values, then these data were fitted as a function of the volume of the added titrant. For both ligands, the assumption of the 1:1 complex was sufficient to simulate the experimental curves with the *FP* being $1.54 \cdot 10^{-2}$ (Sor) and $1.13 \cdot 10^{-2}$ (Man). The obtained stability constants with the literature values are listed in Table 8. Due to the incident medium effects, the error interval for both log β_{11} constant is suggested to be ± 0.1.

The log β_{11} varies between –0.79 and 0.20 for $CaSor^{2+}$ [73,75,77,78,81,82] and between –0.62 and –0.05 for $CaMan^{2+}$ [73,75,82] pointing to the large scattering of the data. Neverthe-

less, the constants determined in the present work are in line with the literature values. Regarding the $CaSor^{2+}$ species, there is good agreement between our constant and the one deduced previously [78] under similar experimental conditions (*i.e.*, temperature, ionic strength, concentrations). (The difference was the use of ^{13}C NMR as method in the presence of 20% V/V D_2O.)

Table 8 Formation constants ($\log \beta_{11}$) of the 1:1 complexes of D-sorbitol (Sor) and D-mannitol (Man). Data correspond to T = 25 °C unless indicated differently; ± 3 *SE* is given in parentheses.

Reaction	Ionic strength and backgr. electrolyte	$\log \beta$	Reference	Method[a]
$Ca^{2+} + Sor = CaSor^{2+}$	≈ 0.006 M[b]	–0.79	77[c]	CON
	0.7 M KNO_3	–0.52	75	POT
	1 M NaCl	0.04(3)	p. w.[d]	POT
	1 M NaCl	0.0(1)[e]	p. w.	POT
	1 M NaCl	0.20(15)	78	^{13}C NMR
	not indicated	–0.09	73	SOL/POT
	not indicated	–0.22(87)	81[c]	^{13}C NMR
	not indicated	0.18	82	SOL/POT/TITR
$Ca^{2+} + Man = CaMan^{2+}$	0.7 M KNO_3	–0.62	75	POT
	1 M NaCl	–0.28(3)	p. w.	POT
	1 M NaCl	–0.3(1)[e]	p. w.	POT
	not indicated	–0.52	73	SOL/POT
	not indicated	–0.05	82	SOL/POT/TITR

[a] CON = conductometry, POT = potentiometry applying Ca^{2+}-ion selective electrode (Ca-ISE), NMR = nuclear magnetic resonance spectroscopy, SOL/POT/TITR = solubility determination *via* Ca-ISE or EDTA titration.
[b] The measurements were carried out with 0.002 M $CaCl_2$.
[c] The measurements were performed at 30 °C (ref. 77) and 36 °C (ref. [81]), respectively.
[d] Present work.
[e] Suggested value for the formation constant (discussed in the text).

Regardless of the uncertainty of the available experimental results, all data – including ours – corroborate that $\log \beta_{11}(CaMan^{2+}) < \log \beta_{11}(CaSor^{2+})$, in agreement with the findings of Angyal and co-workers [71] that polyols having the *threo-threo* sequence (*e.g.*, Sor) coordinate Ca^{2+} stronger than those with the *erythro-threo* sequence (*e.g.*, Man). The reason of this difference is that the *gauche-gauche* arrangement is the desired one for the three adjacent OH groups [71]. For Man, more energy is required to attain this conformation through rotation around the C–C bonds. Based on the data listed in Table 8, $\log \beta_{11}(CaSor^{2+}) - \log \beta_{11}(CaMan^{2+})$ is 0.28 on average (T = 25 °C). One can roughly estimate from this data that the formation of $CaSor^{2+}$ is favored by ≈ 1.5 kJ·mol^{-1} in free energy.

5.2.2. D-gluconate and D-heptagluconate

The titration curves of the $Gluc^-$- and $Hpgl^-$-containing solutions at 25 °C are shown in Figures 24a-b. The observed cell potentials are shifted towards smaller $[Ca^{2+}]$ values to a much higher extent than those observed with Sor and Man. The difference of the potentials between the solutions containing $[Gluc^-]_{T,0} = 0$ and 0.214 M is 9.9 mV, while 9.5 mV was found for $[Hpgl^-]_{T,0} = 0.216$ M ($V = 120$ cm^3). Additionally, the titration curves of the two ligands are essentially identical. In conclusion, 1) the stability constants for $Gluc^-$ and $Hpgl^-$ are similar and 2) the calcium(II) complex(es) of the sugar carboxylates are much more stable than those of the sugar alcohols. The latter clearly reflects the crucial role of carboxylate, which behaves as an anchoring group facilitating the metal ion coordination.

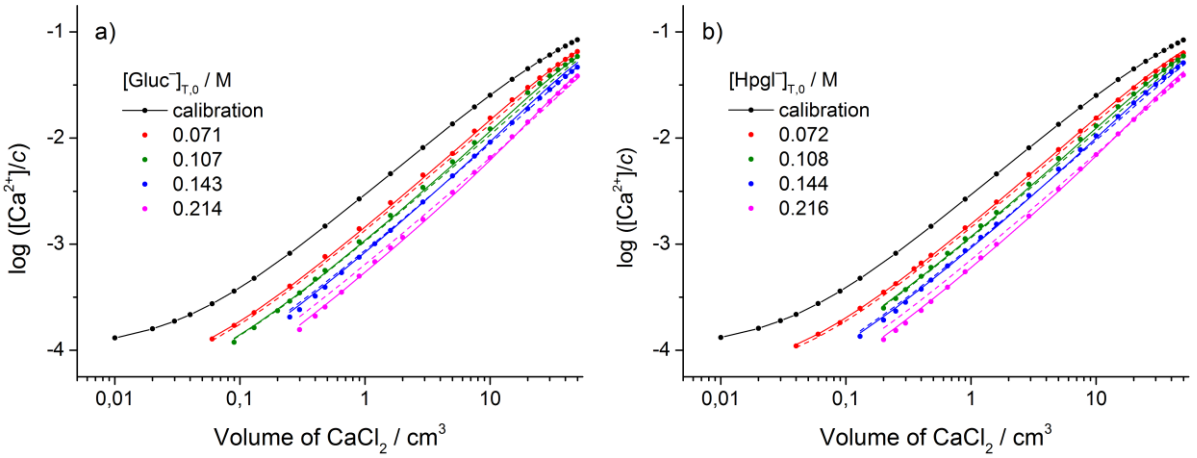

Figure 24 Ca-ISE titration curves of D-gluconate ($Gluc^-$, part a) and D-heptagluconate ($Hpgl^-$, part b). Experimental conditions: $T = (25.0 \pm 0.1)$ °C, $I = 1$ M (NaCl), $V_0 = 70$ cm^3; $[Ca^{2+}]_{T,0} = 10^{-4}$ M. The initial concentrations of the ligands are indicated in the legend. The concentration of the titrant $CaCl_2$ was 0.201 M. Symbols refer to the measured data; dashed or solid lines were calculated by assuming the formation of the 1:1 or the 1:1 and 1:2 complexes.

First, the titration curves were fitted by assuming the exclusive formation of the $CaGluc^+$ and $CaHpgl^+$ species. The results of the calculations are depicted as dashed lines in Figure 24. The *FP* (in log ($[Ca^{2+}]/c$) units) and log β_{11} were calculated to be 0.044 and 1.23 for $Gluc^-$ as well as 0.041 and 1.17 for $Hpgl^-$. These constants agree fairly with literature data obtained *via* Ca-ISE titrations [41,75,87,88,90], especially if one considers the different ionic strength applied.

It is seen, however, that there are systematic deviations between the observed and calculated data; even in the points falling in the linear section of the calibration curve. For instance, the calculated points are under the observed ones in the whole range at 0.071 M NaGluc, while at

0.107 M the same deviation is seen from 5 cm^3. At 0.214 M the calculated curve intersects the experimental one. Expectedly, the same deviations were detected for $Hpgl^-$, too.

In order to improve the fitting of the experimental data, the 1:2 complexes ($CaGluc_2^0$ and $CaHpgl_2^0$) were also included in the chemical model. With this assumption, the above-mentioned errors practically disappear (demonstrated with solid lines in Figure 24). In parallel, the *FP* decreases to 0.023 ($Gluc^-$) and 0.018 ($Hpgl^-$), respectively. Thus, this model was accepted in this study and the corresponding stability products for the 1:1 and 1:2 complexes are presented in Table 9. The concentration distribution diagrams for the two ligands (Figure 25) shows that the formation of the 1:2 species exceeds that of $[Ca^{2+}]_T$ by 30% at high ligand to metal ratios.

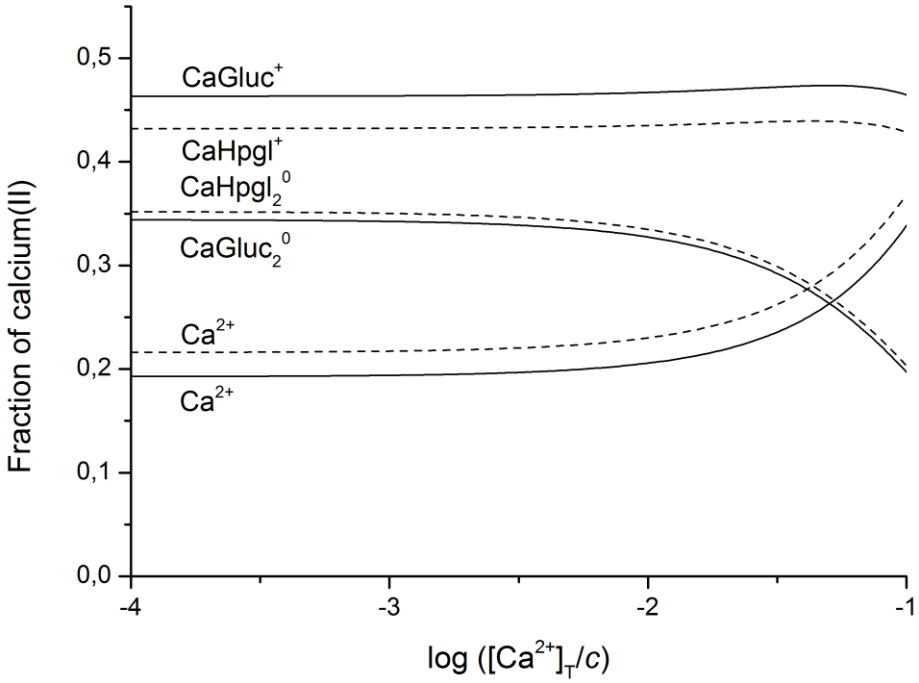

Figure 25 Speciation diagram of the Ca^{2+}/D-gluconate ($Gluc^-$) and Ca^{2+}/D-heptagluconate ($Hpgl^-$) systems as a function of log ($[Ca^{2+}]/c$). The calculations correspond to T = 25 °C, I = 1.0 M and $[Gluc^-]_T$ or $[Hpgl^-]_T$ = 0.200 M. The $Gluc^-$- and $Hpgl^-$-related species are indicated with solid and dashed lines, respectively.

The formation of the $CaGluc^+$ complex should be more preferred than that of the $CaHpgl^+$ analogue, since $Gluc^-$ has *threo*-2,3-*threo*-3,4 triol sequence while $Hpgl^-$ has *erythro*-2,3-*threo*-3,4 triol sequence (Figure 7, p. 17). Conversely, $CaGluc^+$ appears to be more stable, the difference between the $\log \beta_{11}$ constants is only 0.08, which is commensurable with the standard error. On the basis of configuration, Ca^{2+} is likely to be bound to the C2-OH and C3-OH groups of $Gluc^-$, whilst the C3-OH and C4-OH groups should be favored in the case of $Hpgl^-$. Indeed,

the coordination of C2-OH and C3-OH groups for $Gluc^-$ [37] and that of the C2-OH, C3-OH and C4-OH groups for $Hpgl^-$ [41] were observed in the 2D NMR spectra.

Table 9 Formation constants (log β_{pq}) of the $Ca_pA_q^{(2p-q)+}$ complexes where A denotes D-gluconate ($Gluc^-$) or D-heptagluconate ($Hpgl^-$). Data correspond to T = 25 °C unless indicated differently; ± 3 *SE* is given in parentheses.

Reaction	Ionic strength and backgr. electrolyte	log β_{pq}	Reference	Method[a]
$Ca^{2+} + Gluc^- = CaGluc^+$	$I \rightarrow 0$	1.7(3)[b]	37	^{13}C NMR
	$I \rightarrow 0$	1.72(21)	84	GLE POT
	$I \rightarrow 0$	1.89(30)	84	ISE POT
	$I \rightarrow 0$	1.70[c]	85	
	$I \rightarrow 0$	1.94	86	SOL/POT/TITR
	0.1 M KCl	1.6	88	ISE POT
	0.16 M NaCl	1.22	91	IEX
	0.2 M NaCl	1.49(12)	90	ISE POT
	0.2 M KCl	1.21	22[d]	H_2-Pt POT
	0.5 M NaCl	1.05(30)	87	ISE POT
	0.7 M KNO_3	1.31	75	ISE POT
	1 M NaCl	1.08(4)	p. w.[e]	ISE POT
	1 M NaCl	1.02(3)	37	^{13}C NMR
	1 M NaCl	0.37(9)	62	H_2-Pt POT
	1 M NaCl	1.15(27)	90	ISE POT
	1 M $NaClO_4$	1.21(5)	89	GLE POT
	not indicated	1.36	82	SOL/POT/TITR
$Ca^{2+} + 2\ Gluc^- = CaGluc_2^0$	0.5 M NaCl	1.88(24)	87	ISE POT
	1 M NaCl	1.65(9)	p. w.	ISE POT
$Ca^{2+} + Hpgl^- = CaHpgl^+$	1 M NaCl	0.85	41	^{13}C NMR
	1 M NaCl	1.21(12)	41	ISE POT
	1 M NaCl	1.00(4)	p. w.	ISE POT
$Ca^{2+} + 2\ Hpgl^- = CaHpgl_2^0$	1 M NaCl	1.61(7)	p. w.	ISE POT

[a] NMR = nuclear magnetic resonance spectroscopy, GLE/H_2-Pt/ISE POT = potentiometry applying glass, hydrogen or Ca^{2+}-ion selective electrode (Ca-ISE), SOL/TITR/POT = solubility determination *via* Ca-ISE or EDTA titration, IEX = ion-exchange with isotope detection.
[b] Calculated from the data obtained at I = 1 M and 2–4 M (not shown) and from those of refs. [22, 87, 91].
[c] Calculated from the data reported in ref. [91].
[d] The temperature was not indicated.
[e] Present work.

It is possible that more coordination isomers are formed with $Hpgl^-$, which may enhance the otherwise lower stability (entropy effect). Furthermore, $Hpgl^-$ contains an extra OH group, which increases the probability of the coordination of this group when COO^- is already attached to the metal ion (statistical effect). These explanations, however, are still speculative and further information regarding the structure-stability correlation cannot be extracted from the available experimental data.

The binding of the second ligand to Ca^{2+} can be described with the following reaction:

$$CaA^+ + A^- = CaA_2^0 \quad (47)$$

where A^- can be $Gluc^-$ or $Hpgl^-$. The stepwise stability constant, K_{12}, can be expressed as:

$$K_{12} = \frac{[CaA_2^0] \cdot c}{[CaA^+][A^-]} \quad (48)$$

where $\log K_{12} = \log \beta_{12} - \log \beta_{11}$. Accordingly, $\log K_{21} = 0.57$ for $Gluc^-$ and 0.61 for $Hpgl^-$. Both stepwise constants are smaller than $\log \beta_{11}$ which is expected for statistical reasons.

Regarding $CaGluc_2^0$, our value for $\log \beta_{12}$ is commensurable with the one reported previously [87]. (The difference probably results from the difference in the ionic strengths applied.) Additionally, the 1:2 species was detected by polarimetric experiments [92], while ^{13}C NMR [37] and further Ca-ISE [162] measurements implied its formation, though, the variations were too low preventing quantitative evaluation. Nevertheless, this hitherto uncertain species was proposed by various experimental methods (including our measurements), thus, its existence can be postulated. In light of these findings and structural similarity, the formation of $CaHpgl_2^0$ is not surprising.

Summarizing these results, it seems that the formation of the 1:2 complex is preferred if the sugar-derivative ligand has a COO^- anchor and at least two adjacent OH groups. Moreover, the dynamic equilibrium between linkage isomers is even more likely to occur due to the presence of two ligands.

The association of alkaline metal ions are known to affect the optical activity of the ligand [163]. Hence, polarimetric measurements were also performed with solutions containing 0.200 M NaGluc or NaHpgl and 0–0.295 M $CaCl_2$ (Figures 26a-b). The optical rotation of the solutions gradually decreases in both cases with increasing calcium concentration indicating that upon complexation, the optically active complexes formed have specific rotations smaller than that of the uncomplexed anion. Although the direction of this variation is well defined for both ligands, its magnitude is rather small (0.5 and 0.2° for $Gluc^-$- and $Hpgl^-$-containing solutions, respectively) inferring that the prediction of the formation constants is not possible.

By the proposed chemical model, about 75% of the ligand is bound in the two complexes at $[CaCl_2]_T = 0.295$ M. This unexpectedly small effect suggests that the specific rotations of the free ligand and those of the complexes are only slightly different. Analogously to the protonation (eq. 25), the relationship between the optical rotation and free concentrations reads as:

$$\alpha = \alpha_{A^-}[A^-] + \alpha_{CaA^+}[CaA^+] + \alpha_{CaA_2{}^0}[CaA_2{}^0] \quad (49)$$

where $[A^-]$, $[CaA^+]$ and $[CaA_2{}^0]$ are the corresponding equilibrium concentrations while α_{A^-}, α_{CaA^+} and $\alpha_{CaA_2{}^+}$ denote the products of the molar rotation and the optical path length.

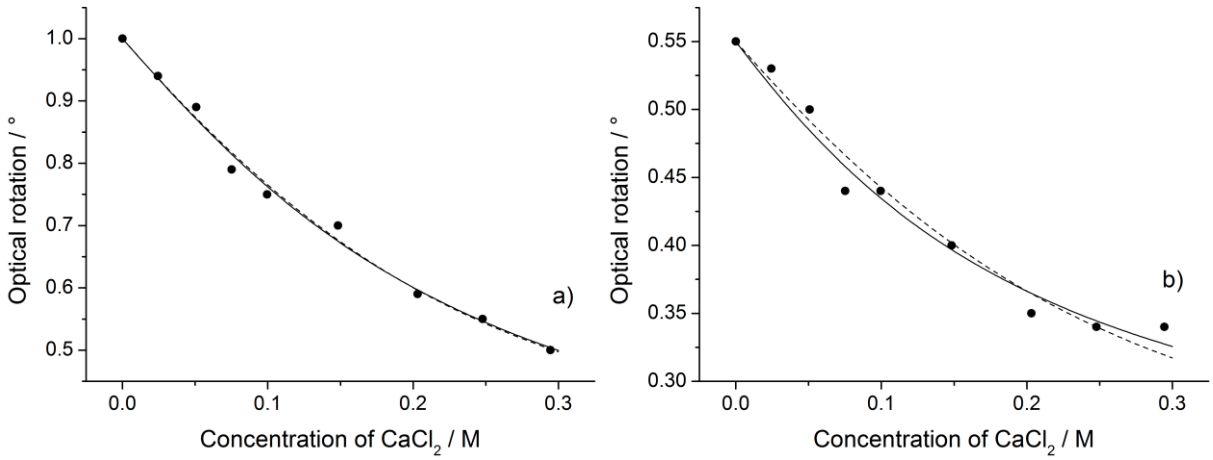

Figure 26 Optical rotation of D-gluconate ($Gluc^-$, part a) and D-heptagluconate ($Hpgl^-$, part b) as a function of $CaCl_2$ concentration. Experimental conditions: T = (25 ± 2) °C and I = 1 M (NaCl); a) $[Gluc^-]_T$ = 0.200 M, $[Ca^{2+}]_T$ = 0–0.295 M, b) $[Hpgl^-]_T$ = 0.200 M, $[Ca^{2+}]_T$ = 0–0.295 M. Symbols refer to the measured data; dashed or solid lines were calculated by assuming the formation of the 1:1 or the 1:1 and 1:2 complexes.

The specific rotations of the various species were estimated with the PSEQUAD program using the 1:1 and 1:2 formation constants from Table 9 as fixed values while $[\alpha_{Gluc^-}]_D$ and $[\alpha_{Hgpl^-}]_D$ were treated as fitted parameters. The results of calculations are depicted in Figures 26a-b and presented in Table 10. It should be noted, however, that the extent of formation of the 1:2 complexes is *ca.* 20%. Therefore the correlation between the stability constants and the specific rotations is high, hence the larger error of the latter. By the same token, fitting only $[\alpha_{CaGluc^+}]$ or $[\alpha_{CaHpgl^+}]$ is also satisfactory and yields similar curve. As a result, the *FP* was calculated to be 0.02° ($Gluc^-$) or 0.01° ($Hpgl^-$) using both models.

These results corroborate that the structure of these hydroxycarboxylates in their uncomplexed and complexed forms are not very much different; in other words, the binding of the metal ion results in minor variations regarding the equilibrium conformation. (Similar experiments were conducted for Glu, Sor and Man as well, but the changes did not exceed 0.1°.)

Table 10 Calculated specific rotations, $[\alpha]_D$, of D-gluconate ($Gluc^-$) or D-heptagluconate ($Hpgl^-$) and their Ca(II) complexes.[a] Data correspond to T = (25 ± 2) °C and I = 1 M (NaCl); ± 3 *SE* is given in parentheses.

Species	$[\alpha]_D$ / $cm^3 \cdot g \cdot dm^{-1}$	Species	$[\alpha]_D$ / $cm^3 \cdot g \cdot dm^{-1}$
$Gluc^-$	12.81[b] 12.98(8)[c]	$Hpgl^-$	6.11[b]
$CaGluc^+$	2.6(4)[d] 1.5(1.8)[e]	$CaHgpl^+$	1.7(3)[d] 1.7(1.4)[e]
$CaGluc_2^0$	9.4(3.5)[e]	$CaHpgl_2^0$	3.8(2.4)[e]

[a] Calculated from the formation constants given in Table 9 on p. 56.
[b] Measured in solutions containing $[Gluc^-]_T$ or $[Hpgl^-]_T$ = 0.200 M.
[c] Calculated from independent calibration.
[d] Only the specific rotation of the 1:1 complex was fitted.
[e] The specific rotation of the 1:1 and 1:2 complexes were fitted simultaneously.

5.2.3. D-glucuronate and D-glucarate

Glucuronate is known to be present as a cyclic anion at pH ≈ 7 [95], which might indicate similar medium effect to the one observed for glucose. If the extent of this effect was significant, a positive shift relative to the calibration curve would be expected in the presence of the ligand for the entire titration range. As the $[Glucur^-]_{T,0}$ increases, however, the free concentration of Ca^{2+} decreases markedly relative to the ligand-free solution (Figure 27a), which indicates complex formation. Fitting the 1:1 complex yields $\log \beta_{11}$ = 0.80 and FP = 0.030 $\log([Ca^{2+}]/M)$, hence, the $CaGlucur^+$ species in itself appears to be insufficient to provide acceptable calculated curves. Dashed lines in Figure 27a show that the deviation between the measured and calculated points becomes significant above V = 10 cm^3 at all concentrations of $CaCl_2$.

Assuming the formation of the binuclear 2:1 complex provides FP as 0.011 $\log([Ca^{2+}]/M)$; the corresponding formation constants are given in Table 11. A plausible explanation for the lack of the 1:2 complex can be that the association of the metal ion and two, structurally rigid ligands of large size makes this association sterically hindered. On the other hand, $Glucur^-$ has a sufficient number of OH groups to bind an additional Ca^{2+} at high metal ion concentrations (> 0.03 M).

Our calculations revealed that the maximum extent of the formation of $Ca_2Glucur^{3+}$ was 17%; thus, its formation cannot be proven unambiguously in this concentration range. Such M_2L^{3+} species was detected between Ca(II) and $Gluc^-$ [62,92] as well as Cu(II) and Man [164], although, these complexes were detected in strongly alkaline medium. Hence, these complexes are stabilized through the displacement of proton(s) from the OH groups.

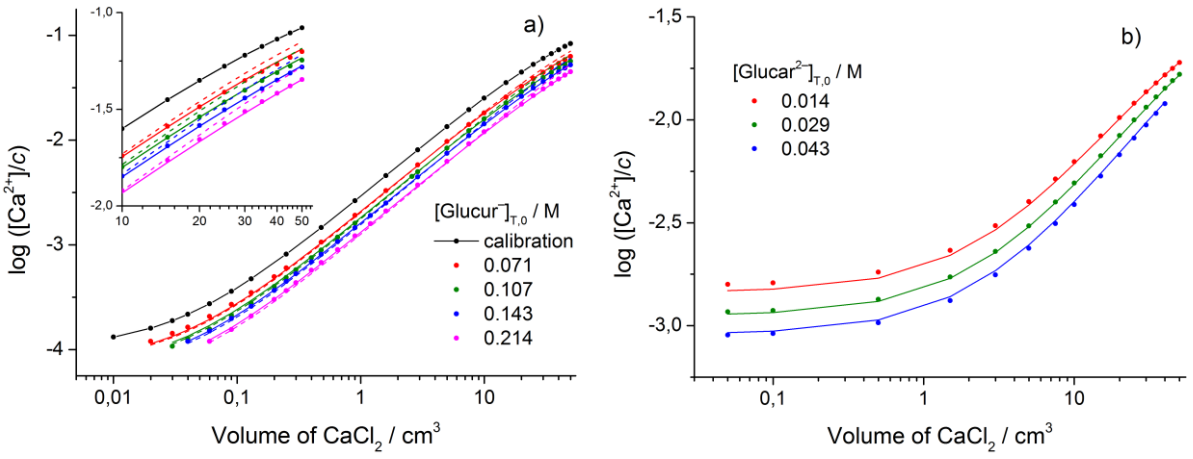

Figure 27 Ca-ISE titration curves of D-glucuronate ($Glucur^-$, part a) and D-glucarate ($Glucar^{2-}$, part b). Inset of part b: enlargement of the range of 10–50 cm^3. Experimental conditions: T = (25.0 ± 0.1) °C, I = 1 M (NaCl), V_0 = 70 cm^3; a) $[Ca^{2+}]_{T,0} = 10^{-4}$ M, b) $2 \cdot 10^{-3}$ M. The initial concentrations of the ligands are indicated in the legend. The concentration of the titrant $CaCl_2$ was a) 0.201 M, b) 0.050 M. Symbols refer to the measured data; dashed orsolid lines were calculated by assuming the formation of the 1:1 or the 1:1 and 2:1 complexes.

Table 11 Formation constants (log β_{pq}) for the $Ca_pA_q^{(2p-q)+}$ complexes where A denotes D-glucuronate ($Glucur^-$)[a] or D-glucarate ($Glucar^{2-}$). Data correspond to 25 °C unless indicated differently; ± 3 *SE* is given in parentheses.

Reaction	Ionic strength and backgr. electrolyte	log β_{pq}	Reference	Method[b]
$Ca^{2+} + Glucur^- = CaGlucur^+$	0.1 M KCl	1.1	88	ISE POT
	0.7 M KNO_3	1.03	75	ISE POT
	1M NaCl	0.80(2)[c]	p. w.[d]	ISE POT
	1 M NaCl	0.76(1)[e]	p. w.	ISE POT
	1 M $NaClO_4$	1.49(3)	98	GLE POT
	not indicated	1.51	95	GLE POT
	not indicated	1.52	95	ISE POT
	not indicated	1.48	95	POL
	not indicated	0.72	97[f]	SPM
$Ca^{2+} + 2\ Glucur^- = Ca_2Glucur^{3+}$	1 M NaCl	1.57(6)[e]	p. w.	ISE POT
$Ca^{2+} + Glucar^{2-} = CaGlucar^0$	$I \rightarrow 0$	3.01(9)	103	ISE POT
	0.1 M KCl	2.2	88	ISE POT
	1 M NaCl	1.48(2)	p. w.	ISE POT

[a] Formation constants correspond to the mixture of α- and β-anomers.
[b] GLE/ISE POT = potentiometry applying glass, hydrogen or Ca^{2+}-ion selective electrode (Ca-ISE), POL = polarimetry, SPM = spectrophotometry.
[c] Calculated constant by omitting the formation of the 2:1 complex.
[d] Present work.
[e] Calculated constant by assuming the formation of the 2:1 complex.
[f] The temperature was not indicated.

Conversely, the formation of the $CaGlucur^+$ complex reaches 55%; its log β_{11} agrees reasonably with those reported in refs. [75,88,97], but it is gnificantly lower than those published in

refs. [95,98]. The presen measurements, however, show clearly that both $Gluc^-$ and $Hpgl^-$ exhibit larger potentiometric effects than $Glucur^-$, hence $\log \beta_{11} \approx 1.5$ (T = 25 °C, I = 1 M) [95,98] seems to be overestimated. From the point of view of structural differences, $Gluc^-$ and $Hpgl^-$ are flexible ligands in contrast with the rigid $Glucur^-$, which should be accompanied by lower stability for the $CaGlucur^+$ species. This was supported by polarimetric experiments since the variation of the optical rotation did not exceed 0.15°.

D-glucarate, which is the most oxidized form of this ligand series, exhibits significant extent of complexation with Ca^{2+} even at much lower ligand concentrations (0.01–0.04 M, Figure 27b). Contrary to the 1:1 species, the formation of the 1:2 complex was not be observed, probably due to the low concentration of $Glucar^{2-}$ (which needed to be applied to avoid precipitation).

The *FP* was found to be 0.013 during fitting while the equilibrium constant is given in Table 11. Compared to $CaGluc^+$, the $\log \beta_{11}$ of $CaGlucar^0$ is remarkably higher; this difference follows from the presence of an additional carboxylate group of $Glucar^{2-}$ rendering its Ca^{2+}-binding ability very strong. Furthermore, it is seen from the stability products that $\log \beta_{11}(CaGlucar^0) \approx \log \beta_{12}(CaGluc_2^0)$ indicating that probably both COO^- groups are attached to the metal ion in the $CaGlucar^0$ complex.

To summarize these results, the order of stability constants of the 1:1 complexes for D-glucose and its derivatives is as follows: Glu < Man < Sor < $Glucur^-$ < $Hpgl^-$ ≈ $Gluc^-$ < $Glucar^{2-}$. This order reflects well the stronger binding ability of COO^- compared to the OH group ($Gluc^-$ *vs.* Sor), the number of COO^- groups ($Glucar^{2-}$ *vs.* $Gluc^-$), the differences arising from structural rigidity and flexibility (Sor *vs.* Glu and $Gluc^-$ *vs.* $Glucur^-$) as well as the role of the configuration (Sor *vs.* Man).

5.3. Complexation of Ca^{2+} by L-gulonate in neutral medium

5.3.1. Complexation equilibria of the Ca^{2+}-gulonate complexes

Similarly to $Gluc^-$ and $Hpgl^-$, Ca-ISE potentiometric measurements were performed with Gul^- to determine the formation constant and composition of the complex(es) formed with Ca^{2+} ions. The titration curves obtained for solutions containing $[NaGul]_{T,0}$ = 0.071–0.214 M are shown in Figure 28. It is clearly seen that upon addition of NaGul to the solutions, the concentration of the unbound calcium ions, $[Ca^{2+}]$, decreases in accord with the observations made for the two other ligands.

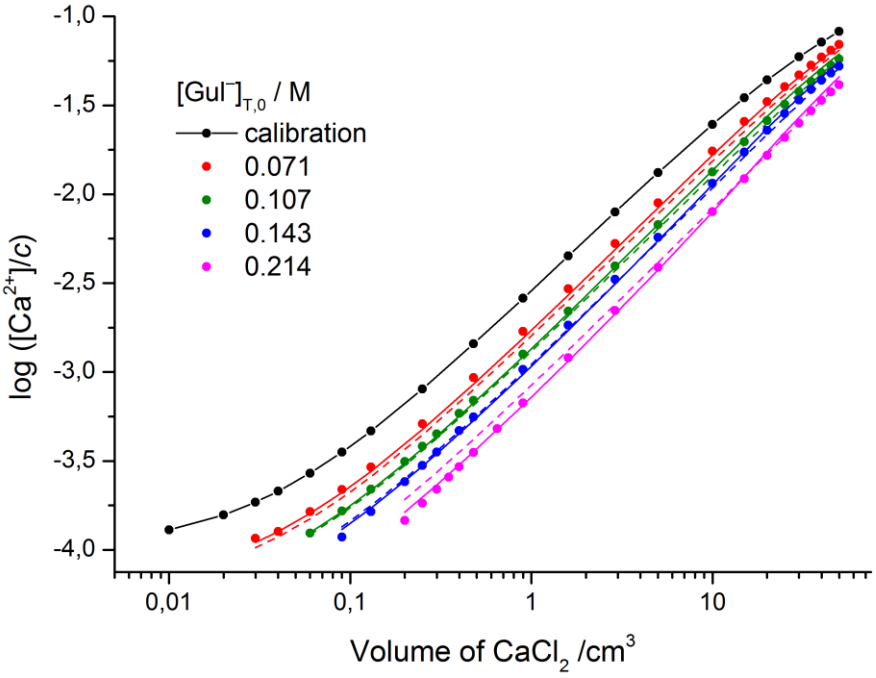

Figure 28 Ca-ISE titration curves of L-gulonate (Gul^-). Experimental conditions: T = (25.0 ± 0.1) °C, I = 1 M (NaCl), V_0 = 70 cm^3; $[Ca^{2+}]_{T,0} = 10^{-4}$ M. The initial concentrations of the ligand are indicated in the legend. The concentration of the titrant $CaCl_2$ was 0.197 M. Symbols refer to the measured data; dashed or solid lines were calculated by assuming the formation of the 1:1 or the 1:1 and 1:2 complexes.

The decrease in the cell potential between the calibration and the sample with $[Gul^-]_{T,0}$ = 0.214 M (at V = 120 cm^3) is 8.3 mV indicating the considerable extent of complexation. On the other hand, this difference, though being slightly smaller, is in line with those found for $Gluc^-$ (9.9 mV) and $Hpgl^-$ (9.5 mV).

The shape of the titration curves is also identical to those of $Gluc^-$ and $Hpgl^-$ as a token of similar structure. It is therefore not surprising that the measured cell potentials can be again fitted better by assuming both the $CaGul^+$ and $CaGul_2^0$ species. As a result, *FP* decreases from 0.041 to 0.022 log ($[Ca^{2+}]/c$) units) while log β_{11} decreases from 1.06 to 0.88. By this model, the 1:2 species is formed more than 30% with respect to $[CaCl_2]_T$, as demonstrated in Figure 29.

The overall smaller drop of $[Ca^{2+}]$ probably stems from the lower stability constants, presented in Table 12 (for comparison, data for the other two anions are also provided). If this difference is not the consequence of the uncertainty of the ion-selective electrode, then it can be attributed to the different configuration. Compared to $Gluc^-$, Gul^- has *erythro*-2,3-*threo*-3,4 arrangement with respect to the OH groups. It follows from the theory of Angyal and co-workers

[71] that $\log \beta_{11}(CaGul^+) < \log \beta_{11}(CaGluc^+)$ and this relation holds for the 1:2 complexes as well. This difference is 0.20, that is, ≈ 1.1 kJ·mol^{-1} in free energy at 25 °C.

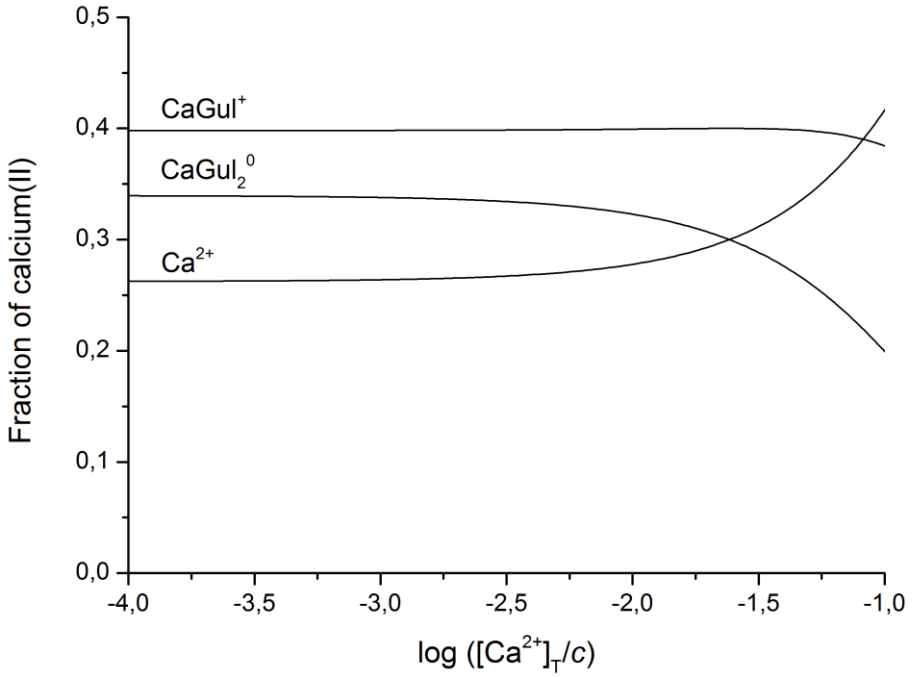

Figure 29 Speciation diagram of the Ca^{2+}/L-gulonate (Gul^-) system as a function of log ($[Ca^{2+}]$/M). The calculations correspond to T = 25 °C, I = 1 M (NaCl) and $[Gul^-]_T$ = 0.200 M.

Table 12 Formation constants ($\log \beta_{pq}$) for the $Ca_pA_q^{(2p-q)+}$ complexes where A denotes L-gulonate (Gul^-), D-gluconate ($Gluc^-$) or D-heptagluconate ($Hpgl^-$).[a] Data correspond to T = 25 °C; ± 3 *SE* is given in parentheses.

Reaction	Ionic strength and backgr. electrolyte	$\log \beta_{pq}$	Reference	Method[b]
$Ca^{2+} + Gul^- = CaGul^+$	0.1 M KCl	1.6[c]	88	ISE POT
	1 M NaCl	0.88(5)	p. w.[d]	ISE POT
	1 M NaCl	1.09(1)	p. w.	^{1}H NMR
	1 M NaCl	1.12(3)	p. w.	^{1}H / ^{13}C NMR
	1 M NaCl	1.0(1)[e]	p. w.	^{1}H / ^{13}C NMR
$Ca^{2+} + 2\ Gul^- = CaGul_2^0$	1 M NaCl	1.51(9)	p. w.	ISE POT
$Ca^{2+} + Gluc^- = CaGluc^+$	1 M NaCl	1.08(4)	p. w.	ISE POT
$Ca^{2+} + 2\ Gluc^- = CaGluc_2^0$	1 M NaCl	1.65(9)	p. w.	ISE POT
$Ca^{2+} + Hpgl^- = CaHpgl^+$	1 M NaCl	1.00(4)	p. w.	ISE POT
$Ca^{2+} + 2\ Hpgl^- = CaHpgl_2^0$	1 M NaCl	1.61(7)	p. w.	ISE POT

[a] Values of $\log \beta$ for $Gluc^-$ and $Hpgl^-$ restricted to those determined in the present work; the literature data are presented in Table 9 on p. 56.
[b] ISE POT = potentiometry applying glass electrode, NMR = nuclear magnetic resonance.
[c] This constant corresponds to D-gulonate.
[d] Present work.

Similarly to the potentiometric method, we tried to exploit the advantages of NMR spectroscopy in determining stability constants. Both the ^{1}H and ^{13}C NMR spectra show that the exchange between the free ligand and its complexes is fast. Assuming only the formation of the 1:1 complex, the observed chemical shift can be expressed as:

$$\delta = \delta_{Gul^-} \frac{[Gul^-]}{[Gul^-]+[CaGul^+]} + \delta_{CaGul^+} \frac{[CaGul^+]}{[Gul^-]+[CaGul^+]} \tag{51}$$

where δ_{Gul^-} and δ_{CaGul^+} are the corresponding limiting chemical shifts in ppm.

Substituting the mass balance equation for gulonate:

$$[Gul^-]_T = [Gul^-]+[CaGul^+] \tag{52}$$

it is readily seen that δ is directly proportional to the free concentration of $[Gul^-]$ and $[CaGul^+]$, while the proportionality coefficient is $\delta_{Gul^-}/[Gul^-]_T$ as well as $\delta_{CaGul^+}/[Gul^-]_T$.

The thus obtained relationship was used to determine the formation constant of the 1:1 complex by measuring a solution series with $[Gul^-]_T$ = 0.200 M and $[CaCl_2]_T$ = 0–0.273 M. It was found that the equilibrium constant correlated significantly with the chemical shift of a certain nucleus, which is due to the fact that the $[CaGul^+]/[Gul^-]_T$ ratio remains below 100% considerably, even at the highest $[CaCl_2]_T$.

Table 13 ^{1}H and ^{13}C chemical shifts of $CaGul^+$ and their relative difference to those of L-gulonate (Gul^-). Experimental conditions: T = (25 ± 1) °C, I = 1 M (NaCl). The shifts of Gul^- were observed experimentally, while those of $CaGul^+$ were calculated. Additionally, ± 3 *SE* is given in parentheses.

Nucleus	δ_{HGul} / ppm	$\delta_{CaGul^+} - \delta_{Gul^-}$ / ppm	Nucleus	δ_{HGul} / ppm	$\delta_{CaGul^+} - \delta_{Gul^-}$ / ppm
H2	4.21(1)	0.22	C1	178.12(7)	–0.22
H3	3.89(1)	0.16	C2	73.66(4)	0.50
H4	3.74(1)	0.08	C3	72.48(4)	0.45
H5	3.77(1)	0.08	C4	69.83(3)	–0.23
H6	3.61(1)	0.03	C5	72.22(3)	–0.04
H6’	3.54(1)	0.06	C6	62.35(3)	0.09

Fitting the ^{1}H chemical shifts, the best *FP* obtained was 0.001 ppm with $\log \beta_{11}$ = 1.09. The ^{13}C shifts were less sensitive upon increasing $[CaCl_2]_T$, hence, they were fitted together with the ^{1}H NMR data. As a result, two minima with acceptable *FP* (0.005 ppm) and $\log \beta_{11}$ values (0.98 and 1.12) were obtained. Having provided better fitting, the second constant was chosen in this work, but both can be accepted; their difference shows the chemical uncertainty and the accuracy of NMR spectroscopy when studying such weak interactions. Hence, as a realistic value,

log β_{11} can be proposed as 1.0(1). (These stability products are listed in Table 12 while the respective chemical shifts are presented in Table 13. The experimental points as well as the calculated curves are depicted in Figures 30a-b.)

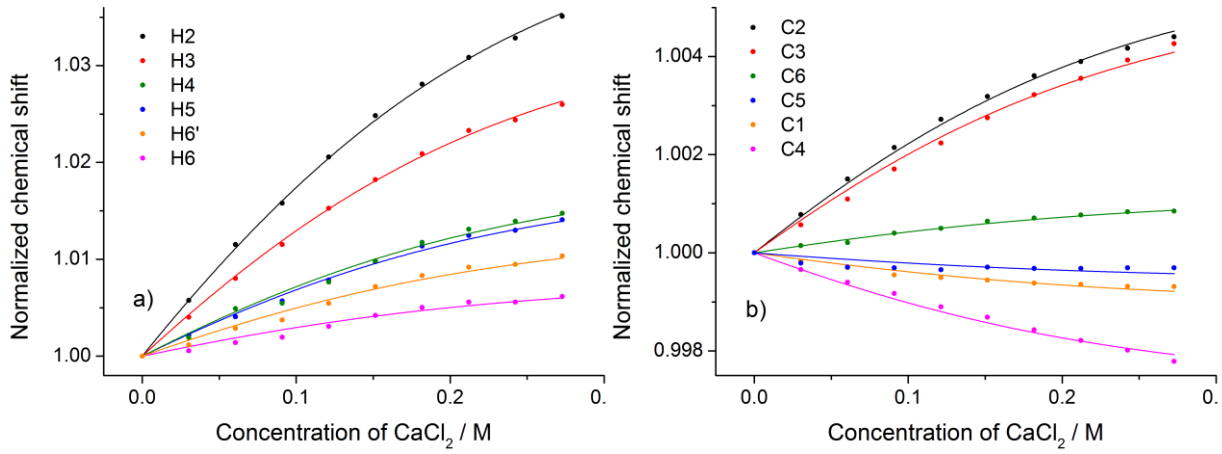

Figure 30 ^{1}H (part a) and ^{13}C (part b) chemical shifts of L-gulonate (Gul^{-}) as a function of $CaCl_2$ concentration. Experimental conditions: T = (25 ± 1) °C, I = 1 M (NaCl); $[Gul^{-}]_T$ = 0.200 M, $[Ca^{2+}]_T$ = 0–0.273 M. Symbols and solid lines refer to the measured and calculated data, respectively. The chemical shifts were normalized to those of Gul^{-} at $[Ca^{2+}]_T$ = 0 M.

Nevertheless, it is readily seen that the constant found *via* NMR is larger than that determined *via* potentiometry. This difference may be the consequence of the formation of the $CaGul_2^0$ species. (Fitting only log β_{11}, the contributions of the 1:2 species will be melted into this constant leading to its increase.) Additionally, the small deviations between the experimental points and calculated curves (Figures 30a-b) refer to (at least) two species of different chemical shifts.

These errors appear mostly below $[CaCl_2]_T \approx 0.11$ M, in agreement with the speciation diagram calculated using the potentiometric data (not shown). That is, the amount of Gul^{-} bound in the 1:2 species reaches its maximum (≈ 25%) at 0.11 M. In parallel, the $2[CaGul_2^0]/[CaGul]$ ratio exceeds 1, then it starts to decrease. It has to be noticed that the formation of two 1:1 species with different coordinations cannot explain the observed variations as their ratio would be the same in the whole range. In conclusion, these NMR measurements indicate the presence of the 1:2 complex but the extent of its formation (≈ 25%) is insufficient to pinpoint it.

5.3.2. Structure of the Ca^{2+}-gulonate complexes *via* different experimental approaches

All the ^{1}H NMR signals of Gul^{-} are displaced downfield with increasing calcium concentration (Figure 30a). The closer a certain hydrogen atom to the carboxylate group, the larger the extent of this displacement. Similar systematic behavior was observed during the protonation of Gul^{-} (Figure 17a, p. 41), that is, the displacement of the ^{1}H NMR chemical shift is clearly correlated with the proximity of the carboxylate group. Thus, the shielding factor of the ^{1}H nuclei appears to be affected mostly by the direct binding of cations (H^{+} or Ca^{2+}). Of these variations, the peaks of H2 and H3 change the most which is consistent with that Ca^{2+} is attached to the COO^{-} and possibly to one or two adjacent OH groups.

Concerning the vicinal coupling constant, $|^{3}J_{H,H}|$, only minor changes are seen except for $^{3}J_{H2,H3}$ which decreases from 5.3 Hz ($[Gul^{-}]_T$ = 0.20 M) to 4.6 Hz ($[Gul^{-}]_T$ = 0.20 M and $[CaCl_2]_T$ = 0.27 M). Though, this difference is not large, it is the opposite of that observed upon protonation (6.1 Hz at pH_{exp} = 2.02) indicating the reverse change of the H2C2C3H3 dihedral angles. Thus, Ca^{2+} is presumably bound not only to the COO^{-} group but also to the C2-OH and/or the C3-OH group.

Conversely, the ^{13}C NMR chemical shifts of some C atoms are displaced upfield, while others are displaced downfield upon calcium binding (Figure 30b). This phenomenon was observed for $Gluc^{-}$ [37] and $Hpgl^{-}$ [41], too, albeit significant differences between the individual directions of these variations were found. These directions for the three ligands are as follows: for, Gul^{-}, upfield: C1, C4, C5, downfield: C2, C3, C6; for $Gluc^{-}$, upfield: C3, C4, C5, C6, downfield: C1, C2; for $Hpgl^{-}$, upfield: C1, C3, C5, C6, C7, downfield: C2, C4. Consequently, the differences in the configuration of OH groups play an important role in these spectral variations.

It seems probable that the shielding factor of the ^{13}C nuclei is sensitive not only to the binding of the metal ion but also to the variations of the conformation. As a result, the extent of the displacement of the ^{13}C NMR signals shows no clear correlation with the proximity of the binding site as opposed to ^{1}H NMR signals (Table 13). That is, the order of the absolute differences between the chemical shifts of the complex and those of the free ligand is as follows: H2 > H3 > H4 ≈ H5 > H6' > H6 and C2 > C3 > C1 ≈ C4 >> C6 > C5.

In conclusion, the assignment of the binding sites is not obvious. On the other hand, the magnitude of these differences implies that the COO^{-}, C2-OH, C3-OH and C4-OH groups are the most probable ones participating in Ca(II) coordination. Concerning $Hpgl^{-}$, the coordination

of the C2-OH, C3-OH and C4-OH groups was proposed *via* NMR spectroscopy [41]. This coordination motif seems probable for Gul^- (both ligands has *erythro*-2,3-*threo*-3,4 sequence).

The effect of Ca^{2+}-complexation on the optical rotation of Gul^- was also studied *via* polarimetry. Upon addition of calcium ions in samples with $[Gul^-]_T$ = 0.200 M and $[CaCl_2]_T$ = 0–0.291 M, the degree of rotation increases by 0.4° with increasing $[CaCl_2]_T$ (Figure 31), which is the same in direction, but smaller in magnitude compared to the effect of protonation. Using the potentiometrically determined stability constants (Table 12), the fraction of the uncomplexed ligand decreases to 32% at $[CaCl_2]_T$ = 0.291 M. Still, the change in the rotation is too small to provide sufficient information to extract the formation constants of the two complexes.

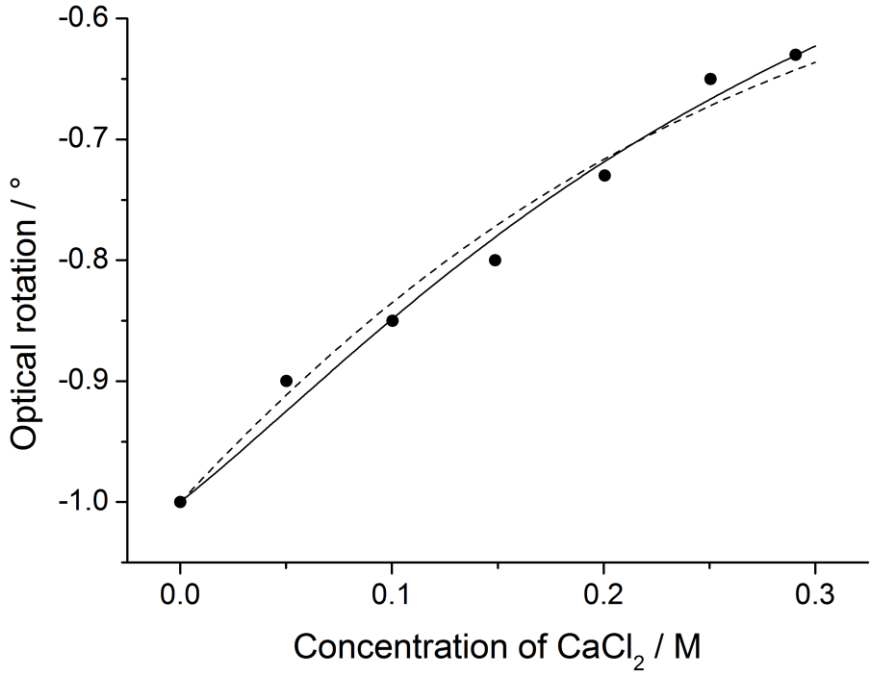

Figure 31 Optical rotation of L-gulonate (Gul^-) as a function of $CaCl_2$ concentration. Experimental conditions: T = (25 ± 2) °C, I = 1 M (NaCl); $[Gul^-]_T$ = 0.200 M, $[Ca^{2+}]_T$ = 0–0.291 M. Symbols refer to the measured data. Dashed or solid lines were calculated by assuming the formation of the 1:1 or the 1:1 and 1:2 complexes.

Similarly to the situation of $Gluc^-$ and $Hpgl^-$, this minor variation arises from the fact that the overall structure of the ligand (which is, in equilibrium, the sum of many coexisting conformations) does not vary markedly upon complexation. This is consistent with the already stated weak metal-ligand interactions which leads to small distortion of the complexed anion.

The specific rotations of $CaGul^+$ and $CaGul_2^0$ were estimated using the expression analogous to eq. 49. Keeping $[\alpha]$ of Gul^- at –12.81° (obtained from the first point) and fitting that of the

1:1 complex, the *FP* was calculated to be 0.02°, which is essentially the same when $CaGul_2^0$ is also included in the model. This can be explained with thelow-extent formation the 1:2 species.

The calculated specific rotations are as follows: $[\alpha_{CaGul^+}] = -4.0(6)$ (only $CaGul^+$ is formed) as well as $[\alpha_{CaGul^+}] = -1.0(3.0)$ and $[\alpha_{CaGul_2^0}] = -13.0(4.5)$ (both species are formed). It is clearly seen that these parameters are accompanied with relatively large errors due to the overall small experimental change (even smaller than that was observed for $Gluc^-$).

5.3.3. Structure optimization of the $CaGul^+$ solution species

In order to obtain further details regarding the structure of the $CaGul^+$ complex, quantum chemical calculations were performed. The ^1H and ^{13}C NMR spectroscopic experiments support the coordination of the second and/or the third OH group to the metal ion (in addition to COO^-). Previously, the binding sites were reported to be the C2-OH, C3-OH, C4-OH groups for Cu(II) [30] and the C2-OH and C4-OH groups for Pr(III) [31]. Considering these observations and our results, the COO^-, C2-OH, C3-OH and the C4-OH moieties can be involved in the metal complexation (depending on the metal ion in question). Thus, structures with such coordination motifs were investigated in the present study.

To get chemically meaningful representation of the first coordination shell of Ca^{2+}, five H_2O molecules were implemented in the initial structures. Hence, the coordination number (CN) of the metal ion was 6 or 7 depending on the denticity of the ligand. (Concerning $CaCl_2$ solutions, the CN varies between 6 and 8 as was deduced from X-ray diffraction (XRD) [165,166], neutron diffraction (ND) [166,167] and EXAFS studies [168,169] as well as molecular dynamics (MD) simulations [170].)

In the two lowest-energy isomers, the hydrated Ca^{2+} ion is bound to the COO^-, C2-OH and C3-OH groups or to the COO^-, C3-OH and C4-OH groups. These structures will be denoted as CaGul_123 and CaGul_134 (Figures 32a-b); the numbers refer to the coordination mode.

In CaGul_123 (Figure 32a) gulonate acts as a tridentate ligand, furthermore, Ca^{2+} is surrounded by three additional water molecules. (The fourth and fifth H_2O molecule included in the initial geometry establishes hydrogen bonds with other metal-coordinated H_2O molecules.) Thus, the CN of the metal ion is 6. Of the three calcium(II) gulonate interactions, the strongest is established with COO^- (2.342 Å) whilst the average Ca(II)-water distance is 2.40 Å. (Selected bond lengths are listed in Table 14). Regarding $CaCl_2$ solutions, the average Ca(II)-O bond

length were found to be between 2.40–2.46 Å depending on the experimental method (XRD, ND or EXAFS) applied [165–169].

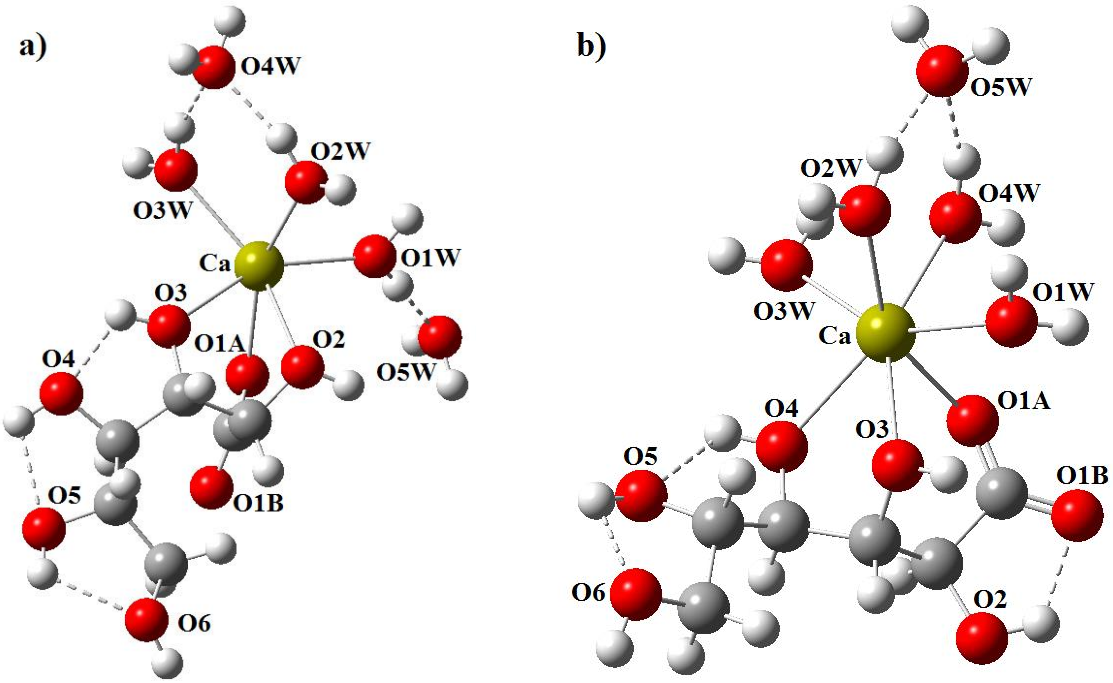

Figure 32 Optimized structures of the $CaGul^+$ complex with different coordination modes (CaGul_123: part a and CaGul_134: part b). The calculations were performed at the B3LYP/6–311++g(d,p) level while solvent effects were taken into account by the IEFPCM model. The hydrogen bonds are visualized with dashed lines.

Additionally, it is seen that two five-membered chelate rings are formed between Ca^{2+} and the C2-OH as well as the C3-OH groups which was found for the $CaGluc^+$ complex (at Hartree-Fock level) [37]. Moreover, there is an intramolecular hydrogen bond network between the OH groups which is probably an additional factor affecting the overall stability.

The other isomer, CaGul_134 (Figure 32b) has lower free energy by 2.3 $kJ \cdot mol^{-1}$, which is not significant as it is commensurate to the energy of thermal motion (2.5 $kJ \cdot mol^{-1}$ at 298.15 K). The metal ion is coordinated stronger by the COO^- group compared to CaGul_123 (2.301 *vs.* 2.342 Å) as well as it is attached to four water molecules (thus, CN = 7). Similarly to CaGul_123, intramolecular hydrogen bonds are formed of which the strongest is the one being between COO^- and C2-OH. The different coordination mode, on the other hand, yields one five- and one six-membered chelate ring.

Table 14 Selected distances for the $[CaGluc]^+$ complex calculated at the B3LYP level applying the 6–311++g(d,p) basis set. Solvent effects were taken into consideration by the IEF-PCM model. The numbering is seen in Figure 32.

Ca-O distances			Hydrogen bond distances				
Atom	Atom	Ca-O(Å)	D[a]	H[a]	A[a]	D-H (Å)	H-A (Å)
			CaGul_123				
Ca	O1A	2.342	O3	H(O3)	O4	0.969	1.957
Ca	O2	2.507	O4	H(O4)	O5	0.966	2.135
Ca	O3	2.469	O5	H(O5)	O6	0.967	2.164
Ca	O1W	2.381					
Ca	O2W	2.420					
Ca	O3W	2.407					
			CaGul_134				
Ca	O1A	2.301	O2	H(O2)	O1B	0.976	1.897
Ca	O3	2.492	O4	H(O4)	O5	0.968	2.115
Ca	O4	2.502	O5	H(O5)	O6	0.966	2.271
Ca	O1W	2.497					
Ca	O2W	2.471					
Ca	O3W	2.456					
Ca	O4W	2.482					

[a] D = donor oxygen, H = hydrogen, A = acceptor oxygen.

The relative stability calculated for these two isomeric forms, however, should be handled with care when describing dynamic equilibrium processes in these systems. The first reason is that these calculations correspond to infinite dilution, which is markedly different from the conditions under which the measurements were performed. Furthermore, numerous other conformations as well as arrangements of the coordinated H_2O molecules can be envisaged.

Regardless of these considerations, the most important results of these calculations is that (at least) two coordination modes, *i.e.*, the COO^-/C2-OH/C3-OH and the COO^-/C3-OH/C4-OH ones are possible, which draws similarities with the $CaGluc^+$ [37] and $CaHpgl^+$ [41] species concerning different linkage isomers.

Furthermore, the calculated Ca-OH_2 distances are shorter by several hundredths of an Å than the Ca-OH distances inferring that water is a very efficient competitor to the hydroxy groups for binding Ca^{2+}. Relating to thermodynamics, this phenomenon appears to be the main reason for the relatively low stability constant of these complexes as was stated previously [63].

5.4. Complexation of Ca^{2+} by L-gulonate in alkaline medium

5.4.1. Deprotonation of gulonate

The pH-potentiometric titrations were carried out in strongly alkaline solution containing $[Gul^-]_T$ = 0.100, 0.150 and 0.200 M. The systematic positive shift of the cell potential with increasing $[Gul^-]_T$ indicates the deprotonation of the anion according to eq. 9 (p. 11).

The at most 7 mV change in the potential, however, points to the low conversion of this process. This arises from that the highest pH_c measured is 13 being significantly lower than the actual pK_a determined (13.72, see also in Table 15). Nevertheless, the *FP* calculated by this model (0.4 mV) is markedly smaller than the one obtained by neglecting this reaction (3.4 mV). Similar pK_a (13.68) was determined for $Gluc^-$ under identical experimental conditions [62], while considerably lower value (13.41) was deduced for $Hpgl^-$ [41]. This difference can be attributed to the statistical effect to the number of OH groups, that is, one additional hydroxyl group decreases the value of pK_a [60].

Table 15 Deprotonation constants (log K_a) for L-gulonate (Gul^-), D-gluconate ($Gluc^-$) and D-heptagluconate ($Hpgl^-$). Data[a] correspond to T = 25 °C unless indicated differently; ± 3 *SE* is given in parentheses.

Reaction	Ionic strength and backgr. electrolyte	log K_a	Reference	Method[b]
$Gul^- + H_2O = GulH_{-1}^{2-} + H_3O^+$	1 M NaCl	–13.72(2)	p. w.[c]	H_2-Pt POT
	1 M NaCl	–13.75(3)	p. w.	^{13}C NMR
$Gluc^- + H_2O = GlucH_{-1}^{2-} + H_3O^+$	0.1 M $NaClO_4$	–13(1)[d]	36	^{13}C NMR/ GLE POT
	1 M NaCl	–13.68(3)	62	H_2-Pt POT
	1 M $NaClO_4$	–13.66(24)	61	H_2-Pt POT
$GlucH_{-1}^{2-} + H_2O = GlucH_{-2}^{3-} + H_3O^+$	1 M $NaClO_4$	–14.02(30)	61	H_2-Pt POT
$Hpgl^- + H_2O = HpglH_{-1}^{2-} + H_3O^+$	1 M NaCl	–13.41(2)	41	H_2-Pt POT

[a] During the calculations, pK_w was taken as 13.76 form ref. [132].
[b] GLE/H_2-Pt POT = potentiometry applying glass or hydrogen electrode, NMR = nuclear magnetic resonance spectroscopy.
[c] Present work.
[d] The measurements were performed at 22 °C.

To confirm that the observed potentiometric effects are associated with the ligand deprotonation, ^{1}H and ^{13}C NMR measurements were performed in solutions containing 0.100 M NaGul and 0–0.996 M NaOH. (By this approach, much broader pH range was available.) The ^{1}H signal positions were not sensitive to the increase of $[NaOH]_T$, but the ^{13}C NMR peaks were shifted

downfield attesting the OH deprotonation (Figure 33). (During protonation, the direction of the variations was the opposite, see Figure 17 on p. 41.)

Since the proton exchange between $GulH_{-1}^{2-}$ and Gul^{-} is fast on the ^{13}C NMR timescale, the following equation could be applied:

$$\delta = \frac{\delta_{Gul^-}[Gul^-] + \delta_{GulH_{-1}^{2-}}[GulH_{-1}^{2-}]}{[Gul^-]_T} \tag{53}$$

where δ_{Gul^-} and $\delta_{GulH_{-1}^{2-}}$ are the chemical shifts of Gul^- and $GulH_{-1}^{2-}$ in ppm, respectively. Substituting eq. (9) into eq. (53), $\log K_a$ can be calculated as a function of $[OH^-]_T$ (the chemical shifts of Gul^- were treated as fixed parameters). The results of these fittings are displayed in Figure 33.

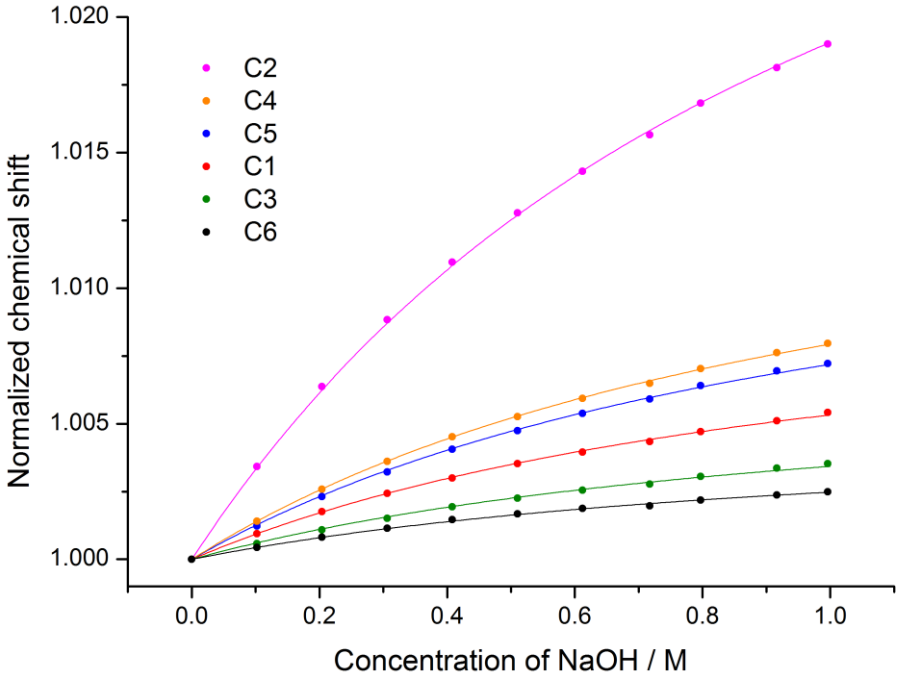

Figure 33 ^{13}C chemical shifts of L-gulonate (Gul^-) as a function of NaOH concentration. Experimental conditions: T = (25 ± 1) °C, I = 1 M (NaCl); $[Gul^-]_T$ = 0.100 M, $[OH^-]_T$ = 0–0.996 M. Symbols and solid lines refer to the measured and calculated data, respectively. The chemical shifts were normalized to those of Gul^- at $[OH^-]_T$ = 0 M.

The thus obtained constant (Table 15) agrees well with the potentiometrically determined one. The corresponding *FP* was calculated to be 0.005 ppm; the limiting chemical shifts are tabulated in Table 16.

The extent of deprotonation is as high as 50%, which pinpoints the formation of the deprotonated species. Additionally, the highest difference between the chemical shifts of Gul^- and $GulH_{-1}^{2-}$ was observed for C2 suggesting that the deprotonation occurs primarily on the C2-OH group. This assumption however, has to be handled with caution, since (unlike ^1H shifts) ^{13}C shifts do not show direct correlation with the proximity to the deprotonation site similarly to protonation (Table 5, p. 41) and Ca(II) complexation (Table 13, p. 64).

Table 16 ^{13}C chemical shifts of $GulH_{-1}^{2-}$ and their relative difference to those of L-gulonate (Gul^-). Experimental conditions: T = (25 ± 1) °C, I = 1 M (NaCl). The shifts of Gul^- were observed experimentally while those of $GulH_{-1}^{2-}$ were calculated. Additionally, ± 3 *SE* is given in parentheses.

Nucleus	$\delta_{GulH_{-1}^{2-}}$ / ppm	$\delta_{GulH_{-1}^{2-}} - \delta_{Gul^-}$ / ppm
C1	180.26(6)	1.92
C2	76.00(9)	2.83
C3	72.56(3)	0.50
C4	71.20(3)	1.13
C5	62.60(3)	1.05
C6	3.54(1)	0.31

Polarimetric measurements performed with solutions containing $[Gul^-]_T$ = 0.202 M and $[OH^-]_T$ = 0–0.996 M showed that the overall change of optical rotation was only 0.15°. This variation is very small despite that 50% of gulonate is deprotonated, therefore it is safe to assume that $[\alpha_{GulH_{-1}^{2-}}] \approx [\alpha_{Gul^-}]$.

5.4.2. Formation of trinuclear Ca(II) complexes

Similarly to the deprotonation measurements, the cell potentials at a certain added titrant volume shifted to higher values upon increasing $[NaGul]_T$ and/or $[CaCl_2]_T$ (Figure 34). Conversely, the magnitude of these variations was much larger and the *FP* was 27.4 mV omitting any complexes forming between Ca^{2+} and Gul^-.

As a next step, the formation of complexes with the general stoichiometry of $Ca_pA_qH_{-r}^{(2p-q-r)+}$ was included in the chemical model. During the course of calculations, the spectroscopically determined deprotonation constant was used. Additionally, the model contained the formation constants of the $CaOH^+$ and $Ca(OH)_2^0$ species reported previously [171].

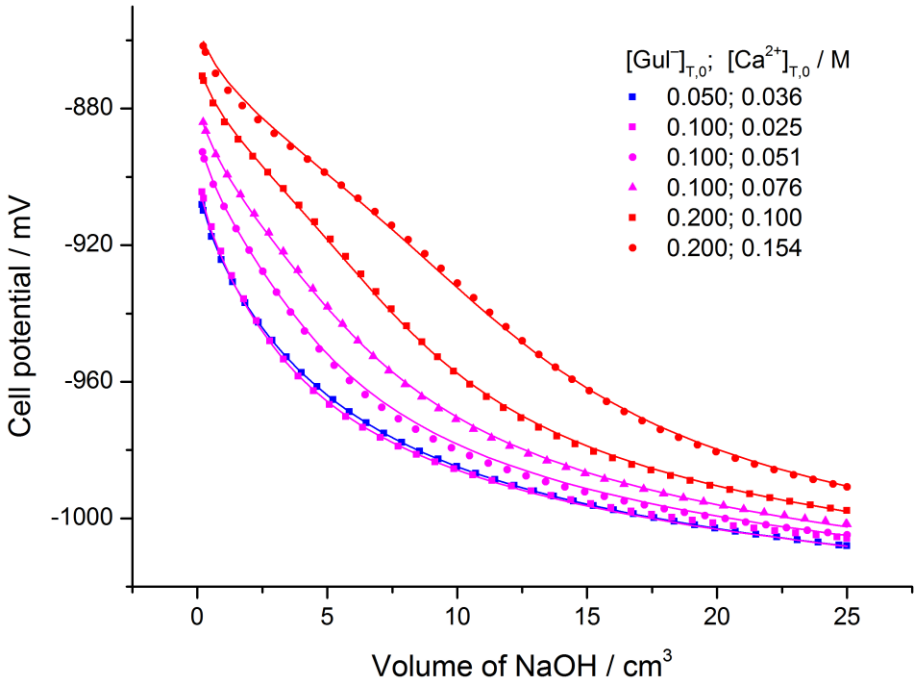

Figure 34 The pH-potentiometric titration curves of solutions containing L-gulonate (Gul^-), $CaCl_2$ and NaOH. Experimental conditions: T = (25.0 ± 0.1) °C, I = 1 M and V_0 = 70 cm^3; the initial concentrations of NaGul and $CaCl_2$ are indicated in the legend. The titrations started in the alkaline region with $[OH^-]_{T,0}$ = 0.005 M. Symbols and solid lines refer to the measured and calculated data, respectively.

Assuming the formation of the mononuclear $CaGulH_{-1}^0$ species, the *FP* could be lowered only to 9.4 mV (the corresponding log β_{11-1} was found to be –10.67). Remarkable decrease (to 0.9 mV) was achieved by taking into account the formation of two trinuclear species, *i.e.* the $Ca_3Gul_2H_{-3}^+$ and $Ca_3Gul_2H_{-4}^0$ ones. Similar observations were made upon the evaluation of the analogous potentiometric titration curves of the two structurally related ligands, $Gluc^-$ [62] and $Hpgl^-$ [41].

Conversely, the formation of 1:1:–1 species was found to be lower than 1% (with respect to $[CaCl_2]_T$), which is also justified by the very large *SE* (0.77) of log β_{11-1}. It should be noted that this complex was detected for the other two ligands, however, those measurements were performed under different analytical concentrations. On the other hand, the stability of $CaGul^+$ complex is lower than that of $CaGluc^+$/$CaHpgl^+$, which may involve the same relation for the onefold deprotonated species as well. Nevertheless, this complex was omitted from the proposed chemical model along with $CaGul^+$ and $CaGul_2^0$, whose ssumption did not improve further the *FP*.

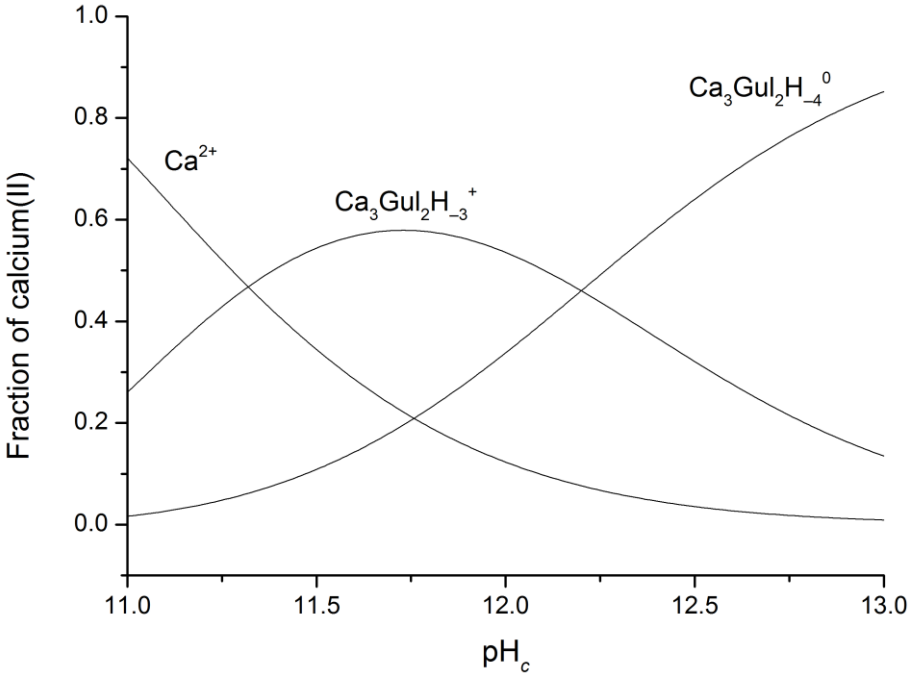

Figure 35 Speciation diagram of the Ca^{2+}/L-gulonate (Gul^{-}) system as a function of pH_c. The calculations correspond to T = 25 °C and I = 1 M (NaCl); $[Gul^{-}]_T$ = 0.200 M and $[Ca^{2+}]_T$ = 0.150 M.

The experimental and simulated data are shown in Figure 34, while the obtained log β_{pq-r} values are presented in Table 17. By the distribution diagram corresponding to $[NaGul]_T$ = 0.20 M and $[CaCl_2]_T$ = 0.15 M (Figure 35), $Ca_3Gul_2H_{-3}^{+}$ predominates between $pH_c \approx 11.3$ and 12.2, then $Ca_3Gul_2H_{-4}^{0}$ becomes the prevailing one.

To compare the results of the three ligands, the formation constants for $Gluc^{-}$ and $Hpgl^{-}$ were recalculated using the equilibrium constants reported previously for CaH_{-1}^{+} and CaH_{-2}^{0} [171]. Additionally, the formation of $CaGluc^{+}$ and $CaHpgl^{+}$ were included in these models with log β_{110} as a parameter to be fitted. This constant, however, was found to be significantly lower than those determined by Ca-ISE titrations. The reason of this difference is that these complexes are formed below 50% and pH-metric titration is an indirect method to detect these otherwise pH-independent reactions.

Concerning the multinuclear complexes found for gulonate, they were detected in solutions of both $Gluc^{-}$ [62] and $Hpgl^{-}$ [41]; however, the $Ca_2GlucH_{-3}^{0}$ was observed solely for gluconate. Interestingly, the originally proposed model of $Hpgl^{-}$ can be substituted by that of Gul^{-} (not shown in Table 17) albeit the *FP* is larger by 0.3 mV. This finding might imply closer similarity between Gul^{-} and $Hpgl^{-}$ than between Gul^{-} and $Gluc^{-}$.

Table 17 Formation constants (log β_{pq-r}) for the $Ca_pA_qH_{-r}^{(2p-q-r)+}$ complexes, where A denotes L-gulonate (Gul^-), D-gluconate ($Gluc^-$) and D-heptagluconate ($Hpgl^-$). Data[a] correspond to T = 25 °C and I = 1 M (NaCl); ± 3 *SE* is given in parentheses.

Reaction	Gul^{-b}	$Gluc^{-c}$	$Hpgl^{-c}$
$Ca^{2+} + A^- = CaA^{+d}$		0.48(8)	0.52(13)[e]
$Ca^{2+} + A^- + H_2O = CaAH_{-1}^0 + H_3O^+$		–10.88(3)	–10.65(5)
$2\ Ca^{2+} + A^- + 3\ H_2O = Ca_2AH_{-3}^0 + 3\ H_3O^+$		–33.20(6)	
$3\ Ca^{2+} + 2\ A^- + 3\ H_2O = Ca_3A_2H_{-3}^+ + 3\ H_3O^+$	–30.46(3)		
$3\ Ca^{2+} + 2\ A^- + 4\ H_2O = Ca_3A_2H_{-4}^0 + 4\ H_3O^+$	–42.66(4)	–42.45(12)	–41.64(9)

[a] During the calculations, pK_w was taken as 13.76 form ref. [132].
[b] Stability constants for Gul^- were determined in the present work.
[c] The stability constants given in refs. [41,62] were recalculated using the formation constants of the hydroxido complexes of calcium(II) from ref. [171].
[d] Further data for log β_{110} are seen in Table 9 (p. 56) and in Table 12 (p. 63).
[e] This species was not included in the original model given in ref. [41].

To summarize these results, it seems reasonable that there are more equivalent models describing the observed experimental effects in alkaline media. On the other hand, the striking similarity between the three systems is the formation of the neutral 3:2:–4 complex. Moreover, its stability was found to be highest for $Hpgl^-$ regardless of the chosen model. This outcome refers to the statistical effect of the OH groups [60], since the increased acidity of $Hpgl^-$ in the presence of metal ions resembles to the situation of ligand deprotonation (Table 15, p. 71).

5.4.3. The metal-induced deprotonation and the binding sites of the ligand

Additional polarimetric measurements were undertaken in the presence of Ca^{2+} ions at 2:1 ligand to metal ratio. Contrary to the deprotonation experiments, the rotation of 0.2 M NaGul decreases to a considerable extent (from –0.85° to –1.95°, see in Figure 36). This variation cannot be attributed to the 1:1 and the 1:2 complexes since their formation causes smaller change and to the opposite direction (Figure 31, p. 67).

This finding is somewhat surprising but can be explained with the metal ion-promoted deprotonation and the simultaneous formation of the highly stable Ca(II) complexes. This assumption is also corroborated by the appearance of an inflection point. Furthermore, it can be deduced that the structures of the free and bound ligands differ remarkably. If the deprotonation took place on one of the water molecules coordinated to the Ca(II) ion, it would not be expected to cause such distortion for Gul^-.

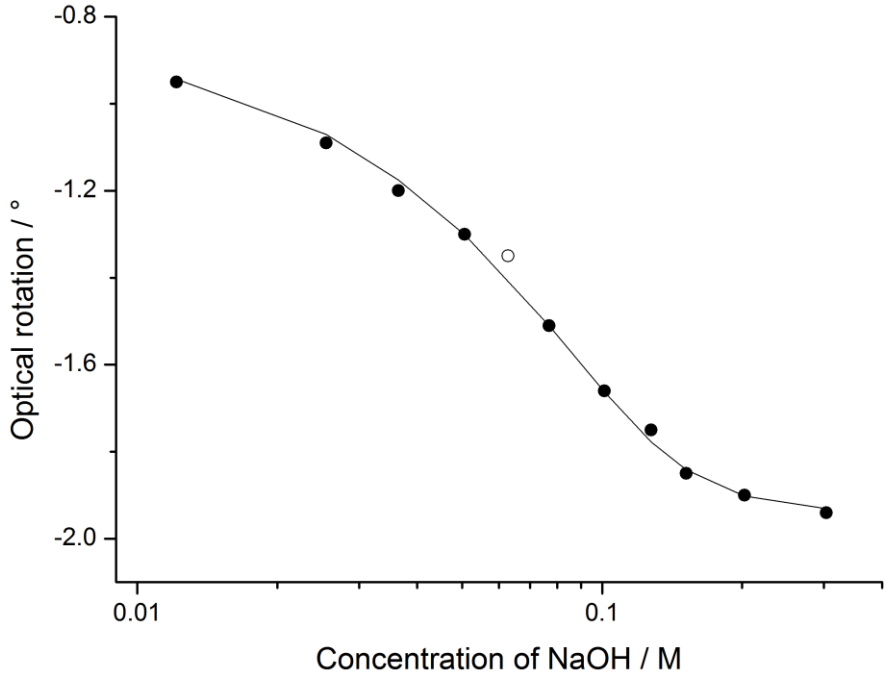

Figure 36 Optical rotation of L-gulonate (Gul^-) as a function of NaOH concentration. Experimental conditions: T = (25 ± 2) °C, I = 1 M (NaCl); $[Gul^-]_T$ = 0.202 M, $[Ca^{2+}]_T$ = 0.100 M, $[OH^-]_T$ = 0–0.304 M. Symbols refer to the measured data; solid lines were calculated by assuming the formation of various $Ca_pGul_qH_{-r}^{(2p-q-r)+}$ complexes with the stoichiometry of 1:1, 1:2, 2:1:–3 and 2:1:–4, respectively. (Empty circle: omitted point.)

Accordingly, the deprotonation at least partly associated with the OH groups. In conclusion, polarimetry – in contrast with potentiometry – is suitable to distinguish these two types of deprotonation. By the distribution diagram (not shown), the ionization of the ligand OH group starts above pH_c = 10.5 in agreement with the general scheme proposed earlier [105].

The observed rotations were evaluated by fixing the specific rotations of Gul^-, $GulH_{-1}^{2-}$, $CaGul^+$ and $CaGul_2^0$ as well as the stability products of the two latter species. Since the measurements were carried out only at one ligand to metal ratio, it was not possible to fit the stability products or the rotations of the two trinuclear species simultaneously. Therefore, the values of $\log \beta_{pq-r}$ from Table 17 were kept constant and only the $[\alpha]_D$ parameters were fitted.

The initial *FP* of 0.73° decreased to 0.02° assuming the formation of the $Ca_3Gul_2H_{-3}^+$ and the $Ca_3Gul_2H_{-4}^0$ species (the calculated curve is shown in Figure 36). The specific rotations for the 3:2:–3 and 3:2:–4 complexes were found to be –41.6(2.2) and –37.7(1.5), respectively. It cannot be deduced, however, whether all of the protons are displaced from the ligand OH groups

or from the coordinated water molecules. Nevertheless, the specific rotation of these deprotonated complexes is considerably lower than that of the free anion providing semi-quantitative proof for the metal ion-induced deprotonation.

In order to reveal the Ca(II) binding sites of the ligand, $[CaCl_2]_T$- and temperature-dependent ^{1}H NMR measurements (Figures 37a-b) were carried out. By increasing $[CaCl_2]_T$, remarkable signal broadening and downfield shift of the H2 peak can be observed (Figure 37a) reflecting the participation of the C2-OH group in the metal ion coordination, probably through its deprotonation. (Under similar conditions, each ^{13}C peak disappears preventing its use for any solution study in strongly alkaline medium.) The binding of an alcoholate group was proposed for both $Gluc^-$ and $Hpgl^-$, for which the variation of H2 signal was found to be similar.

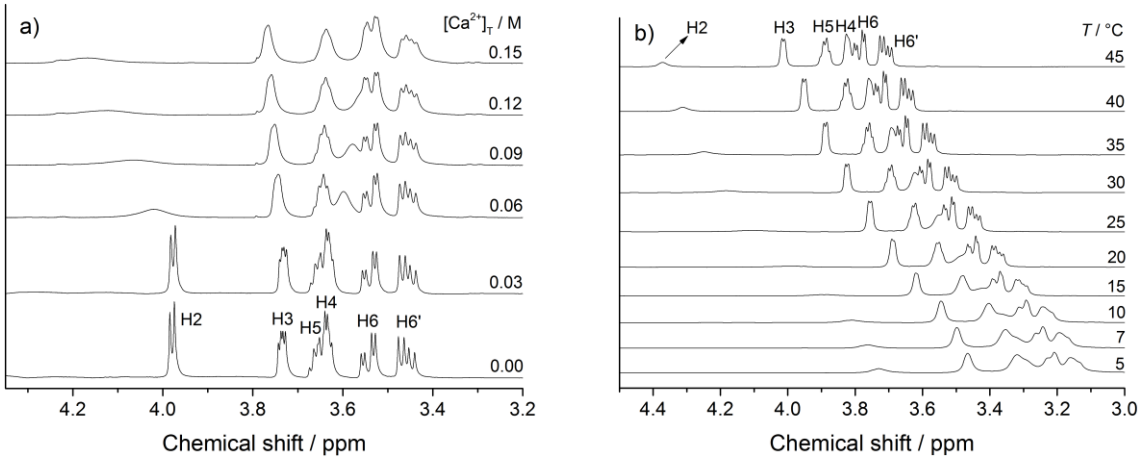

Figure 37 $CaCl_2$- (part a) and temperature-dependent (part b) ^{1}H NMR spectra of the alkaline solutions of L-gulonate (Gul^-). Experimental conditions: a) T = (25 ± 1) °C; $[Gul^-]_T$ = 0.20 M, $[OH^-]_T$ = 0.50 M, $[Ca^{2+}]_T$ = 0–0.15 M. b) T = 5–45 °C; $[Gul^-]_T$ = 0.20 M, $[OH^-]_T$ = 1.01 M, $[Ca^{2+}]_T$ = 0.10 M.

Furthermore, the peak of H4 also undergoes significant signal broadening but, unlike H2, it is shifted upfield. Nevertheless, the C4-OH group can also be considered as a binding site but its deprotonation cannot be deduced unambiguously from these NMR spectra.

The deprotonation of the ligand is supported not only by polarimetric measurements, but by the temperature-dependent (5–45 °C) ^{1}H NMR spectra (Figure 37b) as well. As the temperature decreases, the peaks of H2 and H4 exhibit significant widening due to the decrease of the ligand exchange rate. When Ca^{2+} is bound to Gul^- through the COO^- and several OH groups (neutral medium), the chemical exchange rate remains fast in the ^{1}H and ^{13}C spectra (see Section 5.3.1.,

p. 64). Hence, the present spectral changes entail stronger metal-ligand interactions (*i.e.*, Ca^{2+}-alcoholate in addition to the Ca^{2+}-carboxylate).

In conclusion, the participation of the C2-OH and C4-OH groups in the metal ion-binding can be proposed for $Ca_3Gul_2H_{-4}^0$, which is the predominant species in the concentration range employed. These binding sites found for Gul^-, however, differ from the COO^-/C2-OH/C3-OH sequence suggested for $Gluc^-$ [62] and $Hpgl^-$ [41].

Conversely, it cannot be deduced from these spectra whether the deprotonation takes place solely on the ligand or on the coordinated water molecules are involved, too. Additionally, if two coordination isomers are formed, it is also possible that the binding site is the C2-O^- in the one and the C4-O^- in the other.

5.4.4. The role of configuration: ^{1}H NMR spectra of gluconate and heptagluconate

Comparative ^{1}H NMR measurements were also performed for gluconate and heptagluconate under the same experimental conditions. The corresponding spectra of the two ligands are seen in Figures 38a-b. (The peaks were assigned previously in refs. 37 and 41.)

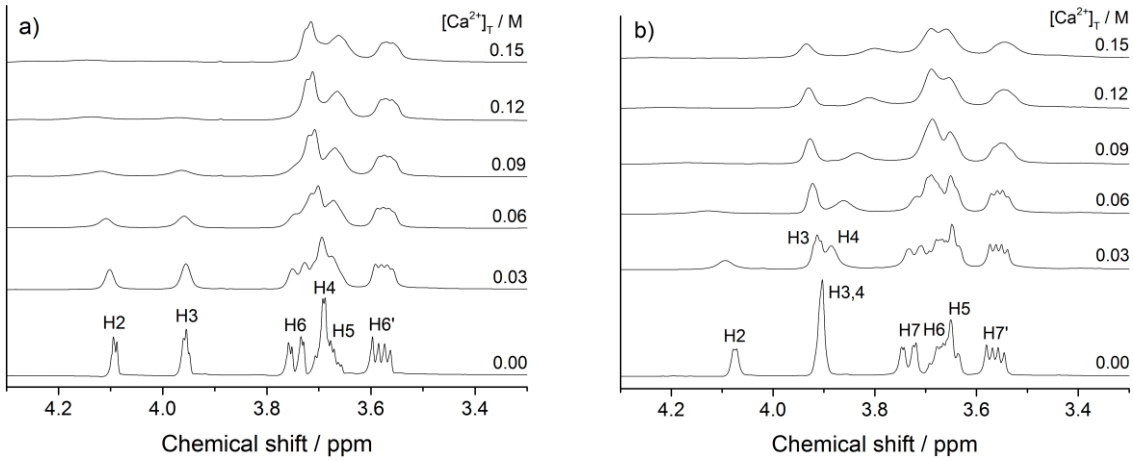

Figure 38 $CaCl_2$-dependent ^{1}H NMR spectra of the alkaline solutions of D-gluconate ($Gluc^-$, part a) and D-heptagluconate ($Hpgl^-$, part b). Experimental conditions: T = (25 ± 1) °C; $[Gluc^-]_T$ or $[Hpgl^-]_T$ = 0.20 M, $[OH^-]_T$ = 0.50 M, $[Ca^{2+}]_T$ = 0–0.15 M.

The peaks of H2/H3 ($Gluc^-$, Figure 38a) or H2 ($Hpgl^-$, Figure 38b) show remarkable peak broadening and downfield shift upon increasing $[CaCl_2]_T$. Thus, the most probable metal-binding sites of the ligand are the C2-OH and C3-OH groups for $Gluc^-$ and the C2-OH group for $Hpgl^-$ in agreement with previous observations [41,62]. The H3 or H4 signal of heptagluconate,

similarly to H4 of gulonate, shifts upfield. Since these two signals are coalesced, the second binding site cannot be unambigously assigned. Hence, a much more alkaline sample was investigated in which these two peaks were well-separated.

The spectra obtained in samples containing 2.0 M NaOH as well as 0 and 0.05 M $CaCl_2$ (Figure 39a) show convincingly that the peak of the lower chemical shift corresponds to the binding site of the complex (in addition to H2). Contrary to previous assignments, this peak is H4 instead of H3. Indeed, up to 0.1 M NaOH, the order of the signals are: H2 > H4 > H3 as it was assigned earlier [41]. However, at 0.5 M NaOH, these two peaks merge as confirmed by NaOH-dependent spectra of $Hpgl^-$ (Figure 39b). Increasing the base concentration further, the peaks are splitted again but the order of the chemical shifts changes to H2 > H3 > H4.

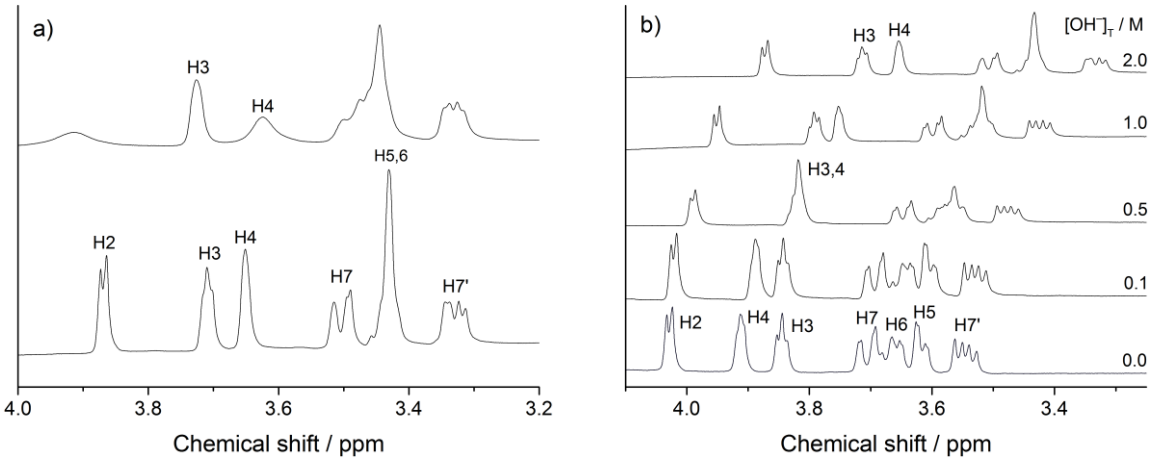

Figure 39 $CaCl_2$- (part a) and NaOH-dependent (part b) ^1H NMR spectra of the alkaline solutions of D-heptagluconate ($Hpgl^-$). Experimental conditions: T = (25 ± 1) °C; a) $[Hpgl^-]_T$ = 0.20 M, $[OH^-]_T$ = 2.0 M, $[Ca^{2+}]_T$ = 0 (lower spectrum) or 0.05 M (upper spectrum), b) $[Hpgl^-]_T$ = 0.10 M, $[OH^-]_T$ = 0–2.0 M.

Accordingly, the coordination sites of $Hpgl^-$ seem to be same as those of Gul^-, *i.e.*, the C2-OH and C4-OH groups: the H2 peak is shifted downfield, while the H4 peak is shifted upfield for both ligands. This allows to conclude that this pronounced similarity stems from the similar arrangement of the OH groups. Although these two compounds differ in the relative configuration, the C2-OH and C3-OH groups are in *erythro*, while the C3-OH and C4-OH groups are in *threo* position (see in Figure 7, p. 17).

On the contrary, the binding sites are the *threo* C2-OH and C3-OH groups for $Gluc^-$ (beside COO^-, see Figure 7). Regarding structural aspects, it seems likely that the *threo* or *erythro* configuration accounts for the differences in the coordination mode. That is, when the

$^{-}$OOC-C2-O^{-} binding moiety has already been formed, the spacing of the C3-OH group (relative to that of C2-OH) determines whether the C3-OH or the C4-OH group is preferred in the Ca^{2+}-coordination.

These results can be regarded as the extension of the coordination rules proposed for sugar alcohols by Angyal and co-workers [71]. Accordingly, the order of complex stabilities in neutral medium is as follows: *threo*-1,2-*threo*-2,3 > *threo*-1,2-*erythro*-2,3 triol. When it comes to deprotonation, both the C2-OH and C3-OH groups can participate in the Ca^{2+} ion coordination in the case of *threo-threo* configuration. On the contrary, the C2-OH and C4-OH groups are preferred in the case of *threo-erythro* arrangement. This proposed scheme is, however, gives only qualitative order. To elucidate the differences at a quantitative level other factors are required to be considered, such as statistical effects, *etc*.

Nevertheless, the present work sheds light on the crucial role of configuration concerning the formation of deprotonated Ca(II) complexes. Furthermore, the proposed coordination properties may be valid for other complexes formed with carbohydrate derivatives, too.

5.5. Complexation of Nd^{3+} by D-gluconate in the pH range of 2–8

5.5.1. The impact of complexation on the absorption spectra and potentiometric titrations

The gluconate-dependent visible spectra of 0.075 M $NdCl_3$ (Figure 40) exhibit considerable redshift as well as increasing absorbance upon increasing $[Gluc^{-}]_T$. Hence, the complex formation is strongly indicated in this series in agreement with previous results [89]. Accordingly, the predominant species are expected to be the $NdGluc^{2+}$, $NdGluc_2^{+}$ and the $NdGluc_3^{0}$ ones.

The spectra differ markedly upon addition of NaOH (Figure 41a). At a ligand to metal ratio of 1:1, the hypersensitive transition of Nd^{3+} is shifted toward higher wavelengths as the pH increases. In parallel, the absorbance increases as well, nevertheless, the shape of the spectra differs significantly from that observed for the previous series. Furthermore, the absence of one single isosbestic point indicates the formation of more than two deprotonated complexes.

Upon increasing the ligand to metal ratio to 2.5:1 (Figure 41b), a new isosbestic point shows up at 583 nm above $[NaOH]_T$ = 0.080 M referring to further deprotonation. Simultaneously, the absorbance starts to decrease above this base concentration, thus, this putative complex has smaller molar absorptivity. Similar changes were observed for the systems with 5:1 molar ratio (not shown).

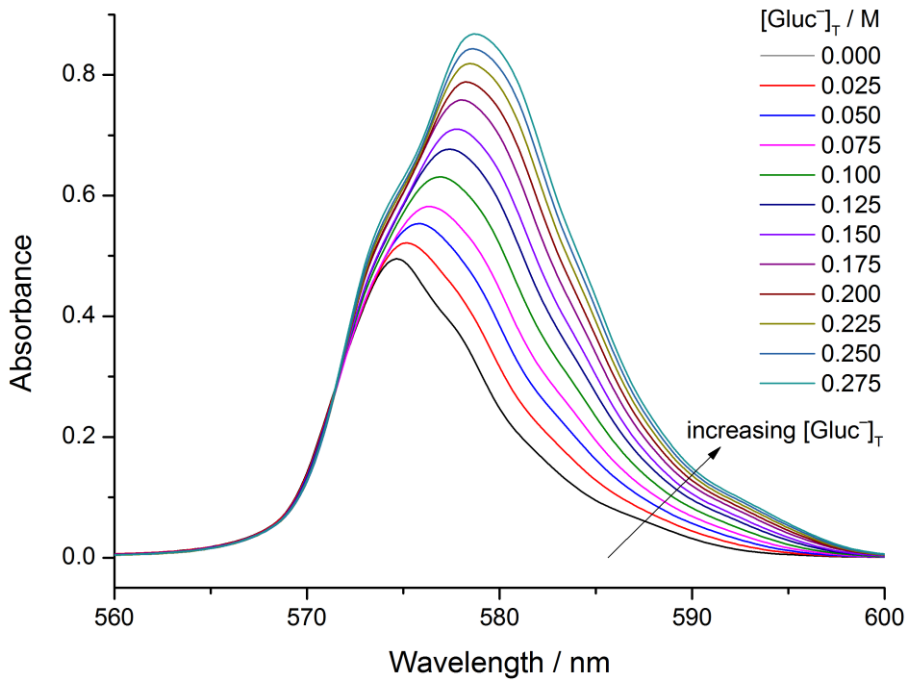

Figure 40 Gluconate ($Gluc^-$) dependence of the visible spectra of $NdCl_3$. Experimental conditions: T = (25 ± 2) °C, I = 1 M (naCl); $[Nd^{3+}]_T$ = 0.075 M, $[Gluc^-]_T$ = 0–0.275 M.

The HCl-dependent spectra (not shown) at 1:1 ratio obviously show that with increasing $[HCl]_T$, the ligand is gradually displaced from the complexes because of its protonation. Further isosbestic points do not appear excluding the formation of any protonated complex. At 2.5:1 and 5:1 ratios, the extent of this displacement is lower due to stronger complex formation.

It is known for Pr(III) and other lanthanides [31,126] that binuclear complexes can be detected when the concentration of the metal ion is varied. Since in the previous works this approach was omitted [121–125], we studied the $NdCl_3$-dependence by applying $[NdCl_3]_T$ = 0.025–0.075 M with varying concentrations of NaGul, NaOH and HCl.

Concerning potentiometry, remarkable effects were observed when solutions with different $[NdCl_3]_{T,0}$, $[NaGluc]_{T,0}$ and $[NaOH]_{T,0}$ were titrated with HCl. These titrations curves are displayed in Figure 42. The presence of the inflection points, similarly to the isosbestic points, corroborates the formation of various deprotonated complexes. At 12:1 and 6:1 ligand to metal ratios (black and blue symbols), the simultaneous protonation of $Gluc^-$ is seen, while this equilibrium cannot be clearly observed at the ratios of 1.6:1 (purple symbols) and 1:1 (red symbols) due to stronger complex formation.

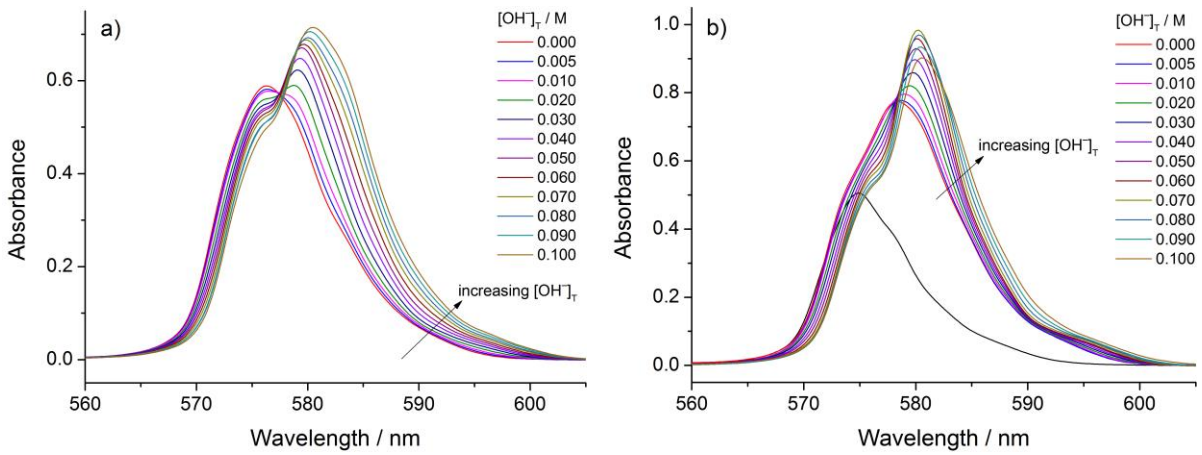

Figure 41 NaOH-dependent visible spectra of the Nd(III) gluconate ($Gluc^-$) system at 1:1 (part a) and 2.5:1 (part b) ligand to metal ratio. Experimental conditions: T = (25 ± 2) °C, I = 1 M (NaCl); $[Nd^{3+}]_T$ = 0.075 M, $[OH^-]_T$ = 0–0.100 M, a) $[Gluc^-]_T$ = 0.075 M, b) $[Gluc^-]_T$ = 0.188 M.

5.5.2. Evaluation of the spectrophotometric and potentiometric data

Despite the sensitivity of the absorption spectra upon complexation, the observed shift is known to be smallercompared to those of transition metals. Thus, the aim of simultaneous fitting was to improve the accuracy of the determined stability constants and to obtain a chemical model, which is supported by both methods.

As a result, the evaluation of the absorption spectra and the potentiometric titration curves revealed the formation of four mononuclear complexes, namely the $NdGluc^{2+}$, $NdGluc_2^+$, $NdGluc_3^0$ and the $NdGlucH_{-2}^0$ ones. The *FP* (which now comprises the differences from both photometric and potentiometric data) was found to be 2.69. The calculated curves are indicated as dashed lines in Figure 42. It is obvious that this model fails to describe the measured data below $V \approx 5$ cm^3.

Assuming the formation of the $NdGlucH_{-1}^+$, then the $NdGluc_2H_{-1}^0$ species proposed previously [121–125], the *FP* decreases to 1.06. In this case, however, the pK_a of $NdGluc^+$ will be higher than that of $NdGluc_{-1}^0$, which is contradiction. Moreover, the lowest *FP* of the potentiometric data set is still 3.8 mV.

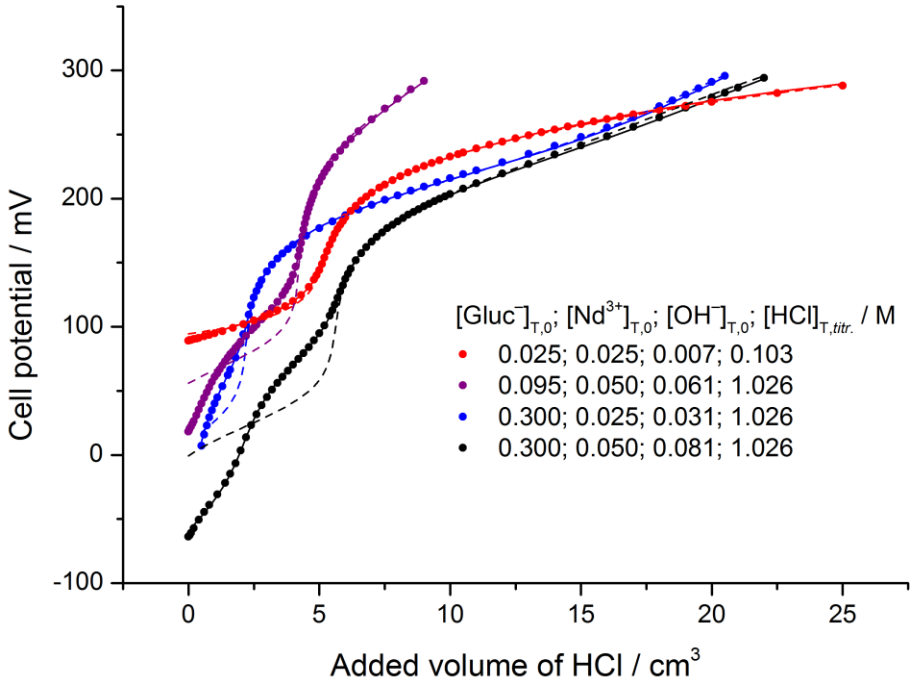

Figure 42 Potentiometric titration curves of solutions containing D-gluconate ($Gluc^-$), $NdCl_3$ and NaOH. Experimental conditions: T = (25.0 ± 0.1) °C, I = 1 M, V_0 = 70 cm^3; the initial concentrations of NaGluc, $CaCl_2$, NaOH and the titrant HCl are indicated in the legend. Symbols refer to the measured data. Dashed lines were calculated by assuming the 1:1, 1:2, 1:3 and the 1:1:–2 species. Solid lines were calculated by including the 2:3:–2 and the 2:4:–2 complexes, too.

These deviations can be appropriately corrected if two binuclear complexes, $Nd_2Gluc_3H_{-2}^+$ and $Nd_2Gluc_4H_{-2}^0$, are included in the model instead of the 1:1:–1 and 1:2:–1 species. The average *FP* decreases to 0.57, while the potentiometric *FP* is between 0.7 and 1.4 mV (solid lines in Figure 42). The average *FP* can be further decreased only by *ca.* 5% with the inclusion of the $Nd_2Gluc_2H_{-3}^+$ complex, whose Cu(II) analogue was reported [30]. The potentiometric *FP*, however, slightly increases and the thus obtained formation constant for $NdGluc_3^0$ ($\log \beta_{13}$ = 5.16) significantly deviates from the literature value (5.53 or 5.60) [89] obtained at the same temperature and ionic strength. Similarly, the involvement of the hydroxido complexes of Nd^{3+} [117,118] does not improve the fit while their molar absorbance spectra are ill-defined.

Based on these considerations, the chemical model consisting of $NdGluc^{2+}$, $NdGluc_2^+$, $NdGluc_3^0$, $NdGlucH_{-2}^0$, $Nd_2Gluc_3H_{-2}^+$ and $Nd_2Gluc_4H_{-2}^0$ was accepted in the present study. It has to be mentioned that the formation of each species (relative to $[Nd^{3+}]_T$) reaches 50%. The calculated stability products with literature data are presented in Table 18. The protonation constant of $Gluc^-$ is in good agreement with those determined under the same temperature and ionic strength including our results, too (Table 4, p. 37).

Additionally, the log β_{11}, log β_{12} and log β_{13} constants are in agreement with the corresponding literature data (Table 18). The stepwise formation constants of the coordination of the second and third gluconate (*i.e.*, log K_{12} = log β_{12} – log β_{11} = 1.88 and log K_{13} = log β_{13} – log β_{12} = 1.23) meet with statistical expectations.

Table 18 Formation constants (log β_{pq-r}) for the $Nd_pGluc_qH_{-r}^{(3p-q-r)+}$ complexes where $Gluc^-$ denotes D-gluconate. Data[a] correspond to T = 25 °C if otherwise not indicated; ± 3 *SE* is given in parentheses.

Reaction	Ionic strength and backgr. electrolyte	log β_{pq-r}	Reference	Method[b]
$Gluc^- + H_3O^+ = HGluc + H_2O$[c]	1 M NaCl	3.352(4)	p. w.[d]	SPM/POT
$Nd^{3+} + Gluc^- = NdGluc^{2+}$	1 M NaCl	2.44(2)	p. w.	SPM/POT
	1 M $NaClO_4$	2.55(5)	89	POT
	1 M $NaClO_4$	2.59(5)	89	SPM
	not indicated	2.72	122	POT
	not indicated	2.66(3)	123	POT
	not indicated	2.37	125[e]	POT
$Nd^{3+} + 2\ Gluc^- = NdGluc_2^+$	1 M NaCl	4.32(2)	p. w.	SPM/POT
	1 M $NaClO_4$	4.45(5)	89	POT
	1 M $NaClO_4$	4.52(7)	89	SPM
	not indicated	4.70(9)	123	POT
$Nd^{3+} + 3\ Gluc^- = NdGluc_3^0$	1 M NaCl	5.45(2)	p. w.	SPM/POT
	1 M $NaClO_4$	5.60(15)	89	POT
	1 M $NaClO_4$	5.53(7)	89	SPM
$Nd^{3+} + Gluc^- + H_2O = NdGlucH_{-1}^+ + H_3O^+$	not indicated	–3.73	122	POT
	not indicated	–3.53	125[e]	POT
$Nd^{3+} + Gluc^- + 2\ H_2O = NdGlucH_{-2}^0 + 2\ H_3O^+$	1 M NaCl	–9.51(2)	p. w.	SPM/POT
	not indicated	–9.96	122	POT
	not indicated	–10.19	125[e]	POT
$2\ Nd^{3+} + 3\ Gluc^- + 2\ H_2O = Nd_2Gluc_3H_{-2}^+ + 2\ H_3O^+$	1 M NaCl	–1.97(3)	p. w.	SPM/POT
$2\ Nd^{3+} + 4\ Gluc^- + 2\ H_2O = Nd_2Gluc_4H_{-2}^0 + 2\ H_3O^+$	1 M NaCl	–0.85(5)	p. w.	SPM/POT

[a] During the calculations, pK_w was taken as 13.76 form ref. [132].
[b] SPM = spectrophotometry, POT = potentiometry applying glass electrode.
[c] Further values for log K_p (= log β_{011}) are seen in Table 1 (p. 7) and Table 4 (p. 37), respectively.
[d] Present work.
[e] The measurements were performed at 32 °C.

The highest discrepancy is observed for the $NdGlucH_{-2}^0$ complex. That is, our log β_{11-2} is about a half order of magnitude higher than those reported in refs. [122,125]. If this difference is not the consequence of the different electrolyte concentration applied, it can be attributed to the binuclear species, whose formation affects considerably the calculated value of log β_{11-2}.

The stoichiometric ratio of the hitherto unknown binuclear complexes is 3:2 and 4:2, which seems reasonable as high ligand to metal ratios were applied during potentiometric titrations. Additionally, as the analytical concentration increases, the formation of these binuclear species

becomes preferred because of the Le Chatelier's principle. By the same token, the formation of deprotonated mononuclear complexes ($NdGlucH_{-1}^{+}$ and $NdGluc_2H_{-1}^{0}$) will be suppressed. Previous studies, on the other hand, were conducted using low metal ion and ligand concentrations, hence the difference between the chemical models.

It is interesting to note that the existence of $Nd_2Gluc_3H_{-2}^{+}$ and $Nd_2Gluc_4H_{-2}^{0}$ reflects the affinity of Nd(III) to dimerize: without gluconate, the metal ion is known to form $Nd_2(OH)_2^{4+}$ [117,188]. It can be envisaged that on the coordination of gluconate, its highly positive net charge can decrease resulting in the stabilization of this species.

With regard to the photometric outcome of data evaluation, the calculated molar absorbance spectra are depicted in Figure 43. The spectra of the 1:1, 1:2 and 1:3 complexes are very similar to those determined before [89].

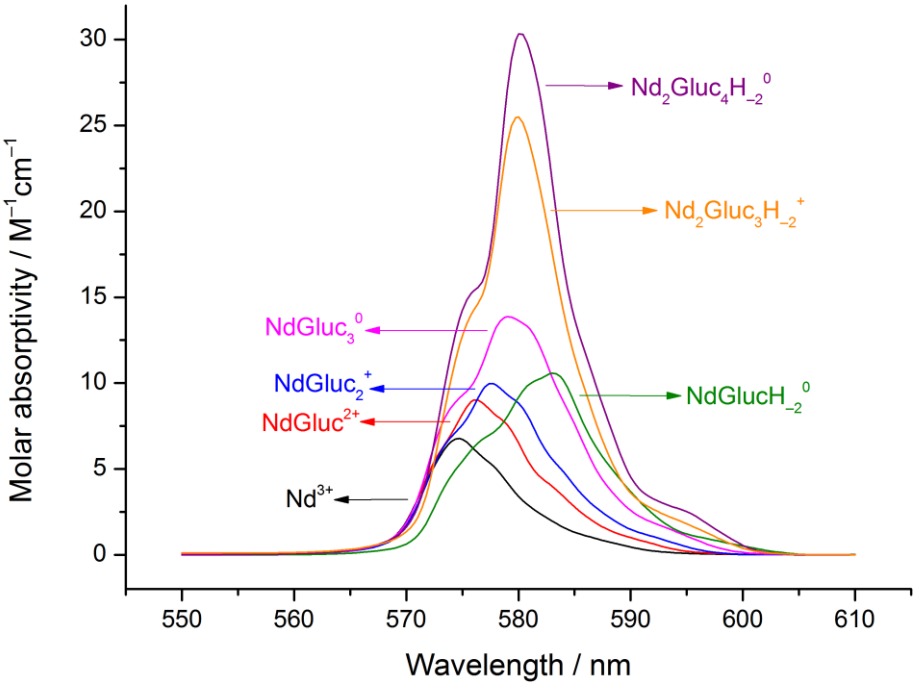

Figure 43 Molar absorbance spectra of the Nd(III) aqua-ion and its gluconate complexes. Experimental conditions: T = (25 ± 2) °C, I = 1 M (NaCl).

The speciation diagram calculated *via* using the stability products obtained in the present study with $[NdCl_3]_T$ = 0.075 M and $[NaGluc]_T$ = 0.188 M is shown in Figure 44. Between pH_c = 2 and 2.5, the $NdGluc_2^{+}$ complex is predominant, then $NdGluc_2^{+}$ is the determining species

up to pH ≈ 5. Above this pH, the two binuclear complexes are preponderant, while increasing the pH further, the neutral $NdGlucH_{-2}^{0}$ becomes the prevailing species.

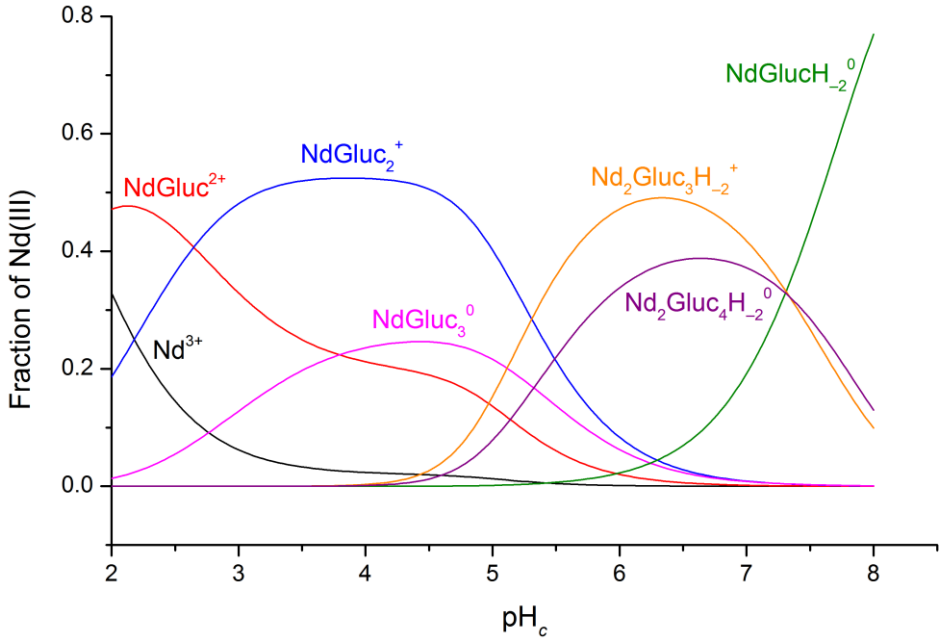

Figure 44 Speciation diagram of the Nd^{3+}/D-gluconate ($Gluc^{-}$) system as a function of pH_c. The calculations correspond to T = 25 °C and I = 1 M (NaCl); $[Gluc^{-}]_T$ = 0.188 M and $[Nd^{3+}]_T$ = 0.075 M.

5.5.3. Solubility aspects and relevance to radioactive waste repositories

Studying 1:1 and 2.5:1 ligand to metal ratios, a mauve-colored precipitate slowly appears at $[NaOH]_T$ > 0.1 M. At 2.5:1 ratio and 0.1 M NaOH, pH_c was calculated to be 7.33 by our model. Without gluconate, the solubility of Nd^{3+} (in terms of log ($[Nd^{3+}]_T/c$)) at pH = 7.3 is about −3.5 (I = 0.5 M, for crystalline $Nd(OH)_{3(s)}$) [2] or −2.8 (I = 1 M, for crystalline $Nd(OH)_{3(s)}$) [117]. Our observations show that in presence of gluconate even 0.075 M $NdCl_3$ (*i.e.*, (log ($[Nd^{3+}]_T/c$ = −1.1) can be kept in the solution phase. Consequently, $Gluc^{-}$ enhances the solubility of Nd^{3+} through complexation by at least one order of magnitude implying its significance in mobilizing radionuclides under the conditions of waste repositories.

A speciation diagram relating to these conditions is depicted in Figure 45. By increasing pH_c from 6 to 8, log ($[Nd^{3+}]_T$/M) decreases from −2.5 to −5.5 when aged $Nd(OH)_{3(s)}$ is the solubility-controlling solid phase [2]. From the point of view of the ligand, $[NaGluc]_T$ = 0.01 M is the upper limit considered in numerous solubility studies [6].

To extend our results to such low concentrations, the 1:1:−1 and 1:2:−1 complexes need to be taken into account. The relation of pK_a ($NdGluc^{2+}$) < pK_a ($NdGlucH_{-1}^{+}$) must be valid in agreement with those reported in ref. [125] (*i.e.*, 5.90 < 6.64 at T = 32 °C). Therefore pK_a = 5.90 was chosen for $NdGluc^{2+}$. In connection with the $NdGluc_2^{+}$ complex, to our best knowledge, pK_a = 6.18 (T = 25 °C, I = 0.2 M) [124] is the only reported data. Using this literature values and our log β_{11} and log β_{12} constants (Table 18), we estimated log β_{11-1} as –3.46 and log β_{12-1} as −1.86. The distribution diagram then was calculated applying these estimated constants together with our data for log β_{11}, log β_{12}, log β_{13}, log β_{11-2}, log β_{23-2} and log β_{24-2}.

It is seen in Figure 45 that the 1:1:−2 complex is formed to the highest extent up to log ($[Nd^{3+}]_T$/M) ≈ −4.8 (the $NdGlucH_{-1}^{+}$ and $NdGluc_2H_{-1}^{0}$ species are also present in considerable amounts). Above this concentration, only the 1:1, 1:2 and 1:3 species are present. In the context of waste repositories, these calculations are still estimations as there can be differences in the ionic strength, temperature, the actual form in the solid phase, furthermore, the log β_{11-1} and log β_{12-1} constants were composed of our and literature data.

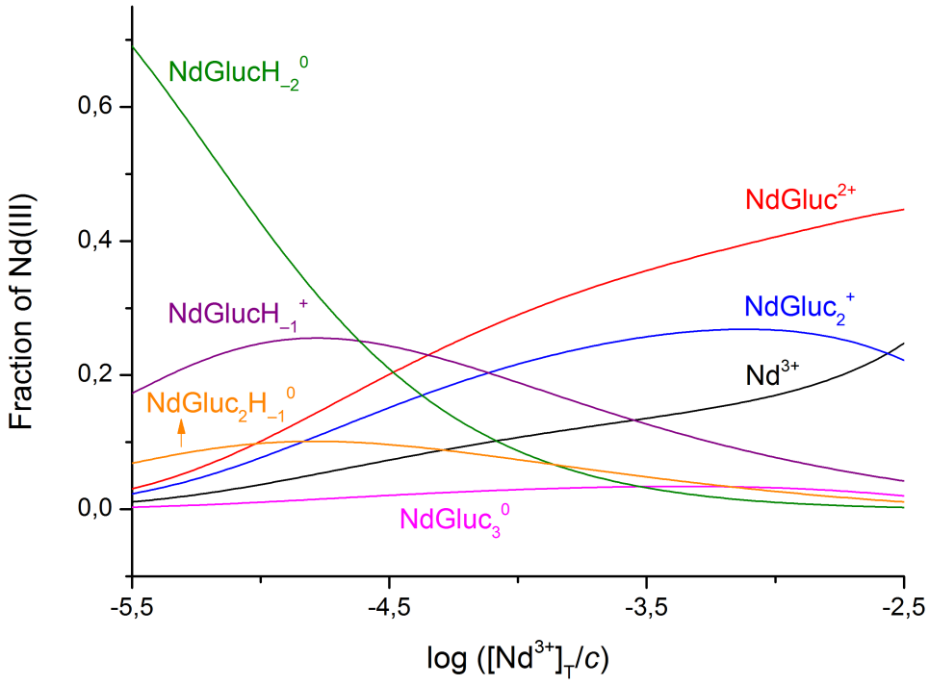

Figure 45 Speciation diagram of the Nd^{3+}/D-gluconate ($Gluc^{-}$) system as a function of log ($[Nd^{3+}]_T$/M). The calculations correspond to T = 25 °C and I = 1 M (NaCl); $[Gluc^{-}]_T$ = 0.01 M and $[Nd^{3+}]_T$ = 0.075 M.

Nevertheless, it is obvious that the binuclear species do not affect the equilibria taking place under the conditions of waste repositories. The situation is the same when the speciation is plotted as a function of pH_c with log ($[Nd^{3+}]_T$/M) being kept at −5.5 (not shown). Based on the physicochemical similarities between Ln(III) and An(III) ions [2,109,112], it may be proposed that only the mononuclear complexes need to be considered when modeling the speciation of the An(III)/$Gluc^-$ systems at 25 °C.

5.5.4. The effect of Nd^{3+} on the ^1H and ^{13}C NMR spectra of gluconate

Lanthanides induce paramagnetic shift, and significant peak broadening occurs due to the interaction between the unpaired electrons and the NMR active nucleus. This effect was scrutinized extensively including neodymium(III) [172]. In the case of strong interactions, some signals are significantly more shifted and/or broadened than the others allowing to find the binding sites of the ligand. These spectral changes were utilized to study the Pr(III)- and Eu(III)-$Gluc^-$ complexes [31,126,127].

As the concentration of $NdCl_3$ increases from 0.005 to 0.020 M, all ^1H peaks of 0.1 M NaGluc exhibit marked shift and broadening even at the highest ligand to metal ratio (Figure 46). Of these multiplets the strongest broadening is seen for the H2 and H3 nuclei (meanwhile, pH_{exp} decreases from *ca.* 7 to 5).

Speciation calculations show that in this solution series the ligand is distributed among the free ion (55%), the $NdGluc_2^+$ (19%) and the $NdGluc_3^0$ complexes (21%). Accordingly, the observed changes can be attributed to these species, for which the main coordination sites are the OH groups attached to the C2 and C3 carbon atoms. (This assumption probably holds for the 1:1 species as well.) This coordination moiety is supported by the ^{13}C NMR spectrum of 0.1 M NaGluc and 0.005 M $NdCl_3$. In addition to the peaks of C2 and C3, the signal of C1 also disappears pointing to the plausible coordination of the COO^- anchor.

The participation of the C2-OH moiety in metal binding was proposed earlier for the $NdGluc^{2+}$ [89], and other $LnGluc^{2+}$ species, including Pr(III) [31] and Eu(III) [126]. Moreover, C3-OH was also identified as a coordination site for complexes such as $EuGluc_2^+$ [127], $CaGluc^+$ [37], $CaHpgl^+$ [41] and $CaGul^+$ (see Section 5.3.2.).

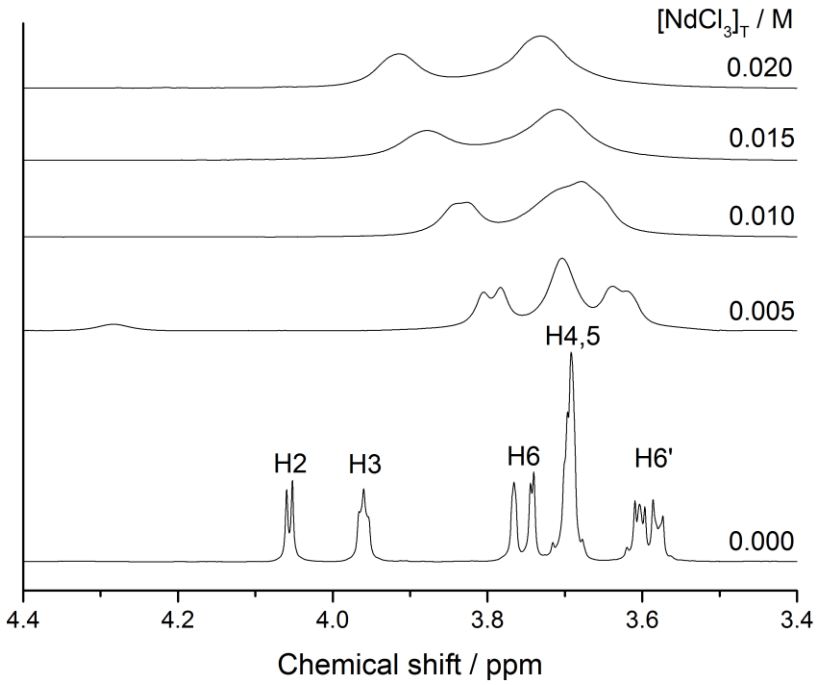

Figure 46 $NdCl_3$-dependent ^1H NMR spectra of D-gulonate ($Gluc^-$). Experimental conditions: T = (25 ± 1) °C; $[Gluc^-]_T$ = 0.100 M, $[Nd^{3+}]_T$ = 0–0.020 M.

The pH-dependence ($4 < pH_{exp} < 8$) provides further insight into the solution structure of these complexes. In the ^1H NMR spectra, the signals of H2 and H3 nuclei are shifted and broadened again markedly (Figure 47a). These observations are confirmed by the ^{13}C NMR spectra (Figure 47b) since the intensities of C2 and C3 decrease significantly (meanwhile, the C5 > C3 order swaps to C3 < C5). By the distribution diagram, these changes belong again to the 1:2 and 1:3 complexes.

From pH_{exp} = 6, further signal broadening can be detected referring to stronger interaction between the paramagnetic metal center and the ligand. The formation of deprotonated complexes accounts for these variations, since the forming alcoholate ions are very efficient binding sites (as the Nd-O bond distance shortens *via* OH deprotonation, stronger paramagnetic effect is induced).

Again the peaks of H2, H3, C2 and C3 are the most significantly affected ones, thus, their chemical environments vary the most. Consequently, either the C2–OH or the C3–OH or both groups undergo deprotonation. The first two scenarios entail that the first deprotonation occurs on a hydroxy (probably the C2–OH) group, while the second one takes place on a coordinated water molecule. The third structure, conversely, means the formation of a diolate moiety. It can

also be envisaged that the deprotonation of C2-OH is accompanied with the peak broadening of both the H2 and H3 peaks. These spectral information, however, do not allow to pinpoint the predominant structure, but the simultaneous formation of isomers is likely to occur, similarly to the Ca(II) complexes of this ligand [37].

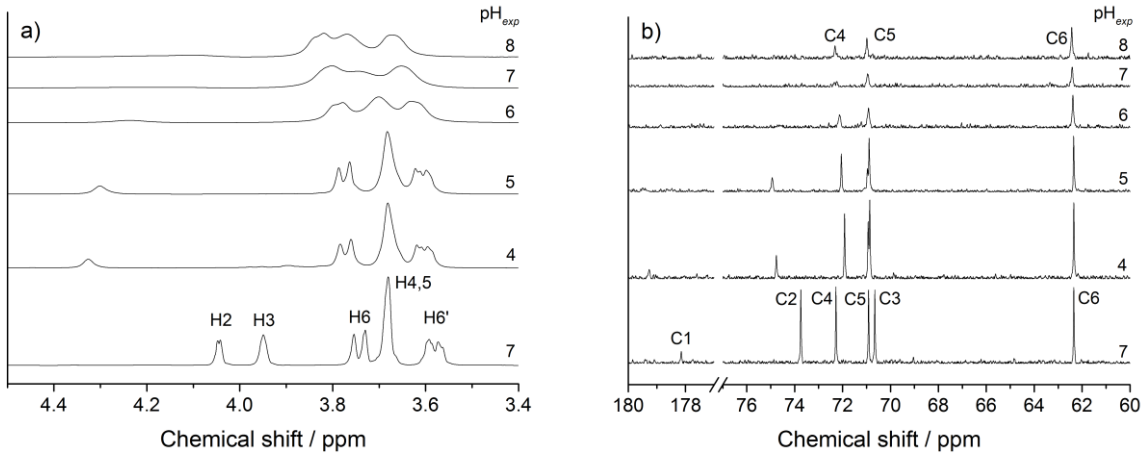

Figure 47 The pH-dependent ^{1}H part a) and ^{13}C NMR (part b) spectra of D-gluconate ($Gluc^{-}$). Experimental conditions: T = (25 ± 1) °C; $[Gluc^{-}]_T$ = 0.100 M, $[Nd^{3+}]_T$ = 0.005 M, pH_{exp} = 4–8. At the bottom of the figure, the spectra of 0.1 M NaGluc at pH_{exp} = 7 are plotted for comparison.

The binding sites found for Nd(III), on the other hand, appear to be the same as those assigned for Ca(II) in neutral [37] or alkaline medium [62]. In other words, the preferred coordination moiety seems to be identical regardless of the metal ion in question. Concerning Ca^{2+} and Nd^{3+}, such similarity may arise from the very similar effective ionic radius. It has to be noted, however, that the C2-OH and C4-OH groups were proposed as binding sites in the $PrGluc_2H_{-1}^{+}$ and $PrGlucH_{-2}^{0}$ complexes [31] (Pr^{3+} has also similar radius).

5.5.5. Possible structures of the $NdGlucH_{-2}^{0}$ complex

During the course of structure optimizations, the initial geometries of the 1:1:–2 species were designed to obtain different coordination modes with the C2-OH and/or the C3-OH group being deprotonated (based on the NMR results). The calculations were carried out adding implicit and explicit water molecules to reach CN (coordination number) = 9 around Nd^{3+}. For $NdCl_3$ and $Nd(ClO_4)_3$ solutions, the average CN was found to be 8.5 and 9 from ND [173] and EXAFS [174] measurements, whilst CN = 8 was deduced *via* NMR relaxation experiments in presence of EDTA [175].

The most stable structure for $NdGlucH_{-2}^{0}$ is seen in Figure 48a (the name NdGluc_12 refers to the coordination mode). The metal ion is attached to the monodentate COO^- and to the C2-O^- moiety. Surprisingly, instead of the deprotonation of the C3-OH group, the proton displacement occurs on a water molecule establishing an Nd-OH bond. The respective bond lengths are listed in Table 19. Accordingly, the Nd-OH distance is shorter than that of the Nd-alcoholate by 0.05 Å.

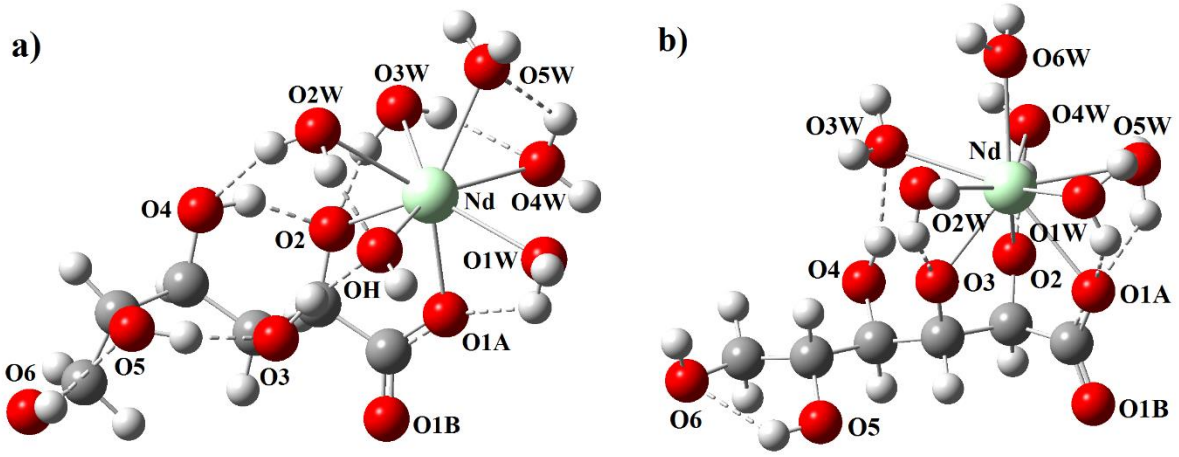

Figure 48 Optimized structures of the $NdGlucH_{-2}^{0}$ complex with different coordination modes (NdGluc_12: part a and NdGluc_123: part b). The calculations were performed at the PBE0 level applying the SDD core potentials for Nd and the def2-SVP basis sets for the lighter atoms. The solvent effect was taken into account by the COSMO model. The hydrogen bonds are visualized with dashed lines.

The CN of Nd^{3+} is 8 since there are five coordinated water molecules for which the bond lengths range from 2.54 to 2.62 Å. For aqueous Nd^{3+} solutions, the average Nd-O distance was determined to be 2.51 Å (EXAFS, XRD, in H_2O) [174,176] and 2.48 Å (ND, in D_2O) [173].

Like $CaGul^+$, extended intramolecular hydrogen-bonding network is established. Of these interactions, the distance of O3-H···H-O is very short (1.645 Å) and in parallel, the O-H covalent bond is considerably elongated (≈ 1 Å). Consequently, the hydroxide ion might capture a proton from the OH^- ion leading to the formation of the second-lowest-energy structure, NdGluc_123 (Figure 48b). At 298.15 K, its free energy is higher by 19.7 $kJ \cdot mol^{-1}$ which is significantly higher than the energy of thermal motion (2.5 $kJ \cdot mol^{-1}$).

The Nd^{3+} is coordinated by the carboxylate, the C2 and C3 alcoholate groups as well as six water molecules yielding CN as 9. It is worth mentioning the metal ion carboxylate distance is longer than that in NdGluc_12, which is a possible reason for the lower stability. Regarding the

hydrogen bonds, O2W-H···O3 is very strong and essentially is the reversed form of the above-mentioned O3-H···H-O bond suggesting an equilibrium process between these two isomers.

Table 19 Selected distances for the $NdGlucH_{-2}^{0}$ complex calculated at the PBE0 level applying the SDD core potentials for Nd and the def2-SVP basis sets for the lighter atoms. The solvent effect was taken into consideration by the COSMO model. The numbering is seen in Figure 48.

Nd-O distances			Hydrogen bond distances				
Atom	Atom	Ca-O(Å)	D[a]	H[a]	A[a]	D-H (Å)	H-A (Å)
			NdGluc_12				
Nd	O1A	2.333	O3	H(O3)	O(OH)	0.999	1.690
Nd	O2	2.278	O4	H(O4)	O2	0.993	1.645
Nd	O(OH)	2.281	O5	H(O5)	O3	0.982	1.737
Nd	O1W	2.542	O6	H(O6)	O5	0.972	2.043
Nd	O2W	2.623	O1W	H(O1W)	O1A	0.972	2.147
Nd	O3W	2.598	O2W	H(O2W)	O3	0.973	2.081
Nd	O4W	2.587	O2W	H(OH)	O(OH)	0.993	1.675
Nd	O5W	2.552	O3W	H(O3W)	O2	0.983	1.817
			NdGluc_123				
Nd	O1A	2.503	O4	H(O4)	O3W	0.971	2.023
Nd	O3	2.234	O5	H(O5)	O5	0.969	2.160
Nd	O4	2.271	O5	H(O5)	O6	0.966	2.271
Nd	O1W	2.567	O1W	H(O1W)	O1A	0.978	1.887
Nd	O2W	2.613	O2W	H(O2W)	O3	0.991	1.683
Nd	O3W	2.609	O4W	H(O4W)	O2	0.988	1.696
Nd	O4W	2.625	O6W	H(O6W)	O1A	0.978	1.916
Nd	O5W	2.571					
Nd	O6W	2.559					

[a] D = donor oxygen, H = hydrogen, A = acceptor oxygen.

6. Conclusions

In the present work, a comprehensive study was carried out concerning the chemistry of L-gulonate (Gul^-) ion in the presence and absence of Ca^{2+} ion at the pH range of 2–13 as well as the complex formation processes between Nd^{3+} and D-gluconate ($Gluc^-$) ions between pH = 2 and 8. In addition to the quantitative description of these complexation equilibria, the structural aspects of the species were also scrutinized *via* invoking NMR spectroscopic, polarimetric and quantum chemical methods.

Below pH = 5, L-Gul^- underwent protonation similarly to its diastereomer, D-$Gluc^-$. For these two anions, the protonation constant, K_p, was determined utilizing various experimental methods, such as potentiometry, polarimetry and NMR spectroscopy. As a result, K_p was found to be similar for both anions. Hence, the basicity of the carboxylate functional group is not significantly affected by the differences in the configuration of the hydroxy groups.

Beside protonation, the acid-catalyzed lactonization also took place in acidic medium. That is, two intramolecular esters, namely the five-membered γ- and the six-membered δ-lactones are formed for both aldonic acids as was attested by the ^1H and ^{13}C NMR spectra. Additionally, the latter method was applied to estimate the lactonization constants. Interestingly, it was found that of the four lactones (γ-HGul, δ-HGul, γ-HGluc, δ-HGluc), γ-HGul was the most stable. The higher stability of γ-HGul over its δ-isomer was confirmed by DFT computations as well.

Regarding lactonization kinetics, NMR and polarimetric measurements revealed that albeit δ-HGul was formed faster the rate of the reverse hydrolysis of γ-HGul was very slow which accounts for its enhanced stability. Moreover, it was found that if HGul was applied in a concentration commensurable to tha of HCl, HGul (in addition to H_3O^+) could catalyze the lactonization and the reverse hydrolytic processes.

In the presence of Ca^{2+}, potentiometric titrations indicated that weak 1:1 complexes were formed with D-sorbitol (Sor) and its diastereomer, D-mannitol (Man), while the formation of the $CaGlu^{2+}$ species could not be observed. The lower stability of $CaMan^{2+}$ relative to that of $CaSor^{2+}$ stems from the difference in stereochemistry. That is, ligands having *threo*-1,2-*threo*-2,3 triol sequence (Sor) form more stable complexes than those with *threo*-1,2-*erythro*-2,3 triol moiety (Man), as was proposed previously in the literature. Considerably more stable complexes

were observed with D-glucuronate and D-glucarate due to the presence of the strongly coordinating COO^- group(s).

In addition to the 1:1 complexes, 1:2 species were found to be formed with D-gluconate and D-heptagluconate ($Hpgl^-$) in solutions with high ligand to metal ratios. Polarimetric measurements, on the other hand, pointed out the weak interactions prevailing in these complexes as the structure of the bound ligands were only slightly different relative to that of the bulk anions.

The structurally similar Gul^- was also capable of forming 1:2 complexes. With respect to solution structure, the minor change in the conformation upon complexation was proven by polarimetry. The NMR spectra and quantum chemical calculations, additionally, suggest that the $CaGul^+$ complex possibly exists as different lingake isomeric forms, in which the binding sites can be the C2-OH, C3-OH or the C4-OH group (beyond COO^-).

In strongly alkaline medium, a proton displacement from a hydroxy group occurred as was deduced from potentiometric and NMR measurements. Adding Ca^{2+} ions to the solutions, strong pH effects were seen implying the formation of deprotonated complexes. Data evaluation revealed the formation of the highly stable $Ca_3Gul_2H_{-3}^+$ and $Ca_3Gul_2H_{-4}^0$ species, the stoichiometry of the latter was reported previously for $Gluc^-$ and $Hpgl^-$ as well.

^1H NMR spectra pointed to the differences in the coordination mode between the Ca(II) complexes of Gul^-/$Hpgl^-$ and $Gluc^-$. That is, the probable binding sites are the C2-OH and C4-OH groups in the case of Gul^- and $Hpgl^-$ while Ca^{2+} is bound to the C2-OH and C3-OH functions of $Gluc^-$. Consequently, if the arrangement of the first and second OH groups is *threo*, the C3-OH participates in the metal ion binding, otherwise C4-OH does. These results infer the definitive role of configuration in the structures of the complexes present in alkaline medium.

With regard to Nd^{3+} and $Gluc^-$ ions, spectrophotometric and potentiometric experiments indicated that complexation equilibria took place to a large extent. In addition to the mononuclear species, two binuclear and previously unknown complexes, $Nd_2Gluc_3H_{-2}^+$ and $Nd_2Gluc_3H_{-2}^+$, were detected. On the other hand, speciation diagrams demonstrate that the extent of formation of these species is negligible under the conditions of radioactive waste repositiories, for which Nd^{3+} is a frequently used model ion.

^1H NMR spectra suggested that the coordination sites of $Gluc^-$ were the COO^-, C2-OH and C3-OH groups while DFT calculations supported the formation of different linkage isomers.

7. Összefoglalás

Munkánk során az L-gulonátion (Gul^-) viselkedését tanulmányoztuk Ca^{2+}-ionok jelen- és távollétében a pH = 2–13 tartományban, valamint vizsgáltuk a Nd^{3+}- és D-glükonátionok ($Gluc^-$) között lejátszódó komplexképződési folyamatokat pH = 2 és 8 között. A kvantitatív jellemzés mellett célkitűzéseink között szerepelt a képződő oldatbeli részecskék szerkezeti jellemzése is NMR-spektroszkópiai, polarimetriás és kvantumkémiai módszerek segítségével.

Megfigyeltük az L-Gul^- savas oldatokban (pH < 5) lejátszódó protonálódását, hasonlóan a diasztereomer D-$Gluc^-$ anionhoz. A potenciometriás, polarimetriás és NMR-spektroszkópiás mérések alapján meghatározott protonálódási állandó nagyon hasonló volt mindkét ion esetén. Ebből arra következtethetünk, hogy a karboxilátcsoport bázicitását a hidroxilcsoportok konfigurációjában jelentkező eltérések nem befolyásolják jelentős mértékben.

Savas közegben a protonálódás mellett a savkatalizált laktonizációs folyamat is végbement. ^1H és ^{13}C NMR-méréseink igazolták, hogy a reakció során két intramolekuláris észter, az öttagú gyűrűs γ- és a hattagú gyűrűs δ-lakton képződik mindkét aldonsav esetén. A négy laktonra (γ-HGul, δ-HGul, γ-HGluc, δ-HGluc) vonatkozó, ^{13}C NMR-spektrumok alapján becsült laktonizációs állandó a γ-HGul esetén volt legnagyobb. Utóbbi δ-HGulhoz viszonyított nagyobb stabilitását DFT-számítások is alátámasztották.

A savkatalizált laktonizáció időfüggését NMR- és polarimetriás mérések segítségével követtük. Kimutattuk, hogy bár a δ-HGul gyorsabban képződik, az ellenkező irányú laktonhidrolízis a γ-HGul esetén sokkal lassabban megy végbe, ami nagyobb laktonizációs állandót eredményez. Ezenkívül bizonyítottuk, hogyha a tanulmányozni kívánt HGul koncentrációja a sósavval összevethető, nemcsak a H^+, de a HGul is katalizálhatja a laktonizációt és a hidrolízist.

A Ca^{2+}-ionokat tartalmazó oldatokban végrehajtott potenciometriás titrálások alapján kis stabilitású, 1:1 összetételű komplexek képződnek D-szorbitollal (Sor) és a diasztereomer D-mannitollal (Man), míg D-glükóz esetén a $CaGlu^{2+}$ képződését nem tudtuk kimutatni. A $CaMan^{2+}$ $CaSor^{2+}$ komplexhez viszonyított kisebb stabilitása az eltérő konfiguráció következménye. Korábbi irodalmi eredmények alapján ugyanis a *treo*-1,2-*treo*-2,3 triol egységet tartalmazó ligandumok (Sor) esetén a komplexképződés kedvezőbb, mint a *treo*-1,2-*eritro*-2,3 triol egység (Man) esetén. Az erős koordinációs tulajdonsággal bíró COO^--csoportot tartalmazó D-glükuronát és D-glükarát jelenlétében jóval nagyobb mértékű komplexképződést figyeltünk meg.

Az 1:1 sztöchiometriájú komplexeken kívül 1:2 összetételű részecskék is képződtek D-glükonáttal és D-heptaglükonáttal ($Hpgl^-$), nagy ligandum:fémion arányú rendszerekben. Polarimetriás kísérleteink ugyanakkor bizonyították, hogy a komplexekben létrejövő, gyenge kölcsönhatások miatt a kötött és szabad ligandum konformációja csak kismértékben tér el.

A szerkezetileg hasonló Gul^- aniont tartalmazó oldatokban is kimutattuk az 1:2 összetételű komplexet. A polarimetriás mérések alapján kijelenthető, hogy a ligandum konformációja a komplexképződés hatására csak kismértékben változik. Az NMR-spektrumok és kvantumkémiai számítások alapján a $CaGul^+$ valószínűleg különböző izomerek formájában fordul elő, melyekben a fémkötőhely a C2-OH és C3-OH vagy a C4-OH csoport (a COO^- mellett).

Az erősen lúgos közegben elvégzett NMR-mérések és potenciometriás titrálások a ligandum egyik OH-csoportjának deprotonálódására utalnak. A Ca^{2+}-ionok jelenlétében tapasztalt, jelentősen nagyobb mértékű potenciometriás effektus ugyanakkor deprotonálódott komplexek jelenlétét igazolja. Az adatok értékelése alapján bizonyítható a nagy stabilitású, $Ca_3Gul_2H_{-3}^+$ and $Ca_3Gul_2H_{-4}^0$ képződése. A 3:2:–4 sztöchiometriájú részecskét korábban $Gluc^-$ és $Hpgl^-$ esetén is kimutattuk.

Az ^1H NMR-spektrumok segítségével megfigyeltük a Gul^-/$Hpgl^-$ és $Gluc^-$ kalciumkomplexei közti, koordinációs módban megnyilvánuló különbséget. Gul^- és $Hpgl^-$ esetén a valószínűsíthető kötőhely a C2-OH és C4-OH csoport, míg $Gluc^-$ esetén a C2-OH és C3-OH csoport a koordinációs hely. Következésképpen, ha az első és második hidroxilcsoport relatív konfigurációja *treo*, a C3-OH csoport, míg *eritro* elrendeződés esetén a C4-OH csoport vett részt a koordinációban. A lúgos közegben képződő komplexek szerkezeti sajátságait tekintve a konfiguráció tehát meghatározó szereppel bír.

A Nd^{3+}- és $Gluc^-$-ionokat tartalmazó rendszerek potenciometriás titrálási görbéi, valamint látható tartományban felvett elektrongerjesztési spektrumai egyhangúan alátmasztották a nagyfokú komplexképződést. A korábban már kimutatott egymagvú komplexek mellett kétmagvú, $Nd_2Gluc_3H_{-2}^+$ and $Nd_2Gluc_3H_{-2}^+$ összetételű részecskék is képződtek. A koncentrációeloszlási diagramok értelmében ugyanakkor képződésük mértéke elhanyagolható a radioaktív hulladéktárolókban uralkodó körülmények mellett.

Az NMR-spektrumok alapján a $Gluc^-$ lehetséges koordinációs helyei a COO^-, C2-OH és C3-OH csoportok, míg a DFT számítások többféle, a fémkötőhelyek tekintetében eltérő izomer képződését valószínűsítik.

8. References

[1] S. Ramachandran, P. Fontanille, A. Pandey, C. Larroche, *Food Technol. Biotech*., 2006, **44**, 185–195.

[2] V. Neck, M. Altmaier, Th. Rabung, J. Lützenkirchen, T. Fanghänel, *Pure Appl. Chem*., 2009, **9**, 1555–1568.

[3] U. Berner: PSI-Report 62, Paul Scherrer Institute, Villigen, Switzerland, 1990.

[4] U. R. Berner, *Waste Manage*., 1992, **12**, 201–219.

[5] C. Bube, V. Metz, E. Bohnert, K. Garbev, D. Schild, B. Kienzler, *Phys. Chem. Earth*, 2013, **64**, 87–94.

[6] X. Gaona, V. Montoya, E. Colàs, M. Grivé, L. Duro, *J. Contam. Hydrol*., 2008, **102**, 217–227.

[7] S. P. Rosenberg, D. J. Wilson, C. A. Heath, In *Essential Readings in Light Metals, Vol. 1: Alumina and Bauxite*, D. Donaldson, B. Raahauge, Eds., John Wiley & Sons, New York, NY, U.S., 2013, pp. 210–216.

[8] B. I. Whittington, *Hydromet*., 1996, **43**, 13–35.

[9] Th. Rabung, M. Altmaier, V. Neck, Th. Fanghänel, *Radiochim. Acta*, 2008, **96**, 551–559.

[10] Furka Árpád: *Szerves Kémia*, Nemzeti Tankönyvkiadó, Budapest, Hungary, 1998, pp. 811–812.

[11] R. M. de Lederkremer, C. Marino, *Adv. Carbohyd. Chem. Bi*., 2003, **58**, 199–305.

[12] H. S. Isbell, H. L. Frush, *J. Res. Nat. Bur. Stand*., 1931, **6**, 1145–1152.

[13] H. L. Frush, H. S. Isbell, *Methods Carbohydr. Chem*., 1963, **2**, 12–15.

[14] H. Li, W. Li, Z. Guo, D. Gu, S. Cai, A. Fujishima, *Collect. Czech. Chem. Commun*., 1995, **60**, 928–934.

[15] P. N. Amaniampong, A. Karam, Q. T. Trinh, K. Xu, H. Hirao, F. Jérôme, G. Chatel, *Sci. Rep.*, 2017, **7**, 1–8.

[16] G. de Wit, J. J. de Vlieger, A. C. Kock van Dalen, R. Heus, R. Laroy, A. J. van Hengstum, A. P. G. Kieboom, H. van Bekkum, *Carbohydr. Res*., 1981, **91**, 125–138.

[17] S. Solmi, C. Morreale, F. Ospitali, S. Agnoli, F. Cavani, *Chem. Cat. Chem*., 2017, **9**, 2797–2806.

[18] O. E. May, H.T. Herrick, A.J. Moyer, P.A. Wells, *Ind. Eng. Chem*., 1934, **26**, 575–578.

[19] R. E. Mitchell, F. R. Duke, *Ann. NY. Acad. Sci*., 1970, **172**, 131–138.

[20] Y. Pocker, E. Green, *J. Am. Chem. Soc*., 1973, **95**, 113–119.

[21] J. Zubiaur, R. Castaño, N. Etxebarria, L. A. Fernández, J. M. Madariaga, *Talanta*, 1998, **45**, 1007–1014.

[22] R. K. Cannan, A. Kibrick, *J. Am. Chem. Soc*., 1938, **60**, 2314–2320.

[23] E. Heinz, *Biochem Z*., 1951, **321**, 314–342.

[24] J. T. H. Roos, D. R. Williams, *J. Inorg. Nucl. Chem*., 1977, **39**, 367–369.

[25] F. Coccioli, M. Vicedomini, *J. Inorg. Nucl. Chem*., 1978, **40**, 2103–2105.

[26] R. J. Motekaitis, A. E. Martell, *Inorg. Chem*., 1984, **23**, 18–23.

[27] K. Blomqvist, E. R. Still, *Anal. Chem*., 1985, **57**, 749–752.

[28] G. M. Escandar, L. F. Sala, *Can. J. Chem*., 1992, **70**, 2053–2057.

[29] W. M. Best, J. M. Harrowfield, T. M. Shand, R. V. Stick, *Aust. J. Chem*., 1994, **47**, 2023–2031.

[30] T. Gajda, B. Gyurcsik, T. Jakusch, K. Burger, B. Henry, J.B., J.-J. Delpuech, *Inorg. Chim. Acta*, 1998, **276**, 130–140.

[31] S. Giroux, P. Rubini, B. Henry, S. Aury, *Polyhedron*, 2000, **19**, 1567–1574.

[32] T. Bechtold, E. Burtscher, A. Turcanu, *J. Chem. Soc., Dalton Trans*., 2002, 2683–2688.

[33] Z. Zhang, S. B. Clark, G. Tian, P. L. Zanonato, L. Rao, *Radiochim. Acta*, 2006, **94**, 531–536.

[34] A. Lakatos, T. Kiss, R. Bertani, A. Venzo, V. B. Di Marco, *Polyhedron*, 2008, **27**, 118–124.

[35] D. T. Sawyer, J. B. Bagger, *J. Am. Chem. Soc*., 1959, **81**, 5302–5306.

[36] Z. Zhang, P. Gibson, S. B. Clark, G. Tian, P. L. Zanonato, L. Rao, *J. Solution Chem*., 2007, **36**, 1187–1200.

[37] A. Pallagi, P. Sebők, P. Forgó, T. Jakusch, I. Pálinkó, P. Sipos, *Carbohydr. Res*., 2010, **345**, 1856–1864.

[38] Dissociation constants (pK_a) of organic acids (at 20 °C), In *Applications of Ion Chromatography for Pharmaceutical and Biological Products*, L. Bhattacharyya, J. S. Rohrer, Eds., John Wiley & Sons, New York, NY, U.S., 2012, pp. 451.

[39] P. M. Dewick: *Medicinal Natural Products: A Biosynthetic Approach, 3rd ed*., John Wiley & Sons, New York, US, 2009, p. 493.

[40] P. A. Levene, H. S. Simms, *J. Biol. Chem*., 1925, **65**, 31–47.

[41] A. Pallagi, Z. Csendes, B. Kutus, E. Czeglédi, G. Peintler, P. Forgo, I. Pálinkó, P. Sipos, *Dalton Trans*., 2013, **42**, 8460–8467.

[42] C. L. Linster, E. Van Schaftingen, *FEBS J*., 2007, **274**, 1–22.

[43] M. u. Hassan, A. L. Lehninger, *J. Biol. Chem*., 1956, **223**, 123–138.

[44] C. Bublitz, A. P. Grollman, A. L. Lehninger, *Biochim. Biophys. Acta*, 1958, **27**, 221–222.

[45] K. Yamada, S. Ishikawa, N. Shimazono, *Biochim. Biophys. Acta*, 1959, **32**, 253–255.

[46] C. Bublitz, A. L. Lehninger, *Biochim. Biophys. Acta*, 1959, **32**, 290–291.

[47] C. Bublitz, A. L. Lehninger, *Biochim. Biophys Acta*, 1961, **47**, 288–297.

[48] C. Bublitz, *Biochim. Biophys. Acta*, 1961, **48**, 61–70.

[49] S. Aizawa, M. Senda, A. Harada, N. Maruyama, T. Ishida, T. Aigaki, A. Ishigami, T. Senda, *PlosOne*, 2013, **8**, e53706.

[50] T. Reichstein, A. Grüssner, *Helv. Chim. Acta*, 1934, **17**, 311–328.

[51] T. C. Crawford, R. Breitenbach, *J. Chem. Soc., Chem. Commun*., 1979, 388–389.

[52] E. Fischer, A. Speier, *Ber. Dtsch. Chem. Ges*., 1895, **28**, 3252–3258.

[53] P. A. Levene, H. S. Simms, *J. Biol. Chem*., 1926, **68**, 737–749.

[54] C. S. Hudson, *J. Am. Chem. Soc*., 1910, **32**, 338–343.

[55] J. E. Baldwin, *J. Chem. Soc., Chem. Commun*., 1976, 734–736.

[56] C. L. Combes, G. G. Birch, *Food Chemistry*, 1988, **27**, 283–298.

[57] H. C. Brown, J. H. Brewster, H. Shechter, *J. Am. Chem. Soc*., 1954, **76**, 467–474.

[58] J. R. Felty: *Thermodynamics of Aldonic Acids and Lactones*, M.Sc. Thesis, Texas Tech University, Lubbock, TX, U.S., 1972

[59] J. Clayden, N. Greeves, S. Warren, P. Wothers: *Organic Chemistry*, Oxford University Press, New York, NY, U.S., 2001, p. 196.

[60] D. D. Perrin, B. Dempsey, E. P. Serjeant: *pK_a Prediction for Organic Acids and Bases*, London, UK; Chapman and Hall, New York, NY, U.S., 1981.

[61] F. Coccioli, M. Vicedomini, *J. Inorg. Nucl. Chem*., 1978, **40**, 2106–2110.

[62] A. Pallagi, É. G. Bajnóczi, S. E. Canton, T. Bolin, G. Peintler, B. Kutus, Z. Kele, I. Pálinkó, P. Sipos, *Environ. Sci. Technol*., 2014, **48**, 6604–6611.

[63] B. Gyurcsik, L. Nagy, *Coord. Chem. Rev*., 2000, **203**, 81–149.

[64] S. J. Angyal, K. P. Davies, *J. Chem. Soc. D: Chem. Commun*., 1970, 500–501.

[65] S. J. Angyal, *Aust. J. Chem*., 1972, **25**, 1957–1966.

[66] S. J. Angyal, *Pure Appl. Chem*., 1973, **35**, 131–146.

[67] S. J. Angyal, R. J. Hickman, *Aust. J. Chem*., 1975, **28**, 1279–1287.

[68] S. J. Angyal, *Chem. Soc. Rev*., 1980, **9**, 415–428.

[69] L.-G. Ekström, A. Olin, *Acta Chem. Scand. A*, 1977, **31**, 838–844.

[70] H. Lönnberg, A. Vesala, *Carbohydr. Res*., 1980, **78**, 53–59.

[71] S. J. Angyal, D. Greeves, J. A. Mills, *Aust. J. Chem*., 1974, **27**, 1447–1456.

[72] A. P. G. Kieboom, T. Spoormarker, A. Sinnema, J. M. van der Toorn, H. van Bekkum, *Recl. Trav. Chim. Pays-Bas*, 1975, **94**, 53–59.

[73] K. K. Mäkinen, E. Söderling, *Calcif. Tissue Int*., 1984, **36**, 64–71.

[74] J. Briggs, P. Finch, M. C. Matulewicz, H. Weigel, *Carbohydr. Res*., 1981, **97**, 181–188.

[75] J. W. Haas, *Mar. Chem*., 1986, **19**, 1986, 299–304.

[76] J.-P. Morel, C. Lhermet, N. Morel-Desrosiers, *J. Chem. Soc., Faraday Trans*. 1, 1988, **84**, 2567–2571.

[77] S. P. Moulik, D. P. Khan, *Carbohydr. Res*., 1974, **36**, 147–157.

[78] Pallagi, Cs. Dudás, Z. Csendes, P. Forgó, I. Pálinkó, P. Sipos, *J. Mol. Struct*., 2011, **993**, 336–340.

[79] F. Franks, J. R. Hall, D. E. Irish, K. Norris, *Carbohydr. Res*., 1986, **157**, 53–64.

[80] H.-A. Tajmir-Riahi, *Carbohydr. Res*., 1988, **183**, 35–46.

[81] J. K. Beattie, M. T. Kelso, *Aust. J. Chem*., 1981, **34**, 2563–2568.

[82] A. P. G. Kieboom, H. M. A. Buurmans, L. K. van Leeuwen, H. J. van Benschop, *Recl. Trav. Chim. Pays-Bas*, 1979, **98**, 393–394.

[83] R. E. Hoffman, T. J. Rutherford, B. Mulloy, D. B. Davies, *Magn. Reson. Chem*., 1990, **28**, 458–464.

[84] L. H. Skibsted, G. Kilde, *Dan. Tidsskr. Farm*., 1972, **46**, 41–46.

[85] K. Vercammen: *Complexation of Calcium, Thorium and Europium by α-Isosaccharinic Acid under Alkaline Conditions*, Ph.D. Dissertation, Swiss Federal Institute of Technology, Zurich, Switzerland, 2000, pp. 28–29.

[86] M. Vavrusova, R. Liang, L. H. Skibsted, *J. Agric. Food Chem*., 2014, **62**, 5675–5681.

[87] M. Masone, M. Vicedomini, *Ann. Chim. (Rome)*, 1981, **71**, 517–523.

[88] M. van Duin, J. A. Peters, A. P. G. Kieboom, H. van Bekkum, *Carbohydr. Res*., 1987, **162**, 65–78.

[89] Z. Zhang, B. Bottenus, S. B. Clark, G. Tian, P. L. Zanonato, L. Rao, *J. Alloy Compd*., **444–445**, 2007, 470–476.

[90] M. Vavrusova, M. B. Munk, L. H. Skibsted, *J. Agr. Food Chem*., 2013, **61**, 8207–8214.

[91] J. Schubert, A. Lindenbaum, *J. Am. Chem. Soc.*, 1952, **74**, 3529–3532.

[92] G. E. Sipes: *Structure and Stability Constants of Boron, Calcium and Magnesium Gluconate Chelates from Optical Rotation and Computer Analysis*, Ph.D. Dissertation, University of Illinois, Urbana, U.S., 1969.

[93] H. A. Tajmir-Riahi, *J. Inorg. Biochem*., 1990, **39**, 33–41.

[94] T. Taga, T. Kaji, K. Osaki, *Bull. Chem. Soc. Jpn*., 1985, **58**, 30–35.

[95] R. O. Gould, A. F. Rankin, *J. Chem. Soc. D: Chem. Commun*., 1970, 489–490.

[96] H.-A. Tajmir Riahi, *Carbohydr. Res*., 1983, **122**, 241–248.

[97] E. Buddecke, R. Drzenieck, *Z. Physiol. Chem*., 1962, **327**, 49–64.

[98] C. Makridou, M. Cromer-Morin and J. P. Scharff, *Bull. Soc. Chim. Fr*., 1977, **12**, 59–63.

[99] L. DeLucas, C. E. Bugg, *Carbohydr. Res*., 1975, **41**, 19–29.

[100] S. E. B. Gould, R. O. Gould, D. A. Rees, W. E. Scott, *J. Chem. Soc., Perkin Trans. 2*, 1975, **0**, 237–242.

[101] J. A. Rendleman, *Food. Chem*., 1978, **3**, 47–79.

[102] P. J. M. Dijkgraaf, M. E. C. G. Verkuylen, K. van der Wiele, *Carbohydr. Res*., 1987, **163**, 127–131.

[103] A. C. García, M. Vavrusova, L. H. Skibsted, *J. Agric. Food Chem*., 2016, **64**, 2352–2360.

[104] T. Taga, K. Osaki, *Bull. Chem. Soc. Jpn*., 1976, **49**, 1517–1520.

[105] M. van Duin, J. A. Peters, A. P. G. Kieboom, H. van Bekkum, *Recl. Trav. Chim. Pays-Bas*, 1989, **108**, 57–60.

[106] C. L. Mehltretter, B. H. Alexander, C. E. Rist, *Ind. Eng. Chem*., 1953, **45**, 2782–2784.

[107] P. J. M. Dijkgraaf, M. E. C. G. Verkuylen, K. van der Wiele, *Carbohydr. Res*., 1987, **163**, 127–131.

[108] R. L. Pecsok, R. S. Juvet, Jr., J. *Am. Chem. Soc*., 1954, **77**, 202–206.

[109] R. Guillaumont, Th. Fanghänel, J. Fuger, I. Grenthe, V. Neck, D. A. Palmer, M. H. Rand: *Chemical thermodynamics series, Vol. 5: Update on The Chemical Thermodynamics of Uranium, Neptunium, Plutonium, Americium and Technetium*, Elsevier, Amsterdam, North Holland, 2003.

[110] V. Neck, M. Altmaier, Th. Fanghänel. *C. R. Chim.*, 2007, **10**, 959–977.

[111] M. Altmaier, X. Gaona, Th. Fanghänel, *Chem. Rev*., 2013, **113**, 901–943.

[112] G. R. Choppin, E. N. Rizkalla, In *Handbook on Physics and Chemistry of Rare Earths, Vol. 18*: *Lanthanides/Actinides: Chemistry*, K. A. Gschneidner, Jr., L. Eyring, G. R. Choppin, G. H. Lander, Eds., Elsevier, Amsterdam, North Holland, 1994, pp. 559–590.

[113] M. Altmaier, V. Metz, V. Neck, R. Müller, Th. Fanghänel, *Geochim. Cosmochim. Acta*, 2003, **67**, 3595–3601.

[114] I. I. Diakonov, B. R. Tagirov, K. V. Ragnarsdottir, *Radiochim. Acta*, 1998, **81**, 107–116.

[115] L. Rao, D. Rai. A. R. Felmy, *Radiochim. Acta*, 1996, **72**, 151–155.

[116] R. J. Silva: LBL Report 15055, Lawrence Berkeley Laboratory, Berkeley, CF, U.S., 1982

[117] J. Kragten, L. G. Decnop-Weever, *Talanta*, 1984, **31**, 731–733.

[118] E. Furia, R. Porto, *J. Chem. Eng. Data*, 2008, **53**, 2739–2745.

[119] L. Helm, M. N. Gaëlle, A. E. Merbach, *Adv. Inorg. Chem*., 2005, **57**, 327–379.

[120] K. B. Yatsimirskii, N. K. Davidenko, *Coord. Chem. Rev*. 1979, **227**, 223–273.

[121] N. A. Kostromina, *Zh. Neorg. Khim*., 1960, **5**, 95–101.

[122] N. A. Kostromina, *Ukr. Khim. Zh.*, 1960, **26**, 299–304.

[123] N. A. Kostromina, *Zh. Neorg. Khim.*, 1963, **8**, 1900–1905.

[124] N. A. Kostromina, *Zh. Neorg. Khim.*, 1966, **11**, 381–385.

[125] C. Panda, R. K. Patnaik, *J. Indian Chem. Soc.*, 1976, **53**, 1079–1083.

[126] S. Giroux, S. Aury, B. Henry, P. Rubini, *Eur. J. Inorg. Chem.*, 2002, 1162–1168.

[127] T. Taga, Y. Kuroda and M. Ohashi, *Bull. Chem. Soc. Jpn.*, 1978, **51**, 2278–2282.

[128] P. Sipos, P. M. May, G. Hefter, *Analyst*, 2000, **125**, 955–958.

[129] G. Peintler: *Spline Calculus, Version 2.12a*, University of Szeged, Szeged, Hungary, 2008.

[130] G. Peintler, B. Kormányos, B. Gyurcsik: *pHCali, Version 1.32a-20070323*, University of Szeged, Szeged, Hungary, 2007.

[131] H. M. Irving, M. G. Miles, L. D. Pettit, *Anal. Chim. Acta*, 1967, **38**, 475–488.

[132] I. Kron, S. L. Marshall, P. M. May, G. Hefter, E. Königsberger, *Monatsh. Chem.*, 1995, **126**, 819–837.

[133] R. G. Bates: *Determination of pH: Theory and Practice*, John Wiley & Sons, New York, NY, U.S., 1964.

[134] *Gaussian 09, Revision A.02–E.01*, Gaussian, Inc., Wallingford, CT, U.S., 2013.

[135] F. Neese, *Wiley Interdiscip. Rev.: Comput. Mol. Sci.*, 2012, **2**, 73–78.

[136] R. Peverati, D. G. Truhlar, *J. Phys. Chem. Lett.*, 2011, **2**, 2810–2817.

[137] F. Weigend, R. Ahlrichs, *Phys. Chem. Chem. Phys.*, 2005, **7**, 3297–3305.

[138] A. D. Becke, *Phys. Rev. A.*, 1988, **38**, 3098–3100.

[139] C. Lee, W. Yang, R. G. Parr, *Phys. Rev. B.*, 1988, **37**, 785–789.

[140] F. A. Momany, M. Appell, G. Strati, J. L. Willett, *Carbohydr. Res.*, 1994, **339**, 553–567.

[141] J. P. Perdew, *J. Chem. Phys.*, 1996, **105**, 9982–9985.

[142] C. Adamo, V. Barone, *J. Chem. Phys.*, 1999, **110**, 6158–6170.

[143] X. Cao, M. Dolg and H. Stoll, *J. Chem. Phys.*, 2003, **118**, 487–946.

[144] A. Schäfer, H. Horn and R. Ahlrichs, *J. Chem. Phys.*, 1992, **97**, 2571–2577.

[145] J. Tomasi, B. Mennucci, R. Cammi, *Chem. Rev.*, 2005, **105**, 2999–3093.

[146] A. K. Rappe, C. J. Casewit, K. S. Colwell, W. A. Goddard III, W. M. Skiff, *J. Am. Chem. Soc.*, 1992, **114**, 10024–10035.

[147] G. Peintler: *ChemMech, Version 5.99g*, University of Szeged, Szeged, Hungary, 2017.

[148] L. Zékány, I. Nagypál, G. Peintler: *PSEQUAD for Chemical Equilibria, Update 5–5.10*, Hungary, 2000–2008.

[149] *OriginPro, Version 8.6*, OriginLab Corp., Northampton, MA, U.S., 2011.

[150] J. C. Cobas, F. Javier Sardina, *Concept. Magn. Reson. A.*, 2003, **19A**, 80–96.

[151] M. L. Ramos, M. M. Caldeira, V. M. S. Gil, *Carbohydr. Res*., 2000, **329**, 387–397.

[152] K. Rehorst, *Ber. Dtsch. Chem. Ges*., 1930, **63B**, 2279–2292.

[153] H. S. Isbell, H. L. Frush, *Bur. Stand. J. Res*., 1933, **11**, 649–664.

[154] M. Karplus, *J. Am. Chem. Soc*., 1963, **85**, 2870–2871.

[155] M. Hummel, M. Leppikallio, S. Heikkinen, K. Niemalä, H. Sixta, *J. Carbohyd. Chem*., 2010, **29**, 416–428.

[156] M. A. Jermyn, *Biochim. Biophys. Acta*, 1960, **37**, 78–92.

[157] T. Takahashi, M. Mitsumoto, *Nature*, 1963, **199**, 765–767.

[158] K. Shimahara, T. Takahashi, *Biochim. Biophys. Acta*, 1970, **201**, 410–415.

[159] Z. Wałaszek, D. Horton, *Carbohydr. Res*., 1982, **105**, 131–143.

[160] Z. Wałaszek, D. Horton, I. Ekiel, *Carbohydr. Res*., 1982, **106**, 193–201.

[161] K. Zhuo, G. Liu, Y. Wang, Q. Ren, J. Wang, *Fluid Phase Equilibr*., 2007, **258**, 78–82.

[162] F. Stumpff, J. A. S. McGuigan, *Anal. Biochem*., 2014, **459**, 46–52.

[163] J. A. Rendleman, *Adv. Carbohydr. Chem*., 1966, **21**, 209–271.

[164] J. Doleźal, K. S. Klausen, F. J. Langmyhr, *Anal. Chim. Acta*, 1963, **73**, 71–77.

[165] T. Megyes, T. Grosz, T. Radnai, I. Bako, G. Palinkas, *J. Phys. Chem. A0*, 2004, **108**, 7261–7271.

[166] T. Megyes, I. Bako, S. Balint, T. Grosz, T. Radnai, *J. Mol. Liq.*, 2006, **129**, 63–74.

[167] Y. S. Badyal, A. C. Barnes, G. J. Cuello and J. M. Simonson, *J. Phys. Chem. A*, 2004, **108**, 11819–11827.

[168] F. Jalilehvand, D. Spangberg, P. Lindqvist-Reis, K. Hermansson, I. Persson, M. Sandström, *J. Am. Chem. Soc*., 2001, **123**, 431–441.

[169] A. Tongraar, T-Thienprasert, J. S. Rujirawat, S. Limpijumnong, *Phys. Chem. Chem. Phys.*, 2010, **12**, 10876–10887.

[170] D. Di Tommaso, K. L. Watson, *J. Phys. Chem. A*, 2014, **118**, 11098-11113.

[171] B. Kutus, A. Gácsi, A. Pallagi, I. Pálinkó, G. Peintler, P. Sipos, *RSC Adv*., 2016, **6**, 45231–45240.

[172] D. F. Mullica, G. A. Wilson, C. K. C. Lok, *Inorg. Chim. Acta*, 1989, **156**, 159–161.

[173] A. H. Narten, R. L. Hahn, *J. Phys. Chem*. 1983, **87**, 3193–3197.

[174] T. Yamaguchi, M. Nomura, H. Wakita, H. Ohtaki, *J. Chem. Phys*., 1988, **89**, 5153–5159.

[175] N. A. Kostromina, N. A. Tananaeva, L. B. Novikova, Yu. B. Schevchenko, *Teor. Eksp. Khim*., 1979, 15, 744–747.

[176] A. Habenschuss, F. H. Spedding, *J. Chem. Phys*., 1979, **70**, 3758–3763.

9. Acknowledgements

First of all, I want to thank my supervisors, Prof. Pál Sipos and Prof. István Pálinkó that they offered an oppurtinity of working in the Material and Solution Structure Research Group (MASOST) to which I joined in 2010. This thesis could not be completed without their guidance, financial support and continuous efforts to establish and maintain the necessary infrastructure.

The other senior group member, Dr. Gábor Peintler also helped me many times to solve any chemical or computational problem and more importantly, he taught me that every topic has many approaches and aspects.

Regarding molecular modeling calculations, the essential help provided by Dr. Alexandru Lupan and Dr. Amr A. A. Attia from the Babeş-Bolyai University is highly appreciated.

I want to give special thanks to my friends and collegues from the MASOST family. Undoubtedly, they helped me a lot to get through all these years. Of the group members, I would especially thank to Csilla Dudás, Ákos Buckó, Norbert Varga and finally, Ilona Halasiné-Varga for their help in the lab.

Last but not least, I express my gratitude to my parents, sister, grandparents and Tünde Pintér; finishing my degree and completing this work would not have been possible without their tremendous support.